Ion exchange coatings for porous separator membranes in RFB applications

Martyna Charyton

UNIVERSITE DE LORRAINE

Ecole Doctorale : **C**himie – **M**écanique – **M**atériaux – **P**hysique

Laboratoire : Laboratoire de Chimie Physique et Microbiologie pour les Matériaux et l'Environnement

Thèse

Présentée et soutenue publiquement pour l'obtention du titre de

DOCTEUR DE l'UNIVERSITE DE LORRAINE

Spécialité : chimie

par **Martyna CHARYTON**

Sous la direction de MATHIEU ETIENNE

ION EXCHANGE COATINGS FOR POROUS SEPARATOR MEMBRANES IN RFB APPLICATIONS

DEPÔTS ECHANGEURS D'IONS POUR MEMBRANES SEPARATRICES DE BATTERIES REDOX FLOW

28.10.2021

Membres du jury

Directeurs de thèse :	**Mathieu ETIENNE**	Directeur de recherche, LCPME, CNRS - Université de Lorraine
	Mateusz DONTEN	PhD, R&D manager, Amer-Sil, Kehlen, Luxembourg
Président de jury :	**Andréea PASC**	Professeure, Université de Lorraine
Rapporteurs :	**Céline CROUTXE-BARGHORN**	Professeure, Université de Haute Alsace
	Maxime PONTIE	Professeur, Université d'Angers
Examinateur :	**Alexander SHAPLOV**	Professeur, Luxembourg Institute of Sciences and Technology
Invité	**Gérard HENRION**	Directeur de recherche, IJL, CNRS - Université de Lorraine

Contents

Acknowledgments

Firstly, I would like to express my sincere gratitude to my supervisors, Dr. Mateusz L. Donten Dr. Mathieu Etienne and Dr. Gerard Henrion for the continuous support of my Ph.D study and related research, for motivation and immense knowledge. Their guidance helped me in carrying the research from and writing of this thesis.

Besides my supervisors, I would like to thank Dr. Peter Fischer for the help in establishing vanadium redox flow battery cycling experiments, all the thoughtful discussions and comments on my work. I am also grateful for the warm welcome I have received from Dr. Cristina Iojoiu during my secondment in LEPMI, Grenoble. She gave insightful remarks and advice related to the synthesis and properties of ion-exchange polymer. I would like to acknowledge for the fruitful collaboration with Dr. Cristina and my colleagues Misgina T. Tilahun and Caterina Sansone during this research stay.

My sincere thanks also go to Dr. Cedric Noel and Dr. Thomas Gries who provided me support and help in laboratory work and spectroscopic measurements at IJL. I would also like to express my gratitude to Dr. Fabienne Quiles for assistance and help related to FTIR and RAMAN spectroscopic measurements and analyses at LCPME.

I thank my fellow labmates from Amer-sil for the stimulating discussions, help and support during the last three years, especially I would like to acknowledge Fruzsina Gerencser, Maxime Henry, Dany Soquay, Frederic Schauli and Daniel Firganek. I would also like to express my gratitude to Joanna Rogińska my colleague from LCPME for her support and help during each of my visit at the university as well guidance with all the administrative work related to the Ph.D.

Last but not the least, I would like to thank the Flowcamp consortium that provided the financial support by European Union's Horizon 2020 research and innovation programme under the Marie Skłodowska-Curie Grant Agreement no. 765289 and gave me the opportunity to join the project receiving priceless experience.

List of abbreviations

AEM	Anion exchange membrane
ASR	Area specific resistivity
BPO	Biphenyl peroxide
CE	Coulombic efficiency
CEM	Cation exchange membrane
DAPCl	*N, N*-diallylpiperidinum chloride
DMEA	*N*-[3-(Dimethylamino)propyl]methacrylamide
EBE 830	Hexafunctional polyester acrylate oligomer (resin) – Ebecryl® 830
EDS	Energy Dispersive X-Ray Spectroscopy
EE	Energy efficiency
ETFE	Poly(ethylene tetrafluoroethylene)
FAP 450	Commercial name of fluorinated anion exchange membrane (Fumatech@)
FTIR	Fourier-transform infrared spectroscopy
HEAA	*N*-hydroxyethyl acrylamide
I500	Irgacure® 500 (50 % 1-Hydroxy-cyclohexyl-phenyl-ketone, 50 % Benzophenone)
IEC	Ion exchange capacity
IEM	Ion exchange membrane
KOH	Potassium hydroxide
MBAAM	*N,N*-methylenebis(acrylamide)
N 115	Commercial name of fluorinated cation exchange membrane (Nafion@)
NBS	*N*-bromosuccinimide
Omnirad 1773	Hydroxy-2-methyl-1-phenylpropanone
PAA	Poly(acrylic acid)
PhCl	Chlorobenzene
PPO	Poly(2,6-dimethyl-1,4-phenylene oxide)
PTFE	poly(tetrafluoro ethylene)
PVC	Poly(vinyl chloride)
PVP	Poly(vinyl pyrrolidone)
RFB	Redox flow battery
TPO	Diphenyl(2,4,6-trimethyl benzoyl)phosphine oxide
VBTAC	(Vinylbenzyl)trimethylammonium chloride
VE	Voltage efficiency
VIMPPO	Poly(2,6-dimethyl-1,4-phenylene oxide) modified with *N*-vinylimidazole (also reported here as vinylimidazolium poly(phenylene oxide)
VRFB	Vanadium redox flow battery
WU	Water uptake

Abstract

There is a growing demand in the development of a sustainable energy storage technology that can mitigate the problem of the intermittent nature of renewable energy sources. Among many energy storage systems, redox flow batteries (RFBs) demonstrate several unique merits: long cycle life, independent power generation and capacity as well as facile scaling up. Different types of electrolytes can be used in this technology, from the organic based one toward the aqueous based in which the charge carrying species are metal cations. Recently, one of the most matured systems are the vanadium redox flow batteries (VRFBs). The development of ion exchange membrane (IEM) that allows passing the charge carrying ions while blocking the redox active species is indispensable to reach high efficiency of VRFBs. Thus, low permeability to vanadium cationic species is crucial in order to prevent self-discharge of the battery and capacity decay. Another key parameter is resistivity of the membrane which should be kept at minimum in order to reach high efficiency of the battery. Besides the ionic transport properties, the IEM should exhibit mechanical and dimensional stability in order to withstand the tension in the battery. Nevertheless, one of the most challenging requirements for the membrane is excellent chemical stability. The electrolyte used in VRFBs is highly acidic and oxidative. Therefore, currently the most commonly used commercial membranes are based on high-cost fluorinated ionomers. Their cost impedes the widespread use of redox flow batteries. Therefore, this study was focused on the fabrication of a composite anion-exchange membrane in an industrially oriented process. From a literature study on different types of ion-exchange membrane it can be concluded that both the chemical structure of the membrane as well as their fabrication highly impact the ionic-transport properties of the membranes. Bearing in mind these aspects, a hierarchical, composite structure of the membrane was considered an advantageous over the dense, self-supported membrane. The presented membrane consists of a porous poly(vinyl chloride) (PVC)-silica substrate (600 μm) and a layer of ionomer (20 – 50 μm) applied on top of it. It is designed so that the substrate ensures dimensional stability and limits the amount of anion exchange material needed, allowing a lower cost of fabrication. Moreover, since the substrate serves as a reinforcement,

the thin ion exchange layer can be formed out of polymers that cannot be used as a self-supported film due to their insufficient mechanical properties. As a result of a composite structure of the anion exchange membrane (AEM), a new range of ion exchange polymers can be considered because the mechanical and ion transport properties are shared between the substrate and the top layer. The ion-exchange layer was applied on the porous substrate using blade-coating technique and UV-curing step, which can be easily adapted in a large-scale roll-to-roll process. Three different approaches for the ion exchange coating layer are described in the corresponding chapter of this thesis:

- UV crosslinking of acrylamide/PVP-based coating layer
- UV curing of acrylamides and poly(2,6-dimethyl-1,4-phenylene oxide) modified with *N*-vinylimidazole (VIMPPO)
- Photocured VIMPPO-based anion exchange composite membranes: Study of the spacing monomer on the properties of AEMs

In the first approach, the ion-exchange layer was fabricated by immobilization of a highly hydrophilic polymer – poly(vinyl pyrrolidone) (PVP) in a dense matrix formed out of acrylamides and acrylic oligomer (resin). All the used chemicals are commodity reagents of a low cost, which can be seen as a great advantage of such coatings over the commercial ion exchange membranes (IEMs). Moreover, varying the content of PVP from 6 wt.% up to 16% wt.% allows controlling the ion transport properties of the membrane. Membranes with lower contents of PVP exhibits less swelling in aqueous media due to the higher amount of a crosslinking matrix. As a result, they exhibit permeability to cations in line with the commercially used fluorinated AEM – Fumatech® FAP 450 on the cost of ion conductivity. The performance tests carried out for a benchmark RFB system – VRFB demonstrated that PVP-based membranes can reach comparable energy efficiency (EE) to the one of a commercial, benchmark membrane (74.7% versus 73.0% for FAP 450 and 75.0% for Nafion® N 115). However, during the charge-discharge experiments, noticeable capacity losses were observed. This can be attributed to possible oxidative degradation of the membrane or partial hydrolysis of the crosslinking agents (acrylic resins).

In the second approach, the anion exchange coating layer was fully crosslinked due to the use of an ionomer that can also serve as a crosslinking agent, stable in the vanadium electrolyte. Thus, poly(2,6-dimethyl-1,4-phenylene oxide) modified with *N*-vinylimidazole (VIMPPO) was synthesized with 25 % of the methyl groups modified with vinyl imidazole to reach high ion exchange capacity. However, UV-cured alone VIMPPO was too densely crosslinked and therefore demonstrated high area-specific resistivity. To improve the ion conductivity of the ionomer, it was used in a combination with acrylamide monomers. This allowed decreasing the content of the synthesized ionomer to even 10 %, which can be seen as an economical advantage. Series of membranes with different content of VIMPPO (max. 25 wt.%) were fabricated and characterized electrochemically in order to optimize the formulation and reach similar ionic transport properties to the one of commercial, benchmarked membranes (Nafion® N 115 and Fumasep® FAP450). VRFB cycling study showed an improvement of the composite membrane performance in comparison to the PVP-based AEMs. In particular, the membrane with 15 wt. % of VIMPPO in the coating layer allowed for high energy efficiencies – 75.1 % (at 80 $mA.cm^{-2}$) during the VRFB cycling experiments and capacity retention in line with the results of the commercial membranes. Nevertheless, some indications of capacity losses were still observed.

The third generation of the composite membranes were fabricated using the same VIMPPO polymer but without acrylamides in order to secure chemical stability. To prevent excessive density of the crosslinking, VIMPPO was formulated with UV-curable monomers which can form spacing molecular bridges between the chains of the ionomer leading to its loosened structure. The membrane fabricated using (vinylbenzyl)trimethylammonium chloride allowed to reach significantly enhanced performance in comparison to the commercial IEMs: higher energy efficiency (77.4 %) and lower capacity decay than in the case of FAP 450 or N 115. Furthermore, the stability of this type of membranes was improved in comparison to the one of the previously fabricated membranes, allowing to perform long-term cycling experiments (75 cycles at 50 $mA.cm^{-2}$) during which the membranes exhibited stable performance.

Resumé en français

Les énergies renouvelables sont au cœur des stratégies pour résoudre les problèmes environnementaux auxquels nous faisons face. En effet, ces sources d'énergie ont en principe un impact beaucoup plus faible sur l'environnement par rapport aux énergies fossiles. Cependant, les sources d'énergie électrique renouvelables telles que l'énergie éolienne ou l'énergie solaire sont intermittentes et fluctuantes, le pic de production d'énergie le plus élevé n'est souvent pas corrélé au pic de demande d'énergie le plus élevé. Afin de surmonter ce problème, le développement de systèmes de stockage d'énergie à grande échelle est crucial pour permettre une alimentation électrique durable. Plusieurs technologies de stockage d'énergie ont déjà été proposées, comme le stockage d'énergie hydroélectrique par pompage ou le stockage d'énergie par air comprimé. Malgré leur haut niveau de maturité, ces systèmes ne sont pas adaptés à toutes les applications, car ils sont limités à une certaine localisation. Une autre façon de stocker l'énergie électrique est de la convertir en énergie chimique, ce qui est la base du fonctionnement d'une batterie. Les batteries rechargeables standards (dites secondaires) sont principalement destinées aux appareils portables ou aux petits systèmes d'alimentation de secours. Le stockage d'énergie à grande échelle nécessite une stabilité à long terme, un rendement élevé, un faible coût d'investissement et une évolutivité flexible. Parmi les nombreux systèmes de stockage d'énergie, les batteries à flux redox présentent des avantages uniques : une longue durée de vie, un rendement élevé, une réponse rapide aux changements de charge ou d'entrée et enfin, une capacité et une production d'énergie indépendantes. Différents types d'électrolytes peuvent être utilisés dans cette technologie, depuis les électrolytes organiques jusqu'aux électrolytes aqueux dans lesquels les espèces porteuses de charge peuvent être des cations métalliques ou des molécules.

Récemment, l'un des systèmes les plus développés et les plus étudiés est la batterie à flux redox au vanadium (VRFB). Cependant, pour atteindre d'excellentes performances, un composant clé des VRFB est une membrane échangeuse d'ions. La membrane transfère les ions équilibrant la charge entre l'électrolyte positif et l'électrolyte négatif et doit donc présenter une conductivité ionique élevée. En parallèle, la membrane doit empêcher le transfert d'espèces redox actives (cations

vanadium : VO_2^+, VO^{2+}, V^{3+}, V^{2+}) car leur croisement entraîne des pertes de capacité et accélère l'autodécharge de la batterie. Par conséquent, afin d'atteindre une performance élevée de la batterie, la membrane doit présenter une faible perméabilité au vanadium et la résistivité de la membrane doit être maintenue au minimum afin d'atteindre une excellente efficacité de la batterie et d'assurer une performance stable à long terme de la batterie. Outre les propriétés de transport ionique, la membrane doit présenter une stabilité mécanique et dimensionnelle afin de résister aux pressions dans la batterie. Néanmoins, un critère essentiel pour la membrane est sa résistivité chimique. L'électrolyte utilisé dans les VRFB est un milieu hautement acide - acide sulfurique 1,5 - 3 M. De plus, lors de la charge, l'électrolyte positif devient également une solution hautement oxydante en raison de la présence d'ions VO_2^+. Par conséquent, les conditions dans la batterie en fonctionnement favorisent la dégradation oxydative et l'hydrolyse acide du matériau de la membrane. Actuellement, les membranes commerciales les plus couramment utilisées sont basées sur des ionomères fluorés qui offrent une excellente conductivité ionique et une faible perméabilité au vanadium ainsi qu'une excellente stabilité chimique dans les milieux acides et oxydants. Cependant, ces échangeurs d'ions fluorés sont fabriqués à l'aide d'ionomères qui sont obtenus par des procédures de synthèse en plusieurs étapes et avec beaucoup de solvants. Leur coût important entrave leur utilisation généralisée dans les batteries à flux redox. Par conséquent, ce travail de thèse s'est concentré sur la fabrication d'une membrane composite échangeuse d'anions dans un procédé industriel potentiellement moins coûteux.

Une étude de la littérature sur les différents types de membranes échangeuses d'ions a permis de conclure que la structure chimique de la membrane ainsi que sa fabrication ont un impact important sur ses propriétés de transport ionique. Compte tenu de ces aspects, une structure de membrane hiérarchique et composite a été considérée comme un avantage pour l'application visée par rapport à une membrane dense et autoportée. Les membranes produites et étudiées dans cette thèse sont constituées d'un substrat poreux en poly(chlorure de vinyle) (PVC)-silice (600 µm) et d'une couche d'ionomère (20 - 50 µm) déposée à sa surface. Cette membrane hiérarchique est conçue de telle sorte que le substrat assure la stabilité dimensionnelle et limite la quantité de matériau échangeur d'anions nécessaire, ce

qui permet de réduire le coût de fabrication. De plus, comme le substrat sert de renfort, la couche mince échangeuse d'ions peut être formée à partir de polymères qui ne pourraient pas être utilisés sous la forme de film autoportés en raison de leurs propriétés mécaniques inadéquates.

Grâce à la structure composite de la membrane, une nouvelle gamme de polymères échangeurs d'ions peut être envisagée pour produire des membranes échangeuses d'anions, car les propriétés mécaniques et de transport des ions sont partagées entre le substrat et la couche supérieure. La couche échangeuse d'ions a été appliquée sur le substrat poreux à l'aide d'une technique de revêtement par lame suivie d'une étape de polymérisation aux UV. Le processus de fabrication présenté peut être facilement adapté à un processus de laminage à grande échelle. Trois approches différentes pour la couche de revêtement échangeuse d'ions sont décrites dans les différents chapitres de cette thèse :

- réticulation UV de couches de revêtement en acrylamide/PVP,
- réticulation UV d'acrylamides et de poly(oxyde de 2,6-diméthyl-1,4-phénylène) modifié par du N-vinylimidazole (VIMPPO),
- membranes composites échangeuses d'anions photodurcies à base de VIMPPO : étude du monomère d'espacement sur les propriétés des membranes échangeuses d'anions.

Dans la première approche, décrite au chapitre 3, la couche échangeuse d'ions a été fabriquée par immobilisation d'un polymère hautement hydrophile - le poly(vinyl pyrrolidone) (PVP) - dans une matrice dense formée d'acrylamides et d'oligomères acryliques (résine). Tous les produits chimiques utilisés sont des réactifs de base d'un faible coût, ce qui peut être considéré comme un grand avantage de ces revêtements par rapport aux membranes échangeuses d'ions commerciales. En outre, la variation de la teneur en PVP dans la couche de revêtement (de 6 % à 16 % en poids) permet de contrôler les propriétés de transport des ions de la membrane. Les membranes à faible teneur en PVP présentent un gonflement moindre en milieu aqueux en raison de la quantité plus élevée de matrice de liaison. Par conséquent, les valeurs d'absorption d'eau ont diminué avec la diminution de la teneur en PVP. Cela a également entraîné une diminution de

la perméabilité aux espèces de vanadium, conduisant à des valeurs de perméabilité conformes à celles d'une membrane fluorée échangeuse d'anions utilisée dans le commerce (Fumatech® FAP 450). Cependant, la diminution de la perméabilité et de l'absorption d'eau des membranes a été suivie d'une augmentation de la résistivité de la membrane. Les tests de performance ont été réalisés en laboratoire pour une batterie à flux redox vanadium.

Deux membranes présentant une combinaison opposée de propriétés ont été sélectionnées afin de trouver une formulation optimale : résistivité modérée - faible perméabilité au vanadium (8 % en poids de PVP dans la couche de revêtement) et résistivité faible - perméabilité modérée au vanadium (14 % en poids de PVP dans la couche de revêtement). Le test de performance démontre que les membranes échangeuses d'anions composites proposées peuvent atteindre une performance de batterie comparable à celle de la membrane commerciale (Fumasep® FAP 450). À la densité de courant appliquée la plus faible, 20 mA cm^{-2}, la membrane avec une teneur plus faible en PVP (8 % en poids) a permis d'obtenir le rendement énergétique le plus élevé (92,6 %) grâce à une excellente efficacité coulombique (96,3 %) et une efficacité en tension satisfaisante (93,0 %). Cependant, à une densité de courant plus élevée, les pertes ohmiques ont un impact significatif sur les performances de la batterie. Ainsi, à 50 et 80 mA cm^{-2}, la membrane la plus conductrice (préparée avec 14 % en poids de PVP dans la couche de revêtement) a permis d'obtenir un rendement énergétique plus élevé (82,8 % et 74,7 % à chaque densité de courant) par rapport à la membrane de référence (80,7 % et 72,7 %). Néanmoins, pendant les expériences de charge-décharge, des pertes de capacité importantes et une plus grande vitesse d'autodécharge ont été observées dans le cas des membranes composites. Ceci peut être attribué à une perméabilité insatisfaisante aux différents ions vanadium ainsi qu'à une possible dégradation oxydative de la membrane ou à une hydrolyse partielle de l'agent de réticulation utilisé pour la préparation de la couche échangeuse d'ions.

Dans une deuxième approche (chapitre 4), la couche de revêtement échangeuse d'anions a été entièrement réticulée grâce à l'utilisation d'un ionomère qui peut également servir d'agent de réticulation et qui est stable dans l'électrolyte de vanadium. Ainsi, le poly(oxyde de 2,6-diméthyl-1,4-phénylène) modifié avec du *N*-vinylimidazole (VIMPPO) a été synthétisé avec 25 % des groupes méthyles

modifiés par le groupement vinylimidazolium. L'ionomère a été obtenu par une procédure de synthèse simple, en deux étapes, qui consiste à introduire le brome sur 25 % des groupes méthyles du poly(oxyde de 2,6-diméthyl-1,4-phénylène), puis à effectuer une réaction d'alkylation en utilisant du *N*-vinylimidazole. Un tel nombre de groupes *N*-vinylimidazolium assure une teneur élevée en groupes quaternaires, chargés positivement, fixés sur le VIMPPO, conduisant à une excellente capacité d'échange d'ions. Parallèlement, le groupe vinyle présent dans la partie *N*-vinylimidazolium permet d'effectuer d'autres réactions de réticulation par polymérisation radicalaire. Cependant, le VIMPPO seul, durci sous rayonnement UV, était trop densément réticulé et présentait donc une résistivité spécifique excessivement élevée. Pour améliorer la conductivité ionique de l'ionomère, il a été utilisé en combinaison avec des monomères d'acrylamide peu coûteux et non toxiques. Cela a permis d'inclure une grande part de matériaux bon marché et hydrophiles dans la formulation, ce qui a conduit à une diminution significative de la quantité d'ionomère synthétisé : jusqu'à 10 % en poids dans la couche de revêtement était suffisant, ce qui peut être considéré comme un avantage économique. Des séries de membranes avec différentes teneurs en VIMPPO (max. 25 % en poids) ont été fabriquées et caractérisées électrochimiquement afin d'optimiser la formulation pour atteindre des propriétés de transport ionique similaires à celles des membranes commerciales de référence (Nafion® N 115 et Fumasep® FAP 450). L'étude démontre que la résistivité de la membrane et la perméabilité au vanadium peuvent être facilement contrôlées en changeant le ratio de VIMPPO par rapport à la fraction d'acrylamide. Lorsque la teneur en VIMPPO a été réduite, la résistivité spécifique de la membrane a été significativement diminuée, devenant même plus faible que dans le cas d'une membrane commerciale dense. Les formulations avec des teneurs réduites en VIMPPO doivent en principe atteindre une plus faible densité de réticulation, permettant une plus grande absorption d'eau et donc, facilitant le transport des ions à travers la membrane. Dans le cas d'une diminution de la densité de réticulation par une teneur réduite en VIMPPO, la perméabilité aux espèces de vanadium à travers la membrane composite a augmenté progressivement. Néanmoins, même avec la plus faible quantité de VIMPPO (10 % en poids dans la couche de revêtement), la perméation des cations de vanadium à travers la

membrane était encore dix fois plus lente par rapport à un substrat nu en PVC-silice. Afin de comparer les performances des membranes enduites avec différentes propriétés de transport ionique, trois des membranes composites proposées ont été sélectionnées pour des tests supplémentaires dans la batterie à flux redox vanadium de laboratoire : 10, 15 et 25 % en poids de VIMPPO dans la couche de revêtement. Les résultats de l'étude du cycle VRFB ont montré une amélioration de la performance de la membrane composite en comparaison avec les membranes à base de PVP et des pertes de capacité plus faibles. Parmi les trois membranes composites, celle contenant 25 % en poids de VIMPPO a permis d'obtenir la plus grande efficacité coulombique à toutes les densités de courant appliquées, grâce à sa faible perméabilité aux espèces de vanadium. Cependant, la résistivité excessive de cette membrane a conduit à une efficacité de tension insatisfaisante, entraînant un faible rendement énergétique global, en particulier à une densité de courant appliquée élevée (67,1 % à 80 mA cm^{-2}). En revanche, la membrane contenant 15 % en poids d'ionomère a permis d'atteindre une efficacité en tension nettement supérieure et une efficacité coulombique légèrement inférieure. En conséquence, cette membrane a démontré la meilleure performance de cyclage en batterie parmi toutes les membranes testées (efficacité énergétique : 75,1 % à 80 mA cm^{-2}) et une rétention de capacité équivalente à celle observée avec les membranes commerciales. Une diminution supplémentaire de la teneur en VIMPPO dans la couche de revêtement a entraîné une détérioration des performances de la batterie. La membrane composite avec 10 % en poids de VIMPPO dans la couche de revêtement a permis un rendement en tension satisfaisant, mais le rendement coulombique a été réduit en raison de la forte perméation des espèces de vanadium à travers la membrane. En conséquence, la membrane avec 10 % en poids de VIMPPO dans la couche de revêtement n'a atteint que 70 % d'efficacité énergétique à la plus haute densité de courant appliquée (80 mA.cm^{-2}). Malgré les performances de cyclage prometteuses des membranes composites échangeuses d'anions présentées, plusieurs problèmes n'ont pas été résolus. Au cours des expériences de charge-décharge, certaines indications de pertes de capacité ont encore été observées. De plus, le taux d'autodécharge de la batterie assemblée avec la membrane composite était encore trop rapide en comparaison avec la membrane commerciale. Enfin, les tests de stabilité chimique ex-situ (réalisés dans une

solution d'électrolyte positif chargé) ont indiqué une dégradation oxydative des couches de revêtement échangeur d'ions.

Le chapitre 5 décrit alors la troisième génération de membranes composites qui a été fabriquée afin d'assurer une stabilité chimique satisfaisante, en utilisant le même polymère VIMPPO mais sans utiliser d'acrylamides. Pour éviter une densité excessive de la réticulation, le VIMPPO a été formulé avec des monomères pouvant former sous rayonnement UV des ponts moléculaires d'espacement entre les chaînes de l'ionomère. Par conséquent, ce ionomère durci sous UV devrait posséder une structure plus lâche que le VIMPPO durci seul. Deux monomères ont été choisis : le chlorure de *N, N*-diallylpipéridine (DAPCl) et le chlorure de (vinylbenzyl) triméthylammonium (VBTC). Ces monomères sont capables d'homopolymérisation linéaire et peuvent réagir avec la partie vinyle présente dans le VIMPPO. Des séries de membranes avec différentes teneurs de chaque monomère ont été fabriquées et caractérisées afin de trouver une formulation permettant d'atteindre une très faible perméabilité au vanadium et en parallèle une faible résistivité. L'augmentation de la teneur en DAPCl ou VBTC dans la couche d'enrobage a entraîné une augmentation significative des valeurs de la capacité d'échange d'ions par rapport à l'ionomère seul polymérisé. De plus, à des teneurs plus élevées en co-monomère, les couches de revêtement ont montré une capacité accrue à absorber l'eau, ce qui a également amélioré la conductivité ionique de la membrane. Ceci peut être attribué à une teneur accrue en groupes polaires, chargés positivement, chimiquement liés à l'ionomère ainsi qu'à une structure plus lâche du polymère résultant. Comme étudié précédemment, l'absorption d'eau est fortement corrélée à la perméabilité des membranes. Dans le cas du monomère DAPCl, l'augmentation de la teneur en monomère a conduit à un taux significativement plus rapide de perméation du vanadium à travers la membrane. Cependant, même à des teneurs relativement élevées en VBTC, la perméabilité est restée plus faible que dans la comparaison avec la membrane fluorée commerciale. Ce n'est que lorsque les valeurs d'absorption d'eau de la membrane ont dépassé 65 % que la perméabilité a sensiblement augmenté. Deux membranes ont été sélectionnées pour des tests supplémentaires : une avec 48% en poids de VBTC dans la couche de revêtement et une avec 27% de DAPCl. Les tests de stabilité ex-situ ont indiqué une certaine dégradation oxydative de la

couche d'enrobage, mais beaucoup moins importante que dans le cas des membranes décrites aux chapitres 3 et 4. Les expériences de cyclage en batterie ont montré que la membrane composite de troisième génération présentait d'excellents résultats, atteignant une valeur supérieure à celle des membranes commerciales (Nafion® N 115 ou Fumasep® FAP 450) à toutes les densités de courant appliquées. En particulier, la membrane fabriquée avec le VBTC a montré la meilleure performance globale grâce à une excellente efficacité coulombique (98,4 % à 80 mA cm-2) et l'efficacité en tension la plus élevée parmi toutes les membranes testées (78,7 % à 80 mA cm^{-2}). De plus, les pertes de capacité au cours des expériences de charge-décharge étaient beaucoup plus faibles dans le cas de la membrane fabriquée à l'aide du VBTC que dans celui de la membrane fabriquée avec du DAPCl. L'expérience d'autodécharge a également démontré que la cellule équipée de la membrane composite fabriquée à l'aide du VBTC a conservé la charge pendant plus longtemps (119 h) que dans le cas de la membrane fluorée de référence, Fumasep® FAP 450 (92 h). Avec ces résultats prometteurs, la membrane composite échangeuse d'anions fabriquée avec VIMPPO et VBTC a été sélectionnée pour un test de cyclage à long terme (75 cycles à 50 mA cm^{-2}) et comparé aux membranes commerciales FAP 450. Au cours de cette expérience, la cellule assemblée avec la membrane composite a montré une meilleure performance de cyclage par rapport à la membrane FAP 450 de référence. La membrane composite a atteint une efficacité coulombique moyenne de 98,6% alors que la membrane commerciale a atteint 97,8%. La principale amélioration de la performance de la membrane est liée à l'efficacité en tension : 85,6 % contre 82,0 % pour une cellule de batterie avec membrane composite et FAP 450, respectivement. Les résultats prouvent que les membranes composites VIMPPO/VBTC présentées peuvent être considérées comme une alternative performante aux membranes échangeuses d'ions de grande valeur disponibles dans le commerce.

General Introduction

Renewable energy sources have gained significant widespread attention owing to the importance of environmental issues and their sustainability. However, due to intermittent and fluctuating nature of the renewables, the energy generation patterns are often shifted from the demand's patterns. Therefore, the development of large-scale energy storage technologies is indispensable for reliable and sustainable power supply.

Some energy storage technologies are very mature, for example compressed air energy storage (CAES) or pump hydroelectric energy storage (PHS). However, these technologies are limited to a specified localization and cannot cover all the need that is foreseen for the coming decades. Another way to store electric energy is to convert it into chemical one. Recently, the conventional secondary (rechargeable) batteries offer a facile energy storage. However, they are mainly dedicated for small portable devices or intermittent backup power system.

Large energy storage requires superior long-term stability (large number of charge/ discharge cycles), high efficiency, rapid response to load or input changes, low capital cost and possible scalability [1]. Redox flow batteries (RFBs) are considered the most suitable technology that meets all of the above-mentioned requirements [2–4].

The RFBs are electrochemical devices that reversibly convert chemical energy into electrical energy using reduction-oxidation reactions of two redox active couples [5]. Figure 1 shows a schematic of RFB system that consists of two electrolytes with dissolved redox active species (anolyte and catholyte - negative and positive electrolyte, respectively) and two electrodes – separated by a membrane. The electrolyte is stored in external reservoirs and circulated through the system to the electrodes where the electrochemical reactions happen during charging or discharging, leading to the conversion of energy.

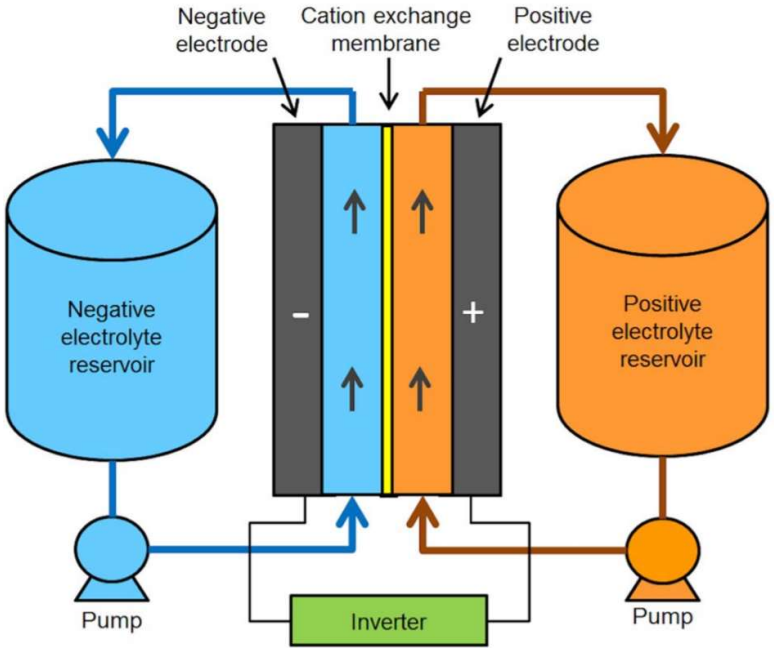

Figure 1. A general schematic of the typical redox flow battery system showing the electrochemical cell and the electrolyte recirculation from holding reservoirs to each of the two half-cells to a holding tank [5].

The energy of the RFB system is defined by concentration of the active species, volume of the electrolyte. In parallel, the power generation highly depends on the kinetics of the redox-active species reactions and the size of electrodes. Power and energy capacity are decoupled thus, they can be independently changed to adapt the system to the actual needs. For example, the capacity needed for certain energy storage application can be easily achieved by changing the volume of electrolyte stored outside the RFB stack making the system a flexible energy storage technology.

The scientific interest in the development of RFBs began with the NASA project in the 1970s. A 1 kW/13 kWh system (aqueous solutions of Fe^{2+}/Fe^{3+} (positive electrolyte) and Cr^{2+}/Cr^{3+} (negative electrolyte)) [6] was demonstrated to store the energy generated by the solar photovoltaic arrays. After that, the interest in other possible chemistries for the RFB were boosted including the new redox active species and the electrolyte solutions (aqueous, non-aqueous, acidic, alkaline or neutral) [7,8]. The all-vanadium redox flow batteries (VRFBs) were firstly proposed by E. Sum *et al.* in 1985 [9]. They are currently considered as the most promising and well-studied technology due to the simple chemistry based on the

same element in the two half cells and high energy densities. In this system, the redox reactions happen between VO^{2+} and VO_2^+ in the positive electrolyte and between V^{2+} and V^{3+} in the negative electrolyte as shown in the equations below (discharge: →, charge: ←).

$$V^{2+} \leftrightarrow V^{3+} + e^-$$

$$VO_2^+ + 2H^+ + e^- \leftrightarrow VO^{2+} + H_2O$$

The possible transfer of vanadium ions across the membrane do not lead to cross contamination of the electrolyte and can be mitigated by simply rebalancing the cell. Despite the advantages of long life-time, deep discharge capability and good reversibility of the redox process, the VRFBs suffers from the high capital cost which impedes their further market penetration [10,11].

Figure 2 indicates that among many components of the VRFB stack such as vanadium electrolyte, bipolar plates, carbon felt electrode, sealings, pumps *etc.* the second highest contribution to the overall cost of VRFB system is related to the use of ion exchange membrane (IEM). Currently the most widespread commercial membranes are the Nafion® series. Their price is estimated between 500 and 1000 \$/m^2 with the possibility to decrease down to 100 - 200 \$/m^2 in future perspective [12]. The reduction of the IEM price should significantly diminish the cost of VRFB and facilitate its further commercialization.

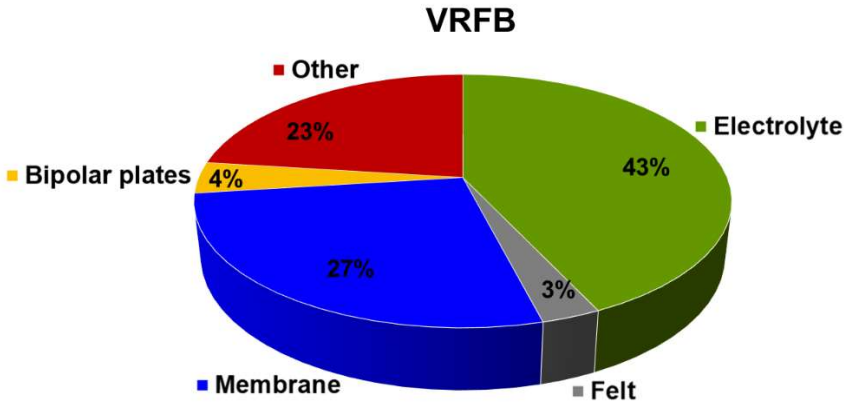

Figure 2. The economic costs associated with 1 MW/4 MWh system using VRFB; estimated contribution for each of the battery components, adapted from the work of B. A. Głowacki *et al.* [13].

The 27% contribution to the overall cost of the VRFB system is addressed to the IEM however, the vanadium electrolyte is related to the second highest cost contribution. An alternative metal-free redox flow battery technologies, based on organic redox active couples, have been proposed. In this case no metal mining is required to obtain the electrolyte [14]. The use of organic molecules offers the advantage of their common abundance and possibility to produce them from a variety of different sources. Furthermore, the synthetic chemistry allows tuning the properties of organic redox active species in order to enhance their kinetics and increase solubility. However, up to now, the organic RFBs exhibit much lower energy density than the metal-based RFBs (especially VRFBs).

IEMs are essential for the sustainable operation of the RFB system. The membrane transfers the charge-balancing ions between positive and negative electrolyte and in parallel physically separates positive and negative half-cells. The ionic transport properties of the membrane have significant impact on the overall battery performance. Highly ion conductive membrane diminishes the resistivity of the RFB cell, allowing reaching high voltage efficiency. In parallel, excellent permeability-selectivity grants high coulombic efficiency and prevents the capacity losses. Furthermore, the membrane has to exhibit outstanding chemical stability in the harsh environment of the cycled RFB. For example, in VRFBs the membrane is exposed to a highly acidic electrolyte (2 – 3 M H_2SO_{4aq}) which during cycling become highly oxidative due to the presence of VO_2^+ ions in the catholyte [15]. The lack of high-performance membrane available at low-cost resulted in numerous research about new possible materials and fabrication methods of the ion exchange membranes. The studies include fluorinated or non-fluorinated membranes and the later may offer lower material cost. In general, the membranes used in RFB can be categorized into two types:

1. Ion exchange membrane:
    - Cation Exchange Membranes (CEM) (Figure 3 a.)
    - Anion Exchange Membranes (AEM) (Figure 3 b.)
    - Amphoteric Ion Exchange Membranes (AIEM) (Figure 3 c.)

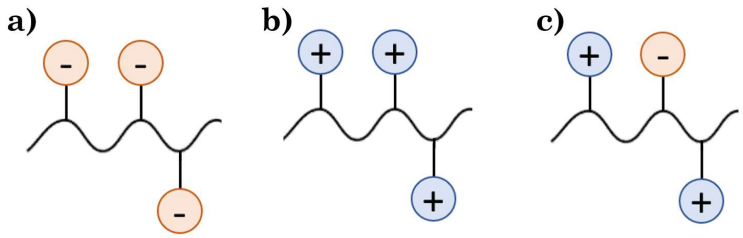

Figure 3. Schematic depiction of three types of ion exchange membranes: a) cation exchange membrane (CEM), b) anion exchange membrane (AEM), c) amphoteric ion exchange membrane (AIEM)

2. Porous separators (nanofiltration membranes)

The most commonly used membranes for RFB testing, especially in lab-scale studies are fluorinated cation exchange membranes (CEM) because of their excellent electrochemical properties and outstanding chemical stability. The perfluorinated sulfonic acid (PFSA) based CEMs were firstly developed by Dupont de Nemours in 1962 under commercial name Nafion®. They were primarily developed for the use in fuel cell application due to their outstanding chemical stability granted by the fluorinated polymer backbone [16,17]. When used in the RFB system, Nafion® membranes exhibits excellent proton conductivity and low permeability to vanadium cations. The fluorinated polymer backbone has hydrophobic properties while the sulfonic acid moieties are hydrophilic. In a hydrated state, the sulfonic acid groups segregate from the fluorinated backbone and form an ion conductive water-filled network that allows transport of ions. As a result, the use of Nafion® membranes in RFBs lead to high efficiencies of the battery and its stable cycling performance.

However, in many of the RFBs the redox active ions are positively charged. Therefore, the use of an anion exchange membrane (AEM) is considered more beneficial for the capacity retention. The positively charged groups present in the polymer structure allow transferring anions across the membrane. Following the Donnan exclusion law, the cationic moieties significantly limit the permeation of ions of the same charge. However, AEMs often exhibit lower ion conductivity in comparison to the cation exchange membrane leading to increased resistivity [18]. Alternatively, amphoteric ion exchange membranes with both negatively and

positively charged moieties have also been proposed as a possible solution to avoid the compromised performance [19].

Besides intensively investigated study on the ion-exchange membranes, nanofiltration membranes are considered a promising alternative, owing to their remarkably lower material cost [20]. However, the need for ion selective transport properties would require not only well-designed porous structure, tortuosity of the pores, pore size distribution but also well controlled pressure inside the RFB cell in order to limit the flow of electrolyte through the membrane.

This thesis was developed with the goal to merge the merits of the porous substrate (mechanical and chemical stability) with the selective ion transport properties of the dense IEMs. Chapter 1 describes the state of the art of the membranes used in redox flow batteries. Firstly, different methods of their fabrication are presented such as extrusion of thermoplastics, solvent-casting, radiation grafting, sol-gel polymerization and layer-by-layer assembly. Subsequently, various types of the membranes are presented depending on their functionality: ion-exchange abilities and structure (dense membranes, porous membranes and composite ones). In chapter 2, methods and materials that were used in this study are described. Chapters 3, 4 and 5 describes composite anion exchange membranes developed during this Ph.D. They consists of a porous poly(vinyl chloride) – silica substrate and a layer (coating) of anion-exchange material on top of the substrate. Depending on the used chemical formulation of the coating layer three types of the composite membranes were fabricated and discussed in chapter 3, 4 and 5, respectively. Chapter 6 summarizes the developed and studied composite AEMs, providing conclusions and outlook.

Chapter 1 – Literature study on the membrane development for the use in a redox flow battery

1.1 Introduction

In RFBs, a membrane separates the two electrolytes to prevent cross-mixing between catholyte and anolyte. The cross-over of redox active species between negative and positive electrolyte has to be prevented, otherwise it would cause capacity losses. In parallel, the membrane has to be permeable to supporting electrolyte ions (such as proton, sulfate or chloride) allowing to balance the changes for the ongoing electrochemical reactions [21,22]. Oswald firstly described the principle of ion transport through the ion exchange membrane in 1890. His study concluded that if the membrane is non-permeable, to either the cations or anions of any electrolyte it can be considered impermeable to the electrolyte. "Membrane potential" was postulated to illustrate the phenomenon at the boundary between membrane and the solution surrounding it. The existence of such boundary was confirmed by Donnan [23] by the development of a mathematical equation that describes the equilibrium concentration – "Donnan exclusion potential". The IEM possess charged moieties in their chemical structure therefore, only certain type of ions can permeate across the membrane. In addition, the high amount of water absorbed into the membrane (water uptake) facilitates the vehicular mechanism of ion transport improving the ion conductivity of the membrane [24].

The challenge of the chemical stability depends on the chosen system. The membrane has to be stable against acid or alkaline catalysed reactions (for example hydrolysis) and oxidation. The high-water uptake helps the absorption of the electrolyte, which may facilitate the degradation of the IEM caused by the harsh electrolyte environment (for example - charged vanadium electrolyte).

Sufficient mechanical properties: dimensional stability and satisfactory flexibility are also important for further use of the membrane. In addition, the water transport from one half cell to the other is driven by osmotic pressure and should be limited by the membrane [25]. Finally, the ideal membrane should be available at lower cost in order to boost the commercialization of RFBs.

In order to meet all of the above-mentioned requirements, a variety of membrane chemistry has been reported including non-ionic, nanofiltration membranes made of porous material and different types of the ion selective ones. Depending on the functional groups present in the membrane, cation exchange membranes (CEMs), anion exchange membranes (AEMs), amphoteric ion exchange membranes (AIEMs) and bipolar membranes can be distinguished [26].

Besides the chemical structure of the ionomer that affects the performance of IEM overall properties, the fabrication method is another important factor that determines its performance. The preparation method has a significant influence on the membrane morphology [27]. Consequently, it affects swelling behaviour of the membrane, ionic transport properties, mechanical stability and even chemical resistivity.

1.2. The methods of membrane fabrication

Depending on the microstructure the IEMs can be divided into heterogeneous (pore-filled, multi-layered, blends or composite with incorporated nanofillers) or homogeneous membranes. In case of the homogeneous membranes, three main categories can be further distinguished depending on the starting material [27]:

- Monomers containing the ion exchange groups that can undergo (co)polymerization reaction with non-ionic monomers in order to form a stable ion-exchange polymer
- Particles or film of polymer that are further modified in order to introduce the ion exchange functionality. The obtained ion exchange polymer can be later processed to form a film (membrane)

In the first case, the most used are vinyl monomers that can easily undergo free radical polymerization, thermally or photo initiated. Divinylbenzene and styrene are considered as good starting materials [28,29]. The ion exchange properties are introduced via radically reactive monomers with the selected ionic group, for example to obtain AEM, *N*-vinylimidazole or 4-vinyl pyridine were used [30,31].

Another way of incorporating the ion exchange functionality is to modify the obtained polymer. In the case of AEM, usually the ammonium group is introduced in a two-step process: chloromethylation and later quaternarization the backbone with a selected tertiary amine [32]. Similar can be applied to the fabrication of CEMs – the divinylbenzene-styrene copolymer can be easily sulfonated [33].

While using a polymer as a starting material, the polymer's solubility is a very important feature that determines preparation methodology.

In case of insoluble polymer, the functionalization can be performed by grafting an ion exchange group or a group that allows later modification. For example, epoxy acrylate or vinyl monomers were grafted on a fluorinated polymer backbone [34].

Soluble polymers can be processed using conventional chemical modification methods such as attachment of the functional moieties or copolymerization to form a multi-block ionomer). The resulting ion exchange polymer is later processed to form a foil (membrane) typically by solvent casting [35–37]. Due to the use of soluble polymer, the membrane fabrication needs to be followed by its post-treatment, for example crosslinking, to improve chemical stability of the resulting film [38].

To fabricate a non-ionic, porous membrane, there are mainly two strategies: dry and wet process, as reported by Zhang *et al.* [39]. The dry process consists of three main steps: extruding, annealing and stretching the homogenous polymer film. In the first step (figure 4), the polymer is heated to a temperature above its melting point. The resulting film needs to exhibit crystalline row structure to allow later formation of "open pores" in the stretching step.

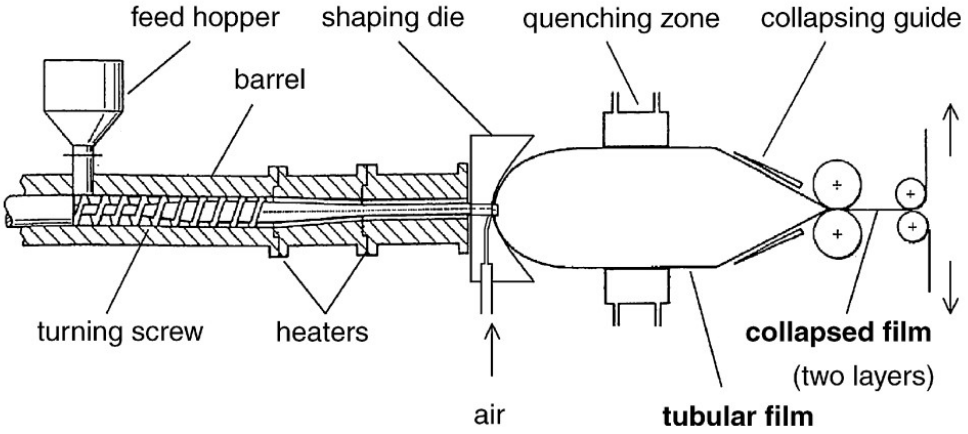

Figure 4. Schematic of an extrusion process [39] for porous stretched foils.

After the extrusion, the polymer film is annealed again to at a temperature slightly below its melting point. This process enhances the crystalline structure of the polymer and facilitates the formation of pores. In the last step, the annealed polymer is stretched to a desired thickness typically ranging from 10 to 100 μm. The stretching step leads to a fragmentary fracture of the film resulting in uniform pores [40].

In the wet process, the microporous membrane is fabricated in three steps process. Firstly, the polymer is mixed with paraffin oil and other additives and the mixture heated to obtain a homogeneous solution. Then the mixture is extruded through a sheet die to obtain a gel-like film and finally the oil or additives are extracted using volatile solvents to form a microporous structure. This process can be applied to both amorphous and crystalline polymers resulting in a non-oriented pore structure and isotropic mechanical strength of the obtained porous separator [39, 40].

1.2.1. Extrusion of thermoplastics

Perfluorinated ion exchange membranes are the benchmarked membranes in many RFB applications owing to their excellent chemical stability. Different fluorinated monomers *e.g.* tetrafluoroethylene, perfluoro(alkylviny1 ether sulfonyl fluorides), perfluoro(3,6-dioxa-4-methyl-7-octene-sulfonyl fluoride or perfluoro(viny1 ether carboxylic acid esters) are copolymerized in an autoclave [41]. The obtained copolymer is extruded as a thin film and consequently the sulfonyl fluoride moieties are hydrolysed into sulfonates groups. Due to the high energy consumption of the melt-extrusion process, nowadays PFSA based membranes (such as commercial Nafion® NR 212) are often manufactured by solution (dispersion) casting [42]. Table 1 lists the most commonly used Nafion® membranes comparing their fabrication methods.

Table 1. Commercial Nafion® membranes [42].

Commercial name	Fabrication	Thickness [μm]
Nafion® N 110	Extrusion	254
Nafion® N 117	Extrusion	183
Nafion® N 115	Extrusion	127
Nafion® NR 212	Casting	50
Nafion® NR 211	Casting	25

1.2.2. Solvent casting

One of the well-established IEM fabrication processes is continuous solution casting. This method is considered as the oldest film manufacturing technology [43]. A schematic illustration of the entire solvent casting process on a belt line is presented in figure 5.

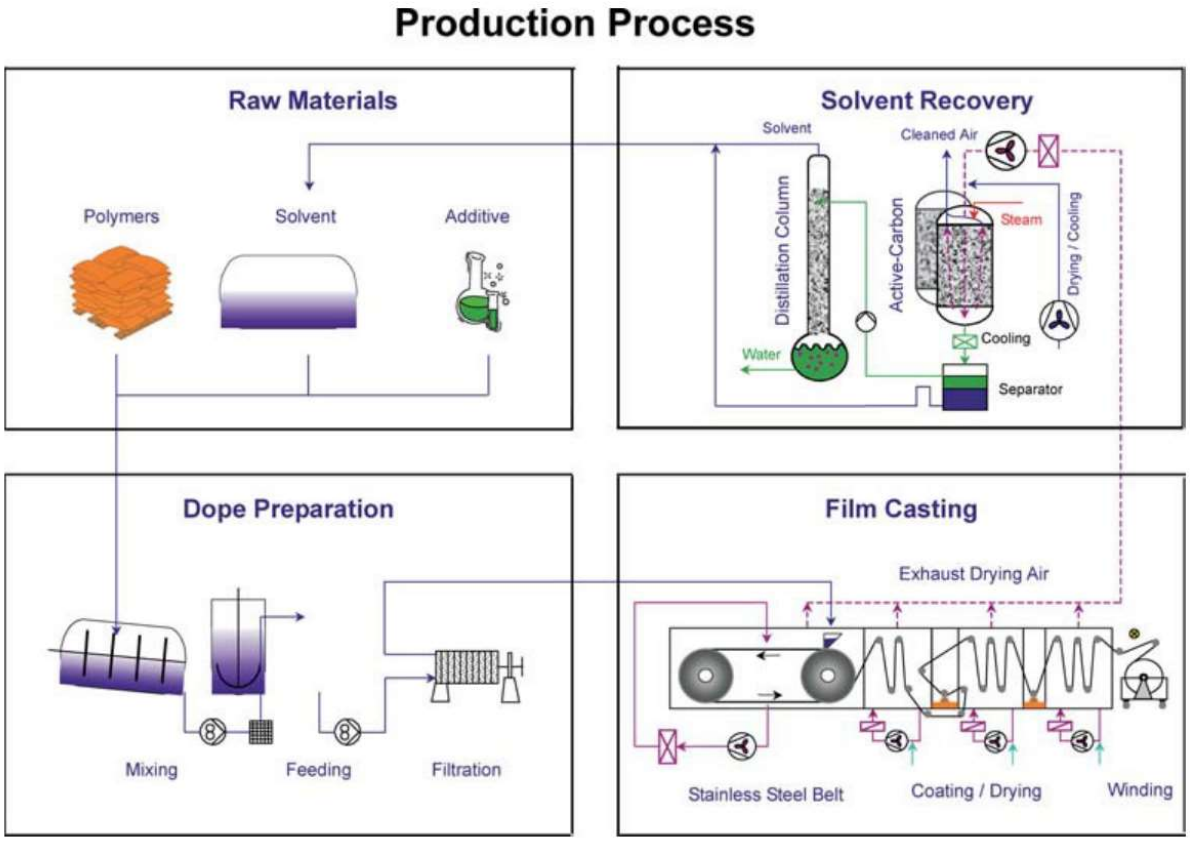

Figure 5. Schematic route for the production of solvent casted membrane [43].

Only the polymers that are soluble in volatile solvent or water can be processed using this method. Moreover, the polymer has to exhibit filmogenic properties allowing obtaining a homogeneous film that can be easily detached from the casting support. Multiple casting steps are sometimes performed to form a film consisting of several layers, in one fabrication process. As soon as the first layer solidifies another one can be applied [44,45].

The main advantage of this fabrication method is the uniform thickness of the obtained membrane. The thickness is of the casted film is mainly affected by the concentration of casting solution [46]. Moreover, the resulting film is in almost perfectly flat form with isotropic dimensional stability. The membrane properties such as mechanical stability can be changed by tuning the individual layers [47]. The solvent also has a key role in determining the membrane final properties. R. Guan *et al.* [48] reported the influence of the used solvent on the properties of sulphonated polyethersulfone (SPES) membrane. The SPES based CEMs were casted using three different solvents: dimethylformamide (DMF), dimethylacetamide (DMAc) and *N*-methylpyrrolidone (NMP) leading to different morphological structure of the films.

In the case of multiblock copolymers, the solvent highly affects the length of blocks as well as the organisation of different domains (for example hydrophilic and hydrophobic ones). Flory-Huggins parameters were suggested as useful indicators allowing to predict solubility and compatibility as well as the swelling degree of the resulting polymer [49]. In similar study [50] the temperature of the film drying was proposed as an important processing parameter that affects the final performance of a multiblock ionomer. The lower temperature of drying facilitates development of a well-organized morphology leading to an increased water uptake. This was attributed to the temperature dependent phase separation of different blocks of the ionomer.

In addition, the solvent casting process enables introducing other component into the membrane structure as long as they are compatible and soluble with the selected solvent [27].

1.2.3. Radiation grafting

Since 1962, radiation grafting is a well-established method for surface modification as it offers a possibility to tune both chemical and physical properties of the treated material [51]. One of the main advantages of radiation grafting is that no chemical initiators, solvents or catalysts are required, and the degree of grafting can be controlled by tuning the applied conditions of the process.

The initiation of such type of treatment can be caused by different radiation sources for example γ-rays or electron beams. This leads to the formation of active species such as ionic groups or radicals on the polymer backbone [52,53]. Especially in the case of hydrophobic, fluorinated polymers radiation grafting seems to be a good alternative to a conventional chemical modification process. J. Qiu et al. [18] used γ-radiation to graft dimethylaminoethyl methacrylate (DMEAMA) on poly(ethylene tetrafluoroethylene) (ETFE) membrane. After immersion in an acidic electrolyte, the tertiary amine groups present in DMEAMA were protonated, forming positively charged moieties. Study in a VRFB cell shows that the resulting grafted membrane exhibited improved ion selectivity, compared to Nafion® N 117. In the work of N.S. Kwak *et al.* [54] γ-radiation was used to graft vinyl benzyl trimethyl ammonium chloride (VBTAC) onto poly(ethylene-co tetrafluoroethylene (ETFE) film. Direct grafting of VBTAC on the hydrophobic substrate was not successful due to the ionization of the monomer. To overcome this problem the fluoropolymer was treated with VBTAC in the presence of 2-hydroxyl ethyl methacrylate (HEMA). Figure 6 shows the synthesis of ETFE-based membrane with grafted VBTAC and copolymerized HEMA (ETFE-g-(VBTAC-co-HEMA).

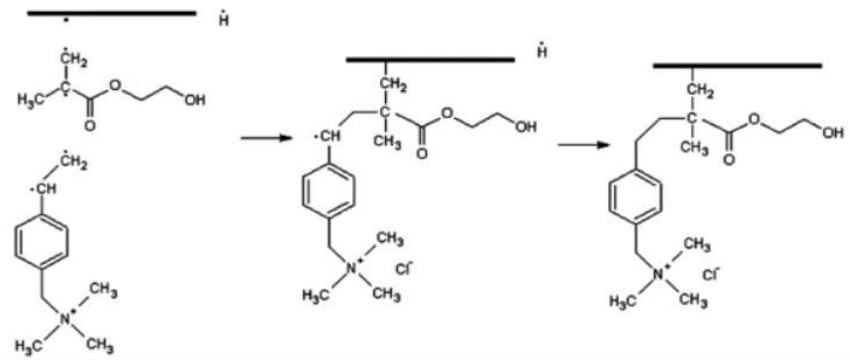

Figure 6. Schematic synthetic route of irradiation-induced grafting of HEMA and VBTAC onto ETFE polymeric film [54].

As a result, the radiation grafting process allowed combining cationic, hydrophilic moieties with incompatible hydrophobic, fluorinated substrate. Espiritu *et al.* [55] studied the influence of the grafting degree on the performance of AEMs. The membranes were obtained by grafting vinylbenzylchloride and trimethyl amine on a polyethylene (PE) sheet (figure 7).

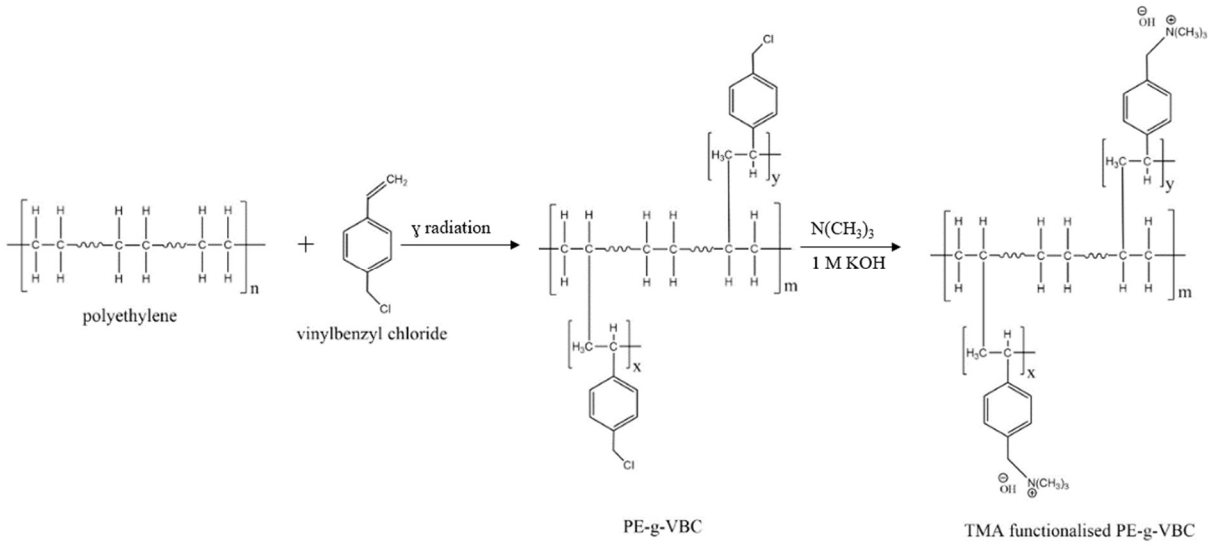

Figure 7. Schematic route for the synthesis of PE based AEM (adapted from [55]).

The degree of grafting (DG) was defined by measuring the weight of membranes before (W_0) and after (W_a) the radiation treatment:

$$DG(\%) = \frac{W_a - W_0}{W_0} \cdot 100\ \%$$

This parameter was controlled by changing the dose of radiation and the concentration of the monomers. The study demonstrated that the mechanical

properties such as tensile strength was lower in the case of higher DG, leading to a consequently increased swelling behaviour of the membrane. Following that trend, the ion conductivity of the AEMs was also improved. This proved that the ionic transport properties of the IEMs can be controlled by the conditions of radiation grafting treatment.

1.2.3.1. Plasma polymerization/modification

This chapter is dedicated for a specific technique that involves the use of plasma treatment. In particular, plasma polymerization involves not only radiation processes but often the use of reactive precursors. Although majority of membranes are prepared using traditional wet chemical processes, such as free radical polymerization, the plasma enhanced chemical vapor deposition (PECVD) has several advantages over conventional polymerization processes. It allows high degree of crosslinking in the resulting plasma polymer leading to an excellent chemical and thermal stability. The films are dense and homogenous, exhibiting good adhesion to almost any substrate with a controllable thickness ranging from nanometers up to micrometers [56]. In addition, plasma polymerization reduces the waste of liquid solvents since they are not needed. Therefore, it can be considered as a more environmentally friendly and cleaner polymerization technique, compared to the conventional methods. However, the complex and non-specific nature of chemical reactions happening in the plasma often lead to less predictable products of the process. Such polymers do not have regular, repeated units, but rather exhibit randomly crosslinked polymeric network. Moreover, their structure highly depends on the external conditions of plasma such as discharge power, pressure or monomer flow rate [57].

Plasma processes have been studied for the fabrication or modification of ion exchange membranes, because they allow depositing an ultra-thin layer of a functional coating on the selected substrate. In 1990 Ogumi *et al.* [58] presented a modified Nafion® N 117 membrane with a thin layer of anion exchange coating that contained pyridine rings. Glow discharge plasma polymerization of 4-vinyl pyridine was performed resulting in a homogeneous thin film (0.2 μm) deposited on the commercial IEM. The modified membrane exhibited improved proton

conductivity and lower vanadium permeability, compared to the pristine N 117. However, the additional layer also led to increased resistivity of the membrane. Similar approach was reported by Zeng *et al.* [59]. Thin layer of anion exchange polymer was deposited on the surface of N 117 membrane by glow discharge plasma polymerization using ethylene and ammonia as precursors.

Weng *et al.* [60] proposed a high performance ion exchange membrane for the use in RFBs prepared from poly(arylene ether sulfone) (PAES) with nano-crack coating. The thin hydrophobic layer with nano-crack structure was obtained by plasma treatment of the PAES membrane with octafluorocyclobutane. Figure 8 pictures the selective ion transport across the membrane.

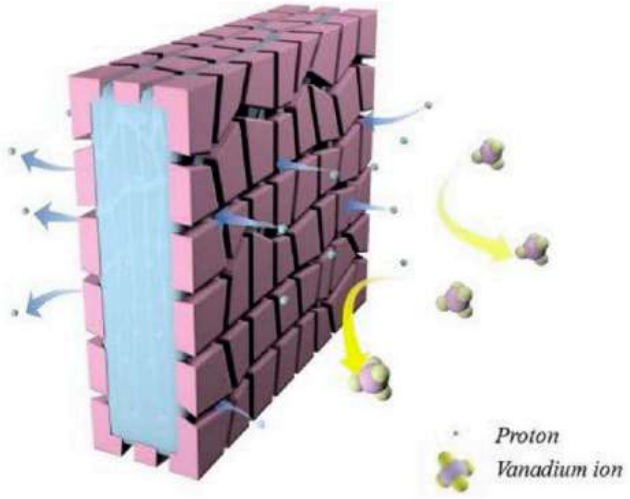

Figure 8. The mechanism of selective ion transport across the plasma modified membrane with "nano-crack" structure of the surface [60].

Performance of the plasma treated membranes was evaluated in VRFB single cells and compared with Nafion® membranes and pristine PEAS membrane. The cycling results shown that the cell assembled with modified membrane exhibited higher coulombic and energy efficiency compared to the one with the pristine PEAS membrane. Furthermore, energy efficiency achieved by the cell with the plasma treated membrane was comparable to the one of Nafion® N 117 (85.37% versus 85.11% respectively). The membrane exhibits stable cycling performance over 200 cycles as the cell efficiencies remained almost constant. This suggested good chemical stability of the membrane and resistivity to oxidative degradation. The

resistivity against vanadium electrolyte was proven in an ex-situ chemical stability test performed in the solution of VO_2^+ ions in sulfuric acid [60].

Matsuoka *et al.* [61] proposed an anion exchange membrane prepared by the plasma polymerization of 4-vinyl pyridine on glass plates or glass porous sheets as substrates. The resulting polymer was rich in pyridine moieties and further treated with 1 vol. % 1-bromopropane to obtain quaternary ammonium groups. Infrared spectroscopy indicated high crosslinking degree of the thin film and scanning electron microscope images show its uniform thickness (c.a. 10 μm). In comparison to the commercial anion exchange membrane (Neosepta AHA), the plasma polymerized membrane exhibited lower resistivity, which can be attributed to the differences in membranes thicknesses (c.a. 10 μm versus 240 μm in case of commercial membrane).

Although plasma polymerisation offers may advantages, this technique is rarely used for the fabrication of IEMs [62]. For example, the need of low pressure or vacuum atmosphere and expensive equipment impedes the industrial application of plasma-based membrane fabrication processes.

1.2.4. Sol-gel method

Since the mid-19th century, sol-gel process has been intensively studied resulting in over 35 00 papers published so far. This method is mainly used to fabricate composite membrane that are organic-inorganic (hybrid) materials. The sol-gel process led to various structures of the membrane depending on the chosen route as shown in figure 9. However, several main typical steps can be distinguished [63,64]. The first one is mixing: the selected metal alkoxides (M(OR)n (where M is the metal and R is an alkyl) are dispersed in a liquid solution. Second step involves crosslinking (gelation) during which, the deposited solution forms different products such as xerogels, wet gels or uniform particles. The third step consists of drying, during which the polymerization of particles is carried out. The reaction is often performed by removing the stabilizing components leading to the formation of gel instead of a continuous network. Lastly, the remaining organic or inorganic components can be removed by heating which leads to crystalline or amorphous type coating [27].

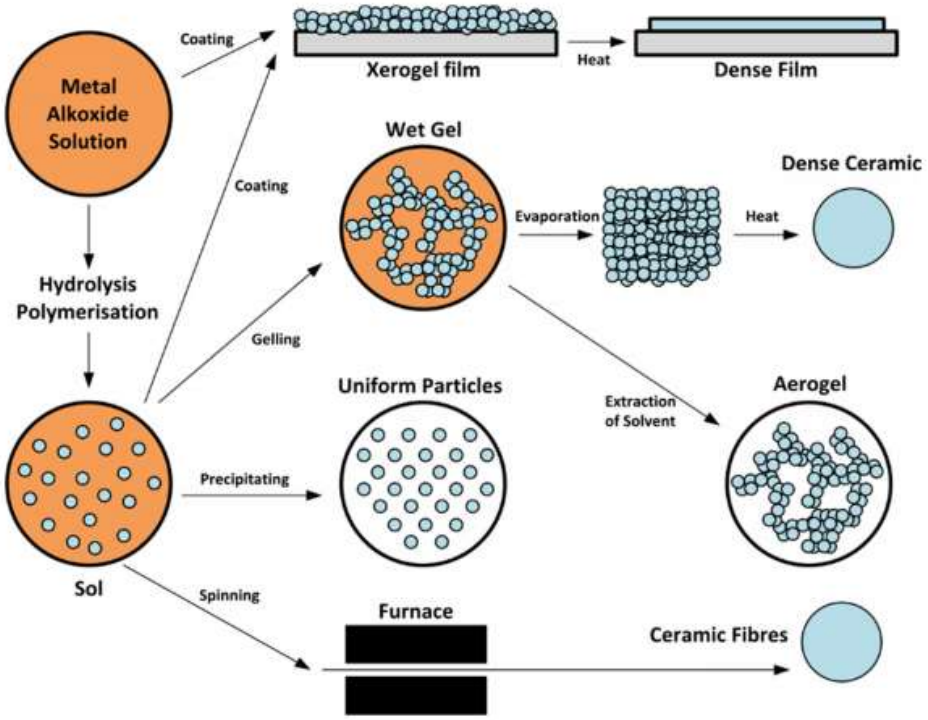

Figure 9. The sol-gel process shown on a belt line [27].

The sol-gel method has many advantages over other fabrication methods. Low temperature processing is used and the resulting product exhibits outstanding thermal and chemical stability depending on the environment as well as chemical purity [65]. Moreover, no melting or machining is needed since in the sol-gel process the precursors are in a liquid form. A wide variation in the ratio of organic to inorganic components is possible in this method, thus the properties of the membrane can be easily adjusted. The ion conductivity and ion selectivity are mainly controlled by organic domains, while the inorganic fractions grant mechanical durability. The membranes obtained in sol-gel technique exhibit similarities between organic and inorganic phases at the molecular level [66].

Mauritz *et al.* reported a microcomposite membrane prepared via sol-gel reaction of silicon tetraethoxide within perfluorosulfonic acid (Nafion®) films [67]. Later the sol-gel method was successfully applied to improve the ion selectivity of Nafion® membranes by the incorporation of TiO_2 or SiO_2 nanoparticles [68,69]. The membranes with modified inorganic nanoparticles exhibited remarkably lower vanadium cation permeability leading to higher coulombic efficiency of the battery cell, in comparison to the cell with pristine Nafion® membrane.

P.K. Leung *et al.* [70] proposed sol-gel method as a possible way to modify commercial AEM (Fumasep® FAP) by the incorporation of silica nanoparticles. The modified AEM exhibited 20% lower permeability of vanadium ions compared to the pristine AEM. This was attributed to the silica particles that serve as barriers blocking the transfer of vanadium species across the membrane. The low permeability was confirmed in cycling experiments, in VRFB cells. The use of the modified AEM allowed reaching the highest coulombic efficiency at a range of current densities (20-80 $mA.cm^{-2}$). The low crossover of vanadium species was also confirmed in a self-discharge test (figure 10).

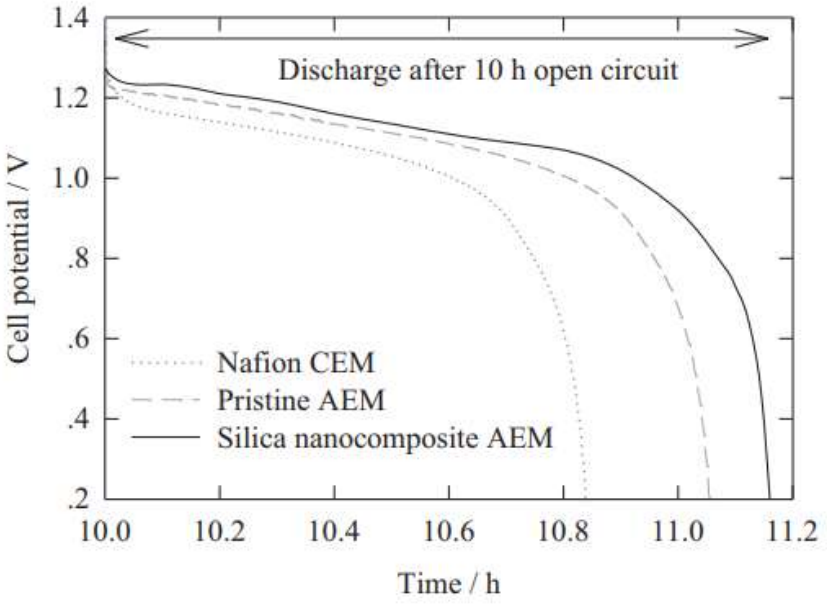

Figure 10. The voltage curves of the fully charged VRFB cells equipped with the silica nanocomposite AEM, pristine AEM (Fumasep®) and Nafion® CEM after 10 h of open-circuit conditions [70].

The sol gel technique can be used not only to modify the commercial IEM, but also to fabricate an IEM out of lower value starting materials. Recently, Ling *et al.*[71] introduced technique sulfonic silica into a porous poly(vinylidene fluoride) (PVDF) membrane via sol-gel. PVDF was selected as a chemically stable, fluorinated base component of the membrane. The incorporated sulfonic silica provided proton exchange moieties leading to a high ion conductivity of the membrane and supressed vanadium permeation, in comparison to a commercial IEM – Nafion® N 115. The VRFB cell assembled with the composite membrane achieved comparable

results to the Nafion® membrane. It was concluded that sol-gel can be considered as a simple way to fabricate an organic/inorganic IEM for the use in redox flow batteries.

1.2.5. Layer-by-layer assembly

The layer-by-layer (LBL) assembly fabrication method is used to obtain multilayer thin films with controlled architecture and composition [72]. The resulting membranes are considered as bipolar ion exchange membranes that consists of both cation exchange layer(s) and anion exchange layer(s). The organized structure of a layer-by-layer system is formed spontaneously without external direction. The procedure involves alternating subsequent immersion of a solid or flexible substrate in the solution of an opposite charge (figure 11). Rinsing step is indispensable between each of the layer deposition to remove weakly attached molecules that may cause partial degradation during later use of the LBL membrane [73].

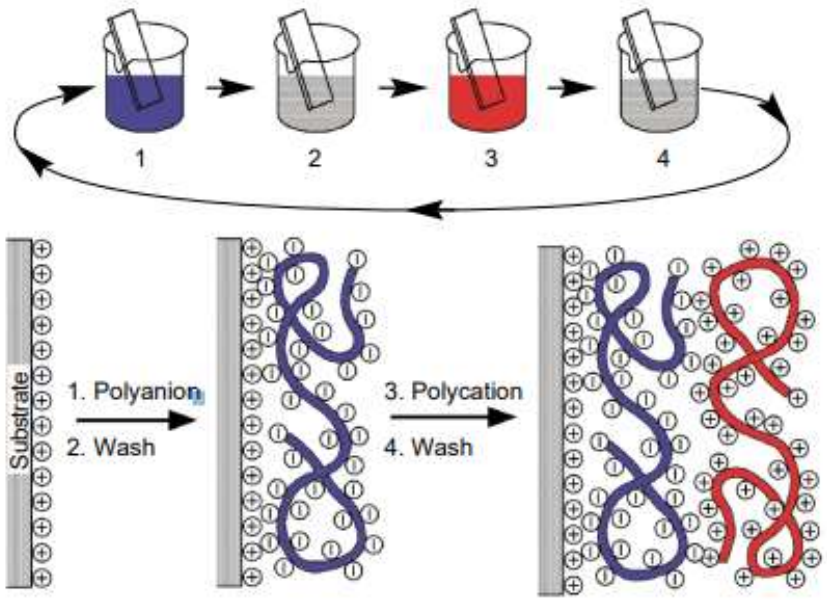

Figure 11. Schematic of the film deposition process in layer-by-layer assembly method (adapted from the study of Decher G. [74]).

The layer-by-layer assembly technique offers very good nanoscale organization and excellent control of the membrane structure. The process allows controlling the thickness of each layer at the nanometre scale [75]. Additionally, the properties of

the fabricated film can be enhanced by changing the type of electrolyte [76]. Teng *et al.* [77] reported polytetrafluoroethylene/sulfonated poly(ether ether ketone (PTFE/SPEEK)) membrane prepared by the LBL self-assembly technique with polycation poly(diallyl dimethylammonium chloride) (PDDA) and polyanion poly(sodium styrene sulfonate) (PSS). The membrane consisted of eight PDDA/PSS bilayers and has very low thickness (only 30 μm). Ion selectivity to vanadium and protons was significantly improved in comparison to the pristine PTFE/SPEEK based membranes as well as the LBL assembled membrane exhibited reduced swelling and water uptake, owing to the decrease of sulfonic groups. The charge-discharge VRFB single-cell tests proved superior performance of the membrane fabricated in LBL process in comparison to the pristine PTFE/SPEEK (figure 12).

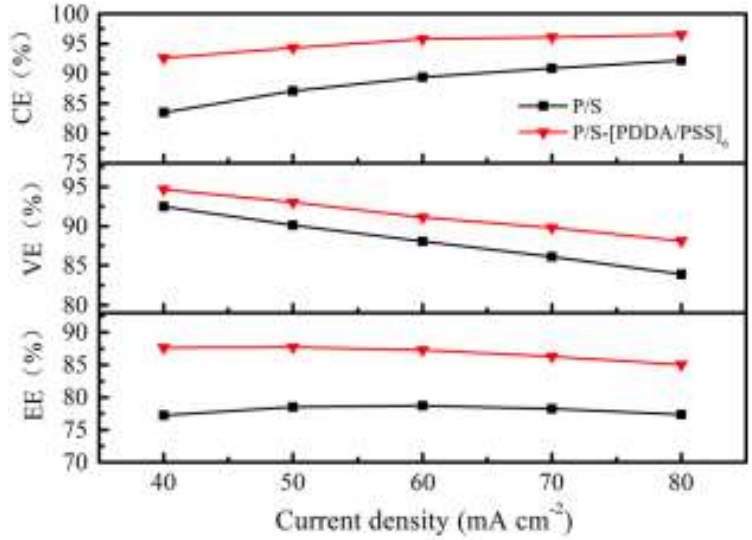

Figure 12. The performance of VRFB cells assembled with pristine PTFEE/SPEEK membrane (black lines and points) and LBL membrane with PDDA/PSS layers added [77], CE – coulombic efficiency, VE - voltage efficiency, EE – energy efficiency.

1.3. Types of membranes

Depending of the type of ionic moieties the membranes are usually classified as cation exchange membranes (CEM) and anion exchange membranes (AEM) [78]. Amphoteric ion exchange membranes (AIEM) possess both cation and anion exchange groups attached to the polymeric backbone. Membranes can be also

categorised based on the morphology into heterogeneous and homogeneous ones. Currently the most commonly used benchmarked membranes are in the form of homogeneous, dense self-supporting foil.

1.3.1. Cation exchange membrane

Cation exchange membranes have negatively charged groups such as: $-SO_3^-$, COO^-, $-PO_3^{2-}$, PO_3H^-. Due to the charge exclusion effect, they are not permeable for anions, while cations or protons can be transferred across the membranes. In the field of RFB application, the most common cation exchange groups are sulfonic moieties. The carboxylic ones are not suitable for the use in RFB as they less easily dissociate into a labile cation and immobilized negatively charged moieties.

Membranes based on fluorinated polymers with sulfonic acid moieties are so far the most studied and commonly used in RFBs, especially the series of Nafion® membrane. The outstanding chemical and mechanical stability are granted by polytetrafluoroethylene backbone polymer. The ionic transport properties are provided by pendant perfluoro vinyl ether chains terminated with sulfonic moiety. These groups are responsible for cation and proton conductivity. The ion selectivity of the perfluorinated sulfonic acid (PFSA) based membranes is attributed to the combination of two types of domains in the polymer structure: hydrophobic fluorocarbon domains and hydrophilic, ionic ones. After immersion in water solution these phases create narrow channels that transport ions. Thus, in aqueous media the membrane consists of dissolved ions imbibed in the hydrophobic (fluorocarbon) domain [79]. Figure 13 shows the separation of hydrophilic and hydrophobic domains resulting in the formation of ion-exchange channels (clusters) [80].

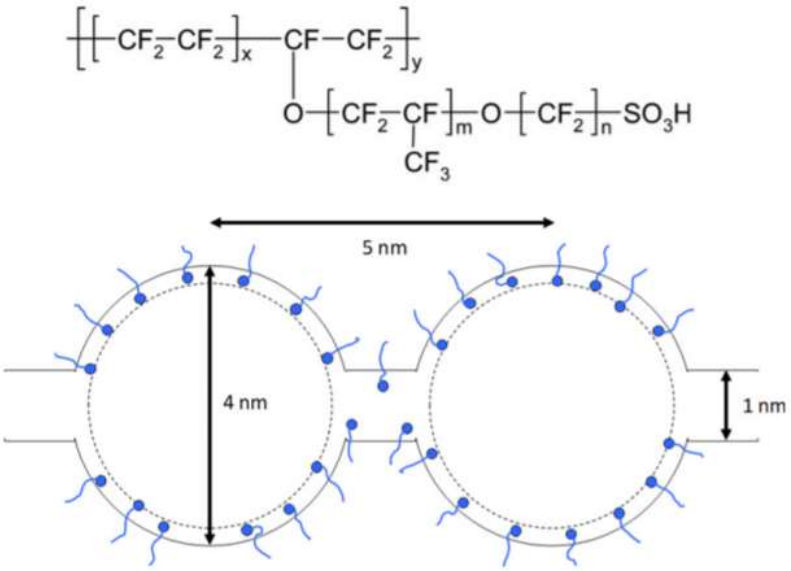

Figure 13. Structure of Nafion® and the ion-channel network model [80].

The use of fluorinated polymer and the well design balance between hydrophilic and hydrophobic domains of the ionomer result in high cost of the Nafion® membranes. Moreover, many studies report the permeation of cationic redox active species across the membrane that later leads to the capacity losses of the RFB (*e.g.* in all Vanadium system) [81,82].

Poly(vinylidene fluoride) (PVDF) is considered as a promising alternative to PFSA membrane due to its excellent chemical stability and lower cost. In order to provide ionic transport properties, a second polymer with charged groups has to be introduced. For example, poly(styrene sulfonic acid) was incorporated to the PVDF-based membrane via solution grafting method reported in the work of Luo et al. [83]. The resulting membrane showed significantly lower permeation of vanadium species in comparison to the commercial membrane - Nafion® N 117. The promising selective ion conductivity was confirmed in VRFB cycling experiment - the values of coulombic efficiency and energy efficiency were higher than in the case of Nafion® N 117 (in the range of 10 – 60 $mA.cm^{-2}$ current density). Moreover, the VRFB cell was cycled for 200 cycles showing to capacity fade and stable battery performance.

In the work of A. Rajput *et al.* [84], PVDF was used with sulfonated styrene-divinylbenzene copolymer. The newly developed proton exchange membrane contained hydrophilic channels that provided ion conductivity while the mechanical properties were granted by hydrophobic, fluorinated fraction of the IEM. The membrane was obtained *via* free radical polymerization followed by sulfonation reaction. The performance in charge-discharge tests using VRFB cell with the fabricated membrane was comparable to the results of Nafion® N 117.

Besides fluorinated or partially fluorinated polymers, the aromatic ones are considered as alternative candidates for CEMs in the RFB application. Membranes fabricated out of sulfonated aromatic polymers have gained significant scientific interest since early 2000s, owing to their lower cost, good chemical stability and high proton conductivity [81,85]. The non-fluorinated, heterochain based polymers include: poly(arylene ether ether ketone) (PEEK) [86], poly(arylene thioether) [87], poly(arylene ether ketone)s (PAEK) [88], poly(arylene ether sulfone) (PAES) [89], poly(imide)s (PI) [90], poly(phthalazinone ether)s (PPEK) [91] or polysulfone (PSU) [36] (see examples in figure 14).

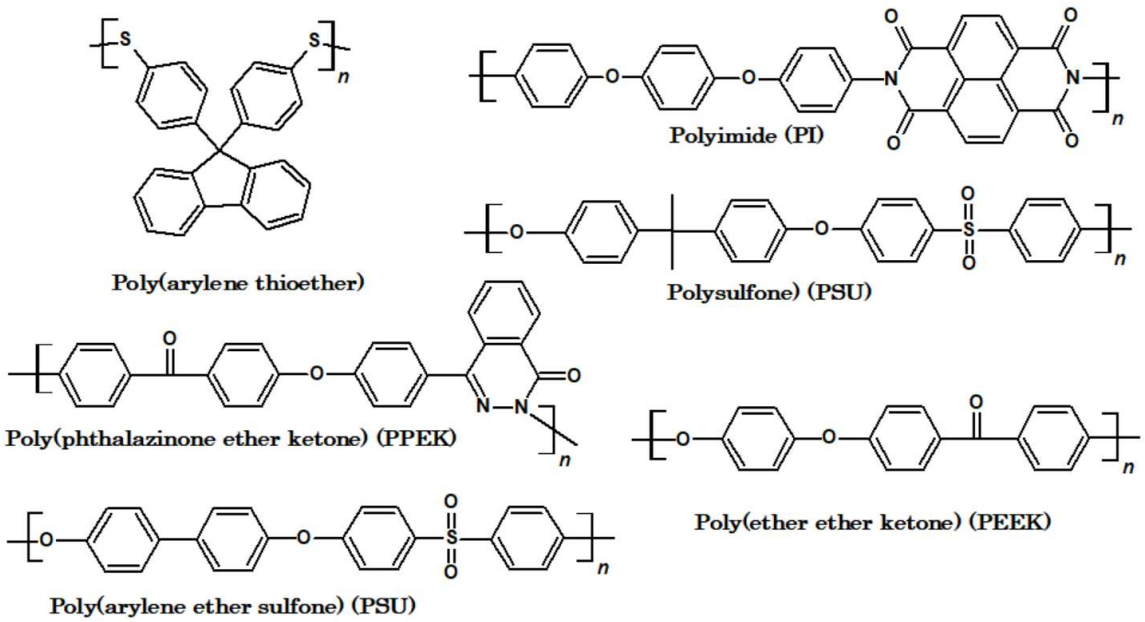

Figure 14. Examples of non-fluorinated, heterochain polymers for ion exchange membranes.

In the case of high degree of sulfonation the hydrocarbon polymers allow to exceed the ion conductivity of the commercial PFSA membranes. Nevertheless, the high amount of charged groups in the polymer backbone leads to high water uptake and swelling of the membrane resulting in insufficient mechanical stability [92]. To improve the durability of the film and maintain the high ionic conductivity, multi block copolymers were proposed. The well-designed structure of the ionomer exhibits significantly improved properties in comparison with a random copolymer. The concept is similar to the one applied in case the of Nafion® membrane, described previously. The block copolymers are formed out of highly hydrophilic sulfonated regions and highly hydrophobic non sulfonated ones. As a result, the block copolymer consists of amphiphilic blocks (figure 15) as described in the work of F. Wang *et al.* [93].

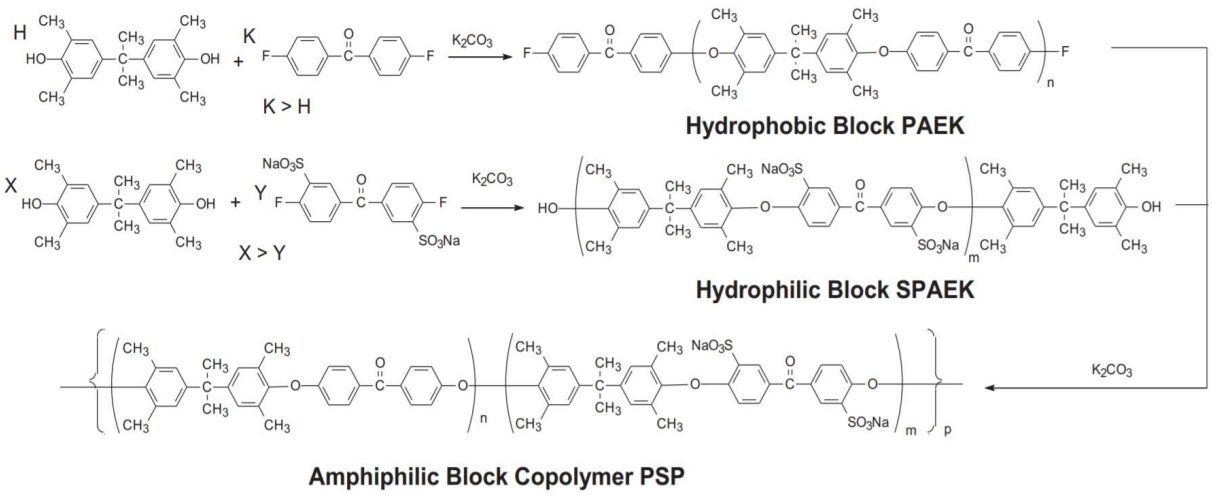

Figure 15. Scheme for synthesis of amphiphilic block copolymer reported by F. Weng [93].

The multiblock membrane exhibited lower ion conductivity than Nafion®. The SPAEK (sulfonated poly(aryletherketone)) based membranes were much stiffer and thus, exhibited good mechanical stability. Moreover, the ion selectivity was improved compared to the commercial membrane. The VRFB cycling performance of the multiblock membranes was stable and indicated higher coulombic efficiency that in the case of Nafion® membrane. However, the overall VRFB performance of the commercial IEM exceeded the results of the SPAEK based one due to lower resistivity of the Nafion® membrane that led to high voltage efficiency.

1.3.2. Anion exchange membrane

Currently, the price of the commercial cation exchange membranes is too high for a large-scale grid RFB application, where the capital cost is a key parameter. The alternative, non-fluorinated, aromatic CEMs despite their potentially low price often do not exhibit performance as good as the commercial, perfluorinated membrane because of the trade-off between ion conductivity and vanadium permeability.

In majority of RFB systems, the electroactive species are in cationic form (metal cations, organic cations) therefore, anion exchange membranes (AEMs) are considered potential candidates that can sufficiently prevent the crossover of the redox active species [94].

AEMs can significantly impede the transfer of cations through the membrane due to repelling forces (charge repulsion) caused by cationic groups bonded to the main polymeric chain. Therefore, common ions that can be transferred across the membrane in the RFB cell are limited to anions or protons. In case of the benchmark VRFB system, the possible charge carriers are SO_4^{2-} or HSO_4^- and H^+ [95].

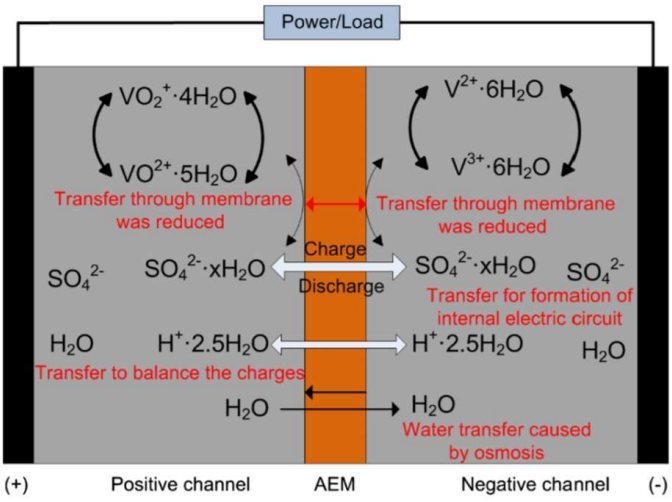

Figure 16. Illustration of the ionic transport in AEMs during operation in VRFB with sulfuric acid as supporting acid [95].

Protons can be transferred through the membrane not only due to water molecules transport and hydrogen bonded species but also because of Grotthus, hopping

mechanism [96]. The second one can occur in the case of AEM with a tertiary amine or other that can be protonated allowing the formation of a labile proton [97].

Besides the advantage of reduced crossover in majority of RFBs, AEMs offers lower costs due to its more facile fabrication and material cost in comparison to the fluorinated membranes. AEMs were applied in the first RFB system – iron-chromium RFB developed by NASA in the 1980's [98]. Later the use of AEMs in the first developed VRFB system was proposed by Maria Skyllas – Kozacos group from University of New South Wales (UNSW) [99]. Despite excellent ionic transport properties, the anion exchange membrane developed at that time suffered from insufficient chemical stability. Therefore, AEMs were later replaced by the PFSA based membranes due to their remarkable chemical stability.

The performance of AEMs in RFB stack was demonstrated in large-scale application by companies such as Sumitomo and Kashima-Kita Electric Power Corporation [100]. The membrane developed in mid-1990s by Kashima Kita Electric Power Corporation [85] was a polysulfone based anion exchange one tested in their large stack VRFB: 2 kW, 10 kW and 200 kW. The membrane exhibited stable performance over 1000 cycles reaching high values of coulombic, voltage and energy efficiencies: 93%, 86% and 80%, respectively (in 200 kW battery). The encouraging results led to the raising interest in the use of anion exchange membranes for RFBs.

Usually, the commercial AEMs are fabricated using poly(styrene) crosslinked with divinylbenzene with quaternary ammonium moiety attached to the resulting copolymer. However, to improve ionic transport properties of the membrane other classes of polymeric backbones were studied such as poly(2,6-dimethyl-1,4-phenylene oxide) (PPO) [101], 6-membered ring polyether imide [102], polysulfone [103], polybenzimidazole [104], polyether ether ketone [105] or copolymers from vinyl monomers [106,107] were investigated due to their satisfactory chemical and mechanical stability. Depending on the type of attached cationic groups the membrane can be classified into several types presented in figure 17 [95].

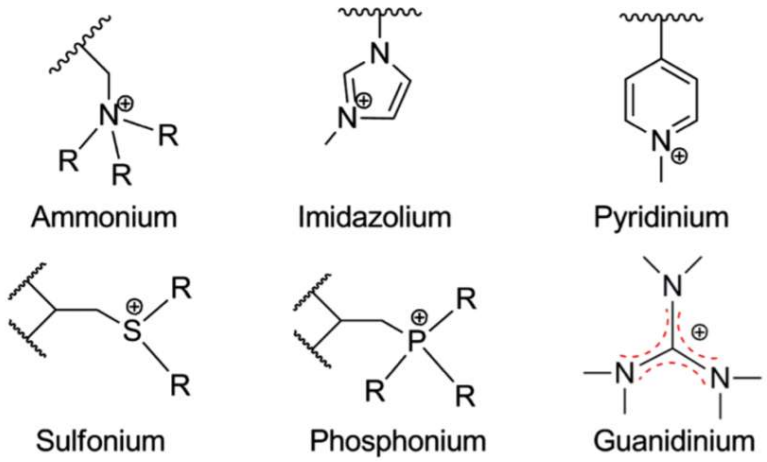

Figure 17. Cationic groups used as anion exchange moieties [95].

The most widely studied cationic groups are ammonium, phosphonium and pyridinium ones. Both sulfonium and guanidinium types of membranes do not exhibit satisfactory chemical stability in RFB environment during a long-term operation. The guanidinium moiety possess unique conjugated structure that stabilize the positive charges [108], however the alkaline nature of this groups leads to its hydrolysis in acidic conditions [109]. As a result, most of the AEMs possess quaternary ammonium groups as anion exchangers.

The ammonium groups are introduced to the polymer chain by attaching halogenated moiety followed by alkylation reaction with tertiary amine. Two similar synthetic routes are used to insert the haloalkyl group: chloromethylation, bromination or iodination The last one is considered more attractive due to shorter reaction time, lower toxicity and easier quaternarization reaction (via SN2 mechanism) since bromine is much better leaving group than chlorine [110]. This approach leads to the development of several types of quaternary AEMs with different ammonium groups starting from small aliphatic ones like trimethylamine or triethylamine [111,112] to heterocyclic amines such as N-methyl piperidine, methyl morpholine or 1.2-dimethyl imidazole [113].

An example of chemically and mechanically stable AEM was reported in Mai's work on quaternarized polysulfone based membrane for VRFBs [114]. The cell mounted with the proposed membrane achieved remarkably high coulombic efficiency – 99% and high energy efficiency – 81 % (at 80 mA.cm^{-2}). The excellent

ion selectivity was attributed to Donnan exclusion effect and rigidity of the aromatic polymer backbone which led to the reduced size of hydrophilic domains in comparison to Nafion® N 115 (used as a reference in this study).

The promising results encouraged many scientists to focus on the optimization of the anion exchange membranes performance. One of the main goals was to develop a membrane available at lower cost than the commercially available ones. Therefore, non-fluorinated, hydrocarbon polymers were preferred. To improve their chemical and mechanical stability, crosslinking of the ionomer was often proposed. In the work of M. S. Cha *et al.* [115] polysulfone based AEMs were prepared using primary diamine based crosslinkers (diaminobenzophenone) (Figure 18).

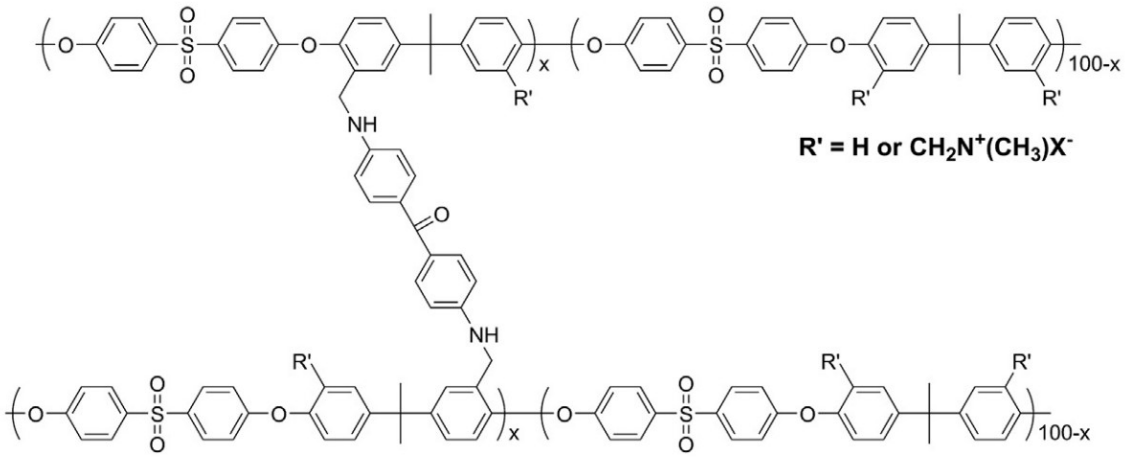

Figure 18. Chemical structure of polusulfone based AEM crosslinked by diaminobenzophenone [115].

The crosslinked membranes showed significantly improved dimensional stability and durability in comparison to a non-crosslinked ionomer. The increasing degree of crosslinking also reduced water uptake and ion exchange capacity. Following that trend, the membranes became more dimensionally stable and less permeable to vanadium cations. The ion conductivity of the crosslinked AEMs was maintained high, despite the low ion exchange capacity values. Chemical stability investigated *via* ex situ soaking tests in solution of VO_2^+ (0.1 M VO_2^+ in 5 M H_2SO_4) proved excellent chemical stability of the crosslinked membranes in the oxidative and highly acidic media. The VRFB cells assembled with the proposed AEMs (CAPSU-

2.5) exhibited outstanding performance reaching 73 % of energy efficiency at high current density (150 $mA.cm^{-2}$) exceeding the performance of Nafion® N 115 (66 %). The majority of up-to-date AEMs are fabricated out of random copolymers based on rigid aromatic backbones [116]. Those ionomers have to exhibit high ion conductivity caused by the presence of polar cationic groups, hydrophilicity of the polymer backbone or the charge delocalization. Multi-block copolymers with well-defined phase-separated, hydrophilic-hydrophobic morphology have been proposed to enhance electrochemical properties of the AEMs in a similar manner as in the case of proton exchange membranes [117,118]. Moreover, the high density of hydrophobic blocks enhances mechanical properties of the membrane, especially when is swollen or hydrated in the electrolyte [119]. The AEMs based on multi-block copolymers have been mainly reported for the use in alkaline fuel cell application [120–122] and less commonly applied in the field of flow batteries [123]. Jiangju *et al.* [124] reported AEM for the VRFBs with microscopically segregated phase morphology. The ionomer was synthesized out of quaternary ammonium poylsulfone with attached hexane side chains (C6QPSF). The performance of the C6QPSF membrane was compared with a similar quaternary membrane yet without attached hydrophobic side chains (QPSF) and two commercially available ion exchange membranes: Fumasep® FAP PP 475 and Nafion® N 212. The membrane with multiblock structure exhibited enhanced ion conductivity despite lower water uptake, compared to the random equivalent anion exchange polymer. Cycling tests in a VRFB cell showed a superior performance of the membrane with phase segregated morphology (figure 19).

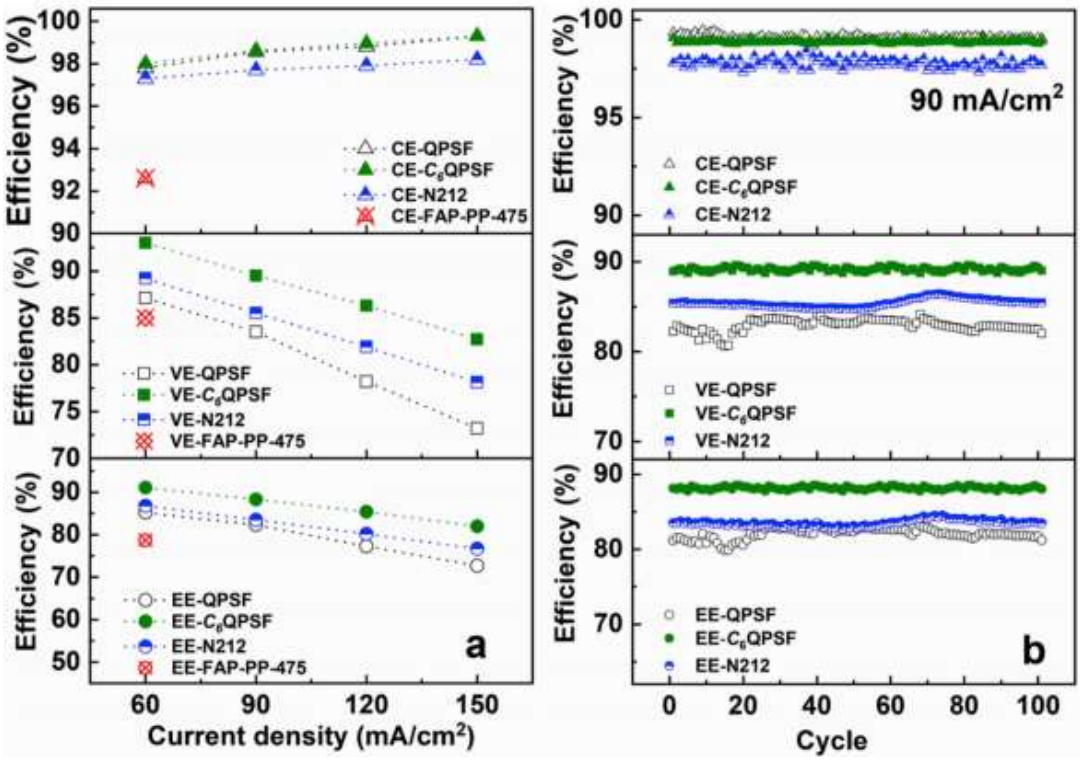

Figure 19. 4. (a) The efficiencies of VRFB cells assembled with N212, QPSF, C6QPSF, and FAP-PP-475 membranes at different current densities in the range of 60–150 mA.cm^{-2}, (b) Cycling performance at 90 mA.cm^{-2} of the VRFBs installed with QPSF, C6QPSF and N 212 [124].

The VRFBs assembled with C6QPSf exhibited the highest voltage and energy efficiency among all tested membranes. The coulombic efficiency was very close to the one of QPSF membrane. At higher current densities, the voltage efficiency was decreasing slower in the case of C6QPFS, comparing to other tested membranes. This was attributed to lower ohmic losses of the cell mounted with phase segregated AEM. The long-term cycling experiments indicated stable performance of the VRFB cell with the QC6PSF membrane. No obvious decay in coulombic, voltage or energy efficiency was evident for 100 cycles.

Currently, the benchmark anion exchange membrane are the series of Fumasep® membranes [125]. They offer lower cost in comparison to Nafion® membrane, but often exhibits higher resistance and unsatisfactory long-term stability leading to compromised overall cycling performance of a flow battery.

1.3.3. Membranes with both cation and anion exchange groups

T. Mohammadi *et al.* [126] compared the performance of VRFB assembled with cation exchange membrane and anion exchange membrane. It was concluded that AEMs usually offer the advantage of remarkably low crossover of the vanadium species across the membrane. In parallel, the CEMs typically exhibit improved ion conductivity and thus, allow for a high voltage efficiency of the battery. In order to find the trade-off between those two trends, Mohammadi and Maria Skyllas-Kozacos [99] proposed to introduce cation exchange groups (anionic moieties) into the anion exchange membrane that possess cationic groups (Selemion AMV and Selemion type 2, Asahi Glass Japan). Subsequently in 2003 Sukkar *et al.* [25] proposed incorporation of anion exchange groups into cation exchange membrane. The resulting membranes can be considered as an amphoteric ion exchange membrane (AIEM) that possess both positively and negatively charged groups. Historically, Sollner firstly developed the amphoteric membrane in 1932 [127] describing a membrane with both weak acidic and weak basic moieties in its chemical structure.

Recently, there are several strategies to obtain the membranes that exhibits cation and anion exchange properties. The simplest method of their fabrication is blending two different ionomers (cationic and anionic). J. Kerres *et al.* [128] proposed acid – base blend membrane based on sulfonated PEEK or PSU (acidic polymer) and poly(4-vinylpyridine), polybenzimidazole or aminated PSU (basic polymer). The acidic and basic polymers were ionically crosslinked by the interaction between *N*-containing group and sulfonic acid group. In the work of S. Liu *et al.* [129] SPEEK was blended with polyimide (PI) – a commercially available polymer that exhibits satisfactory chemical stability and high ion conductivity. The occurring ionic interaction between SPEEK and PI is demonstrated in figure 20.

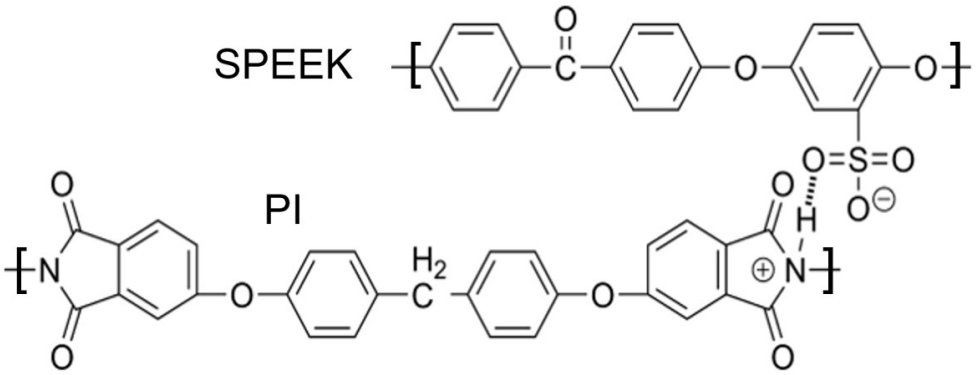

Figure 20. Schematic of the ionic interaction between PI and SPEEK [129].

The proposed SPEEK/ PI blend membranes exhibited excellent tensile strength and dimensional stability. The ionic transport properties were dependent on the ratio between polyetherimide and SPEEK. The characterization study performed in conditions of VRFB environment showed excellent proton conductivity of the blend membrane, granted by the presence of ionic channels formed by sulfonic acid groups. In parallel, the vanadium permeation was remarkably low due to the Donnan exclusion effect.

Another strategy to form an AIEM is to attach functional groups to the same side chain. Therefore, high anion exchange capacity is possible without affecting cation exchange capacity, contrarily to the blend membranes. For example, Yan *et al.* [130] proposed to use inexpensive sulfonated aromatic polymer (polysulfone) with amphoteric side-chain that consists of methyl imidazolium moiety and sulfonic moieties (figure 21).

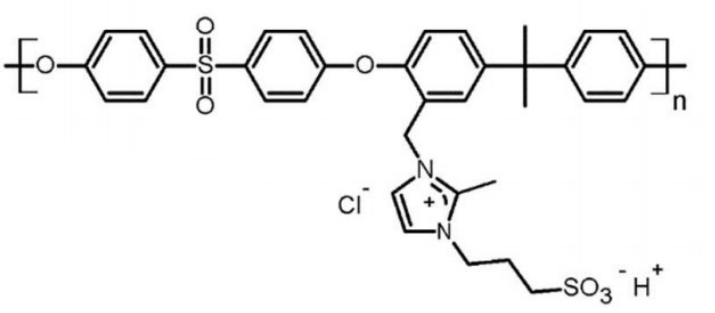

Figure 21. Structure of amphoteric-side-chain polymer [130].

The resulting ionomer exhibited cation exchange capacity (2.02 mmol g^{-1}) and relatively low swelling ratio. Thus, its vanadium permeability was over 25 times lower in comparison to Nafion@ N 212. The VRFB cell assembled with the fabricated membrane reached high coulombic efficiency (98.9 %) and energy efficiency (77%) at high applied current density (200 $mA.cm^{-2}$). Moreover, after 200 cycling no visible signs of capacity fade were observed.

Alternatively, the cationic and anionic moieties can be attached to different side chains of the ionomer. The performance of such membrane can be tailored by changing the content of the component with one of the functional groups. Therefore, the cation exchange capacity and anion exchange capacity can be independently changed [131]. Qiu *et al.* reported a novel poly(ethylene-co-tetrafluoroethylene) (ETFE) based AIEM. The membrane was fabricated in a two-step radiation induced grafting process resulting in ETFE based film with grafted sulfonated styrene and dimethylaminoethylmethacrylate (DMAEMA) figure 22.

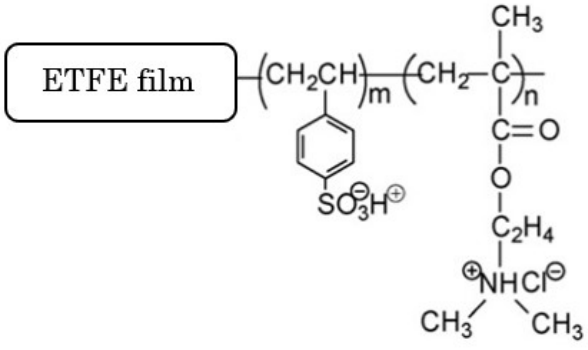

Figure 22. Schematic of the chemical structure of the AIEM [131].

The proposed AIEM shown excellent perm-selectivity, that led to higher coulombic efficiency (95.6% at 40 $mA.cm^{-2}$) of VRFB cell in comparison to the cell mounted

with Nafion® N 117 membrane (87.9 %). However, the ion conductivity was lower than the one of the commercial membranes resulting in lower voltage efficiency (78.6 % vs 82.6%) reached by the cell assembled with the AIEM. Nevertheless, the energy efficiency of the VRFB cell with presented membrane was reported as slightly higher (75.1% vs 72.6%) than in the case of using the commercial membrane.

In the work of J. Liao *et al.* [132] the amphoteric membrane was prepared using the similar approach. Both types of functional groups were attached to different side chains. The membrane was prepared from fluoro-methyl sulfonated poly(arylene ether ketone-co-benzimidazole) and demonstrated promising performance in energy storage application. The VRFB cell mounted with the fabricated AIEM achieved voltage efficiency close to the one of Nafion® N 117 and significantly improved coulombic efficiency. The overall energy efficiency at 70 $mA.cm^{-2}$ reached the value of 75 %, exceeding the performance of the commercial Nafion® membrane. Moreover, the *ex*-situ chemical study confirmed excellent resistivity to oxidation degradation of the proposed AIEMs.

1.3.4. Porous separator

The symmetric types of RFB systems such as all vanadium [133], all iron [134] or copper based RFB [135] the same element is used in both positive and negative electrolyte. As a result, the crossover of the redox-active species does not lead to irreversible contamination of electrolytes. Therefore, the porous separators can be considered as a potential low-cost alternative to the ion-exchange membranes.

The porous membranes do not exhibit any charged moieties however, depending on their pore size, such separators have size-exclusive properties. Nowadays commercially available membranes are classified as: microfiltration membranes (pore size: 10 – 0.1 μm), ultrafiltration membrane (pore size: 100 – 2 nm) and nanofiltration membranes (pore size: 2 – 0.5 nm) [136]. The size exclusive properties of porous separator can provide satisfactory coulombic efficiency and prevent capacity losses in the case of batteries in which the redox active species are made of large molecules for examples polymers. Such species are employed in polymer-based redox flow batteries. Figure 23 shows a schematic principle of the

size exclusion phenomena happening while using the porous membrane in the polymer-based RFB.

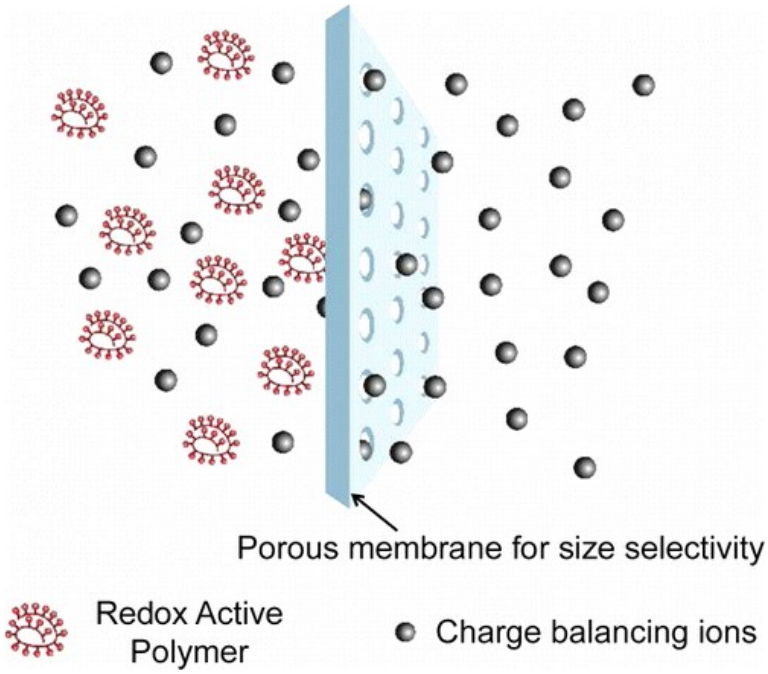

Figure 23. Schematic of size exclusion-based selectivity of porous separator applied in polymer RFB [137].

For example, commercial porous membrane Celgard® 2400 (pore size: 21.5 nm) and Celgard 2325 (pore size:14 nm) were proposed to prevent the cross-over of polymer redox active species: poly(vinylbenzylethylviologen) derivatives in a non-aqueous organic RFB system [137]. The rejection of polymer active species was increasing with higher molecular weight of the specie and with lower pore size of the membrane. 93 % of the polymer electrolyte was rejected using Celgard® 2400. Ultrafiltration membrane were also applied in aqueous polymer RFB system proposed by T. Janoschka *et al.* [138]. The solutions of polymers containing TEMPO (2,2,6,6-tetramethylpiperidinyloxy) radical and 4,4'-bipyridine derivatives (viologen) were used as catholyte and anolyte, respectively. Separation of those two electrolytes was provided by a simple cellulose base dialysis membrane.

Due to the significantly lower cost in comparison to IEMs, many studies were focused on the use of porous separator in other RFB systems, including VRFBs. Zhang *et al.* [139] proposed polyacrylonitrile (PAN) or polysulfone/sulfonated poly(ether ether ketone) (PSF/SPEEK) blend membranes fabricated using phase

inversion method. The pore size distribution was controlled by changing the concentration of polymer. The porous separators allowed to reach even 95 % of coulombic efficiency and 76% of energy efficiency in VRFB cell during charge-discharge test at 80 mA.cm^{-2}. In order to further improve the coulombic efficiency of the porous membrane, silica particles were incorporated into the polymer matrix in order to reduce the pore size of the separator [140] (figure 24).

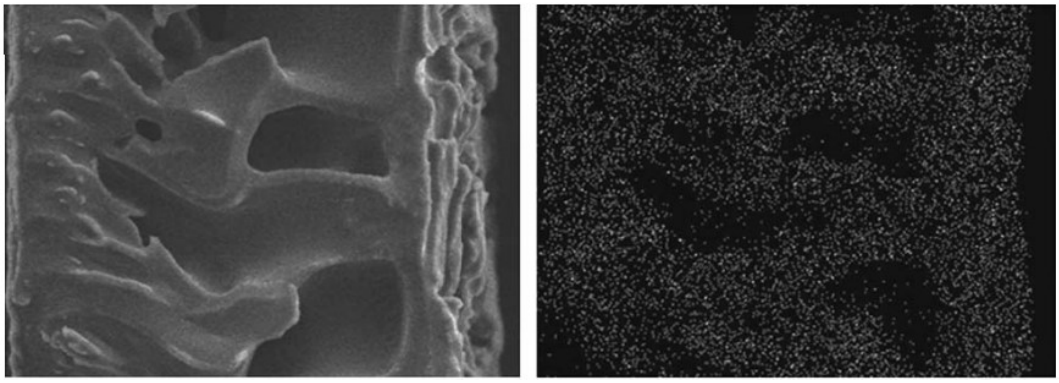

Figure 24. The EDS image of silica modified PAN membrane (left – cross-section of porous membrane, right – EDS of Si element) [140].

SiO_2 was introduced to nanofiltration PAN membrane by in situ hydrolysis of tetraethylorthosilicate (TEOS). The resulting membrane exhibited decreased permeability to vanadium and in parallel, the incorporated nanoparticles of silica facilitated proton conductivity. The enhanced conductivity was attributed to the increased absorption of sulfuric acid into the membrane. As a result, the membranes modified with silica shown improved proton/vanadium selectivity reaching 98% of coulombic efficiency during charge-discharge test in the VRFB cell. At 80 mA.cm^{-2}, the cell demonstrated excellent energy efficiency (79%) proving that PAN/silica-based membrane can be considered a lower cost alternative to the commercial ion exchange membrane.

Xiaoling Wei *et al.* [141] proposed the use of commercially available poly(vinyl chloride) (PVC)/silica- based porous separator (Amer-sil, Kehlen, Luxembourg) for the application in VRFBs. The porous membrane was a 400 μm thick separator with average pore size of 45 nm. The VRFB cell equipped with PVC/silica membrane exhibited average energy efficiency of 79 % and coulombic efficiency of 90 %. Especially at high applied current densities (above 100 mA.cm^{-2}) the energy

efficiencies were becoming very close to the one achieved using Nafion® N 115 membrane (figure 25).

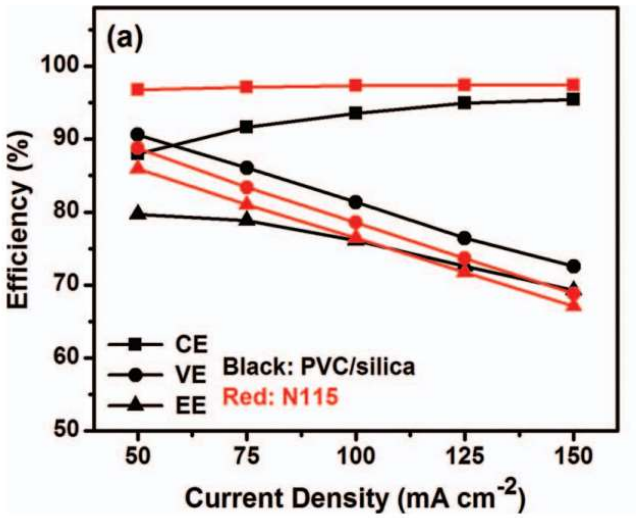

Figure 25. Efficiencies achieved by the VRFB cell using PVC/silica separator and Nafion® N 115 [141].

The ohmic losses of the cell are increasing with higher applied current, significantly deteriorating the overall battery performance. Therefore, the less resistive membrane (in this study the porous separator) became the better performing one and its excellent voltage efficiency can compensate for the slightly lower coulombic efficiency.

1.3.5. Composite membranes

Besides the most commonly used dense, self-supported IEMs, other alternatives are composite membranes that offer a unique ability to independently control ionic transport properties and mechanical stability. Among different types of the composite IEMs three main categories can be distinguished:

- pore-filled membranes
- layered membranes
- membranes with inorganic fillers.

1.3.5.1. Pore-filled membranes

At the early stage of the RFBs development (in particular the all vanadium RFBs), Mohammadi and Skyllas – Kozacos [142] proposed a composite membrane prepared by the incorporation of anion exchange resin – Amerlite® CG 400 into the pores of a commercial Daramic porous separator. The ion exchange resin was further crosslinked with divinylbenzene to ensure high density of the ionomer and thus, limit the permeation of the vanadium species. The VRFB cell with the composite membrane exhibited energy efficiency of 85 % at 20 $mA.cm^{-2}$. The membrane was also tested in a long-term cycling experiment (700 cycles – 4000 h) at 40 $mA.cm^{-2}$ resulting in average energy efficiency of the cell - 75 %. The cycling results were reported as comparable to the one of commercial ion exchange membrane – Selemion® CMV (Asahi Glass Co., Japan). This concept of pore-filled membranes (PFM) is one of the most common strategies to fabricate a composite IEM. In general, the polyelectrolyte is introduced to the pores of substrate (figure 26).

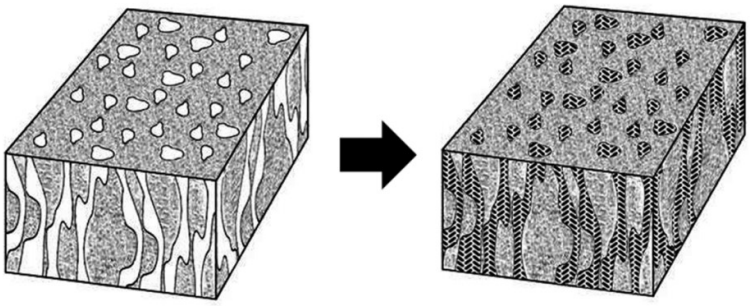

Figure 26. The schematic of the pore-filled membrane concept [143].

PFMs are known to exhibit excellent dimensional and chemical stability granted by the tough porous substrate [144]. The chemically robust substrate can be fabricated using such polymers as polyethylene (PE) [145], polypropylene (PP) [146], poly(tetrafluoroethylene) (PTFE) [147], polyacrylonitrile (PAN) [148], poly(ether sulfone) (PES) [149] or polyimide (PI) [150]. Besides organic porous substrates, also inorganic ones, such as porous alumina [151] were proposed. The pore size distribution is more uniform in the case of inorganic substrate and the size of pores can be smaller in comparison to polymeric porous materials, leading to improved selectivity of the membrane.

The most facile method to obtain PFM is pouring the ionomer solution on the surface of the porous substrate or immersion of the substrate in the solution of the ion exchange material [152]. The ionomer penetrates the pores and subsequently the usually volatile solvent is evaporated. Typically, high concentration of ionomer with sufficiently viscosity is preferred to secure retaining the polyelectrolyte inside the pores. Often, the process is repeated to improve membrane quality and avoid possible defects. In the work of Y. Oshiba *et al.* [153] a proton exchange membrane was prepared using perfluorosulfonic acid (PFSA) polymer as ionomer and a mechanically robust, porous ultra-high molecular weight polyethylene (UHMWPE) substrate (Teijin Limited) for the use in fuel cells. The solution of PFSA ionomer was applied on UHMWPE substrate followed by drying the membrane at 100 °C for 13.5 h. The porous separator used as a mechanical reinforcement limited the excessive swelling of the PFSA ionomer. In parallel, the high content of ionic groups in PFSA granted high proton conductivity of the PFM. Similar methodology of was presented by Y. Ahn *et al.* [147]. A sulfonated poly(arylene ether ketone) (SPAEK) was incorporated into the pores of PTFE porous substrate. The PTFE support was hydrophilized chemically to facilitate the ion transfer across the membrane. The composite membrane exhibited significantly improved mechanical stability and decreased vanadium permeability in comparison to a pristine SPAEK membrane.

Another method to fabricate a PFM is to impregnate the pores of substrate with a mixture of monomers and their *in-situ* polymerization inside the pores. In this case the ion exchange polymer was reported as a crosslinked copolymer (figure 27 [81]).

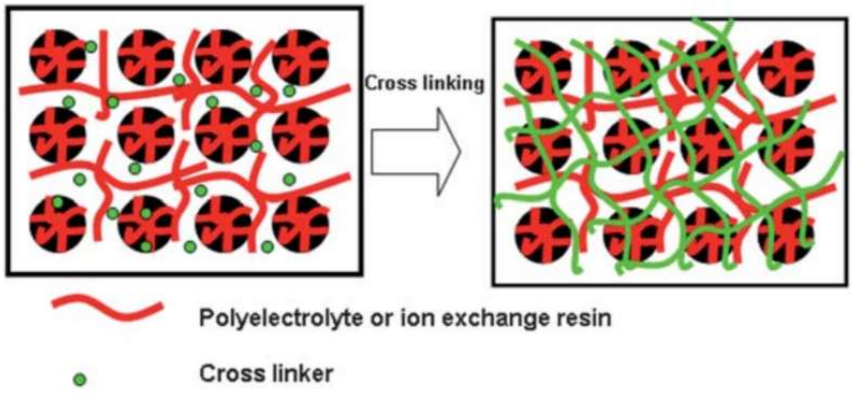

Figure 27. Schematic of the preparation of crosslinked pore-filled membrane, figure adapted from [81].

Miyake *et al.* [154] proposed to use a mixture of divinylbenzene (crosslinker), 4-vinylpyridine and 1-vinyl imidazole as precursors of anion-exchange copolymer. A PTFE porous film was impregnated with the precursors mixture and subsequently exposed to a UV irradiation. Thus, the precursors underwent a free-radical polymerization resulting in a crosslinked ionomer.

The anion exchange group can be introduced to the PFM either by the use of monomer or polymer possessing such a functional group, or by later chemical modification of the polymeric membrane. Maurya *et al.*, [155] presented the fabrication of an anion-exchange PFM by the immersion of porous PE film (Celgard® a battery separator with a thickness of 20 µm and 40–50% porosity) into the solution of non-ion selective monomers (divinylbenzene, 4-vinylbenzene chloride and thermal initiator benzoyl peroxide). After the polymerization the resulting copolymer was quaternized using different amines (Trimethylamine (TMA), triethylamine (TEA), 1,4-diazabicyclo[2.2.2]octane (DABCO), N,N,N,N-tetramethylethylenediamine (TMEDA), tris(2,4,6-trimethoxyphenyl)-phosphine (TTMPP). The composite PFM quaternized with TEA was tested in a non- aqueous $V(acac)_3$ RFB showing encouraging voltage efficiency of 95.7 % and 58.7 % energy efficiency at low current density (0.1 $mA.cm^{-2}$).

The performance of the membrane can be changed by modifying the crosslinking degree of the ionomer as well as by the hydrophilic properties of the porous substrate. D.H. Kim and M. S. Kang [156] reported PFMs prepared using porous PTFE film of a different hydrophilicity impregnated with a mixture of *N,N'*-dimethylaminoethyl methacrylate and divinylbenzene. The monomers were polymerized via photo-induced radical polymerization followed by simultaneous quaternarization and crosslinking reaction using *p*-xylylene dichloride (figure 28).

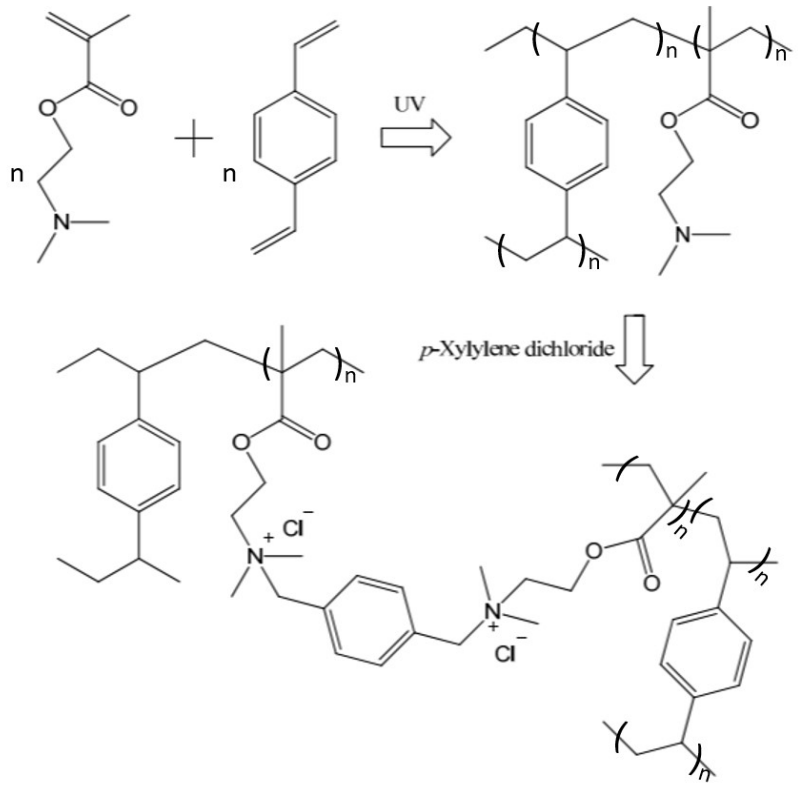

Figure 28. Schematic of the synthesis of anion-exchange polymer with quaternary ammonium moieties crosslinked by divinylbenzene and *p*-xylylene dichloride [156].

The resulting polymer had a double crosslinked structure owing to the use of divinylbenzene and *p*-xylylene dichloride. The crosslinking degree of the PFMs was controlled by varying the content of divinylbenzene. The optimal amount of divinylbenzene was indicated as 10 wt.%, higher contents of crosslinker led to the rapid increase of ASR. The use of less hydrophilic PTFE porous substrate was concluded as more desirable in VRFB application since higher energy efficiency was achieved using such membrane that in the case of a membrane fabricated with more hydrophilic substrate (86.9 % versus 83.0 %, current density – 20 $mA.cm^{-2}$). The improved performance of the cell assembled with more hydrophobic membrane's substrate was attributed to the higher coulombic (97.2 % versus 90.9 %) that compensated slightly lower voltage efficiency (89.4 % versus 91.3 %). Chemical stability tests carried out in a 0.1 M V_2O_5 solution in 5 M H_2SO_4 at 40 °C for 200 h indicated signs of the membrane oxidative degradation. Nevertheless,

comparing to commercial anion exchange membrane (Neosepta® AMX Astom Corp., Tokyo, Japan), the rate of oxidation was significantly reduced.

1.3.5.2. Heterogenous, layered membranes

Another type of the composite membranes is those in which two (or more) layers can be distinguished. Typically, they consist of the initial membrane (porous or ion exchange) whose surface is modified by the application of an additional material in order improve the membrane performance. Several methods have been developed to introduce new thin layer on the membrane surface [157] such as: solution casting, *in situ* polymerization, electrodeposition or spin coating. Figure 29 shows schematic illustration of most commonly applied technique for the modification of base membrane surface.

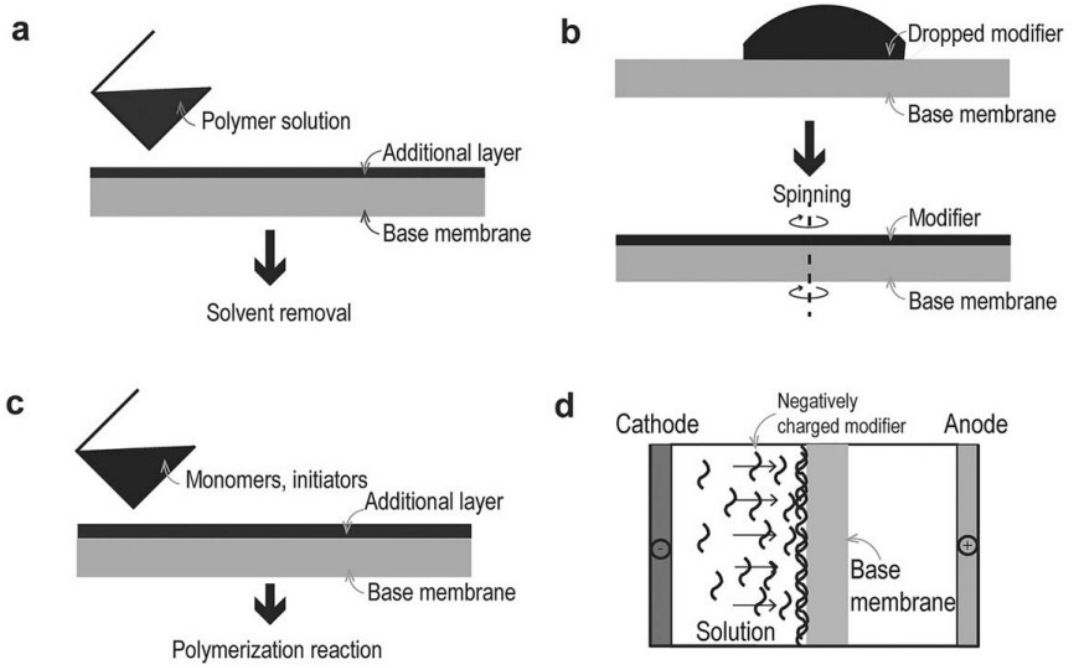

Figure 29. Schematic representation of (a) solution casting, (b) spin-coating, (c) in-situ polymerization and (d) electrodeposition , adopted from [157].

Qingtao Luo *et al.* [158] proposed to coat the surface of Nafion® N 117 with a PEI-based polyelectrolyte. The additional layer was introduced *via* interfacial polymerization of the amino reach ionomer – polyethyleneimine (PEI). Moreover, the Nafion® N 117 was modified by introducing chlorosulfonyl groups to improve adhesion to PEI. Applying the anion-exchange layer led to a decreased permeation

of cationic species (vanadium). Consequently, a VRFB cell with the composite, layered membrane achieved higher coulombic efficiency in comparison to the pristine Nafion® N 117 (96.2% versus 93.8 %). However, both ion exchange capacity and proton conductivity of the composite membranes were reduced in comparison to Nafion® N 117. Thus, the voltage efficiency was lower (88.4 %) than in case of the commercial membrane (90.7 %). As a result, the overall cell performance achieved using the composite membrane was matching the performance of Nafion® N 117 (energy efficiency 85.1 % and 85.0 %, respectively).

To reduce the material cost of the IEM, non-fluorinated polymers were also investigated as an alternative polymer for the composite, layered membranes.

Study of Jia *et al.* [159] proposed a novel multi-layered membrane consisting of polypropylene membrane sandwiched between two layers of SPEEK/ tungstophosphoric acid [159]. The SEM pictures of the multi-layered membrane's cross-section clearly indicated a hierarchical structure of the membrane (figure 30).

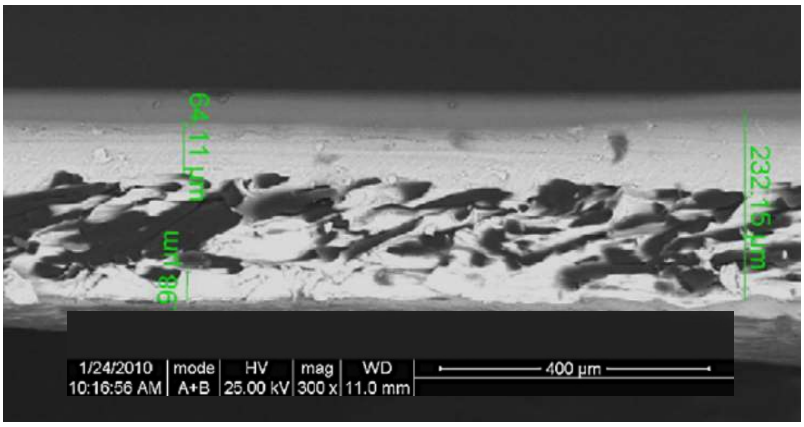

Figure 30. SEM image of the cross-section of the sandwich type, hierarchical membrane [159].

The newly developed, sandwich type membrane exhibited significantly lower permeability to vanadium species in comparison to commercial membrane (Nafion® N 212). A VRFB single cell employing the composite membrane achieved higher coulombic and energy efficiency that in the case of Nafion® N 212. The rate of self-discharge was also lower than in case of cell with Nafion® N 212. A long-

term charge-discharge test carried out at 35.7 mA.cm^{-2} indicated stable cycling performance of a VRFB cell with the membrane throughout 80 cycles (> 350 h). Upon completing this test, no decrease in voltage, coulombic or energy efficiency was observed. W. Lee *et al.* [160] proposed a polybenzimidazole (PBI) layer applied on a porous poly(vinylidene difluoride) (PVDF) substrate. PBI has been indicated as a promising ionomer for the use in RFBs [161–163]. The imidazole groups undergo protonation in contact with acidic electrolyte while the sulfuric acid molecules are absorbed by hydrogen interactions. As a result, the polymer became proton and sulphate conducting ionomer. The open porous structure of PVDF support facilitated absorption of electrolyte into the pores. Furthermore, the substrate exhibited good chemical stability and sufficient adhesion to PBI thin ion selective layer. The composite membrane was prepared by spray-coating technique using 1 wt.% of PBI solution in 2.5% KOH/ethanol. The performance tests carried out in a VRFB three-cell stack shows that the composite PVDF/PBI membrane allowed to achieve higher energy and coulombic efficiency than with a commercial membrane Nafion® N 117 (figure 31).

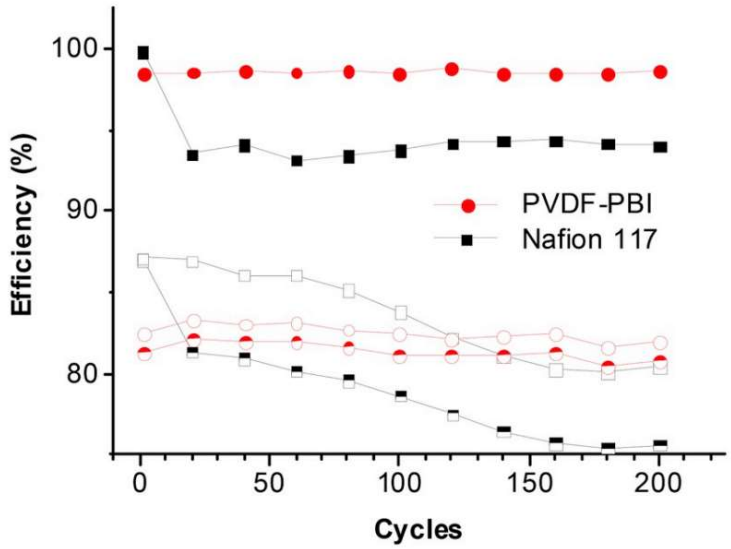

Figure 31. Coulombic (full symbols), voltage (empty symbols) and energy efficiency half-filled symbols) for a three-cell stack, 60 mA.cm^{-2} [160].

Moreover, the study also demonstrated a significant impact on the orientation of the PBI layer in the cell. The lowest capacity fade was achieved in the case of having the ion exchange layer exposed towards the positive electrolyte.

1.3.5.3. Membranes with inorganic fillers

Another category of composite membranes is the one consisting of ion-exchange polymer and inorganic fillers. Wang *et al.* proposed a sulfonated poly(phthalazinone ether ketone) SPPEK/ WO_3 hybrid membrane prepared by a hydrothermal reaction [164]. The role of the inorganic particles was to improve proton conductivity of the membrane as the hydrated WO_3 particles can form a proton conducting channels. The results of a cycling experiment performed in a single cell VRFB showed stable performances of the hybrid membrane during 100 cycles. Moreover, the VRFB cell with the SPPEK/WO_3 membrane exhibited lower self-discharge rate and increased coulombic and energy efficiency, compared with commercial membrane (Nafion® N 212). Inorganic nanofillers can be also used to enhance ion selectivity and chemical stability of the ion exchange membrane. For example, the incorporation of silica or titanium oxide nanoparticles into SPEEK [76,105] resulted in decreased vanadium permeation across the membrane and improved stability, compared to the pristine SPEEK membrane.

Nano-fillers were also incorporated to the anion exchange membrane to enhance the stability of the membrane. Those nanofillers include metal oxide [165]. Vinodh *et al.* [166] investigated the influence of different nano-scale metal oxides on the ion transport properties of anion exchange membrane. The composite membranes were fabricated from quaternarized polystyrene-b-poly(ethylene-r-butylene)-b-polystyrene and quaternarized polysulfone by incorporation of SiO_2, TiO_2 and ZrO_2 nanoparticles (size: 10-15 nm). Although water uptake and ion conductivity increased in the composite membranes, the ion selectivity was also improved. The results were attributed to the higher number of water molecules absorbed by the composite membranes that facilitated the ion

transfer while ionic channels became partially blocked by the nanoparticles.

Besides the incorporation of metal-oxides, graphene oxides are becoming promising nanofillers for IEMs. Dai Wenjing *et al.* [167] proposed nanocomposite SPEEK/graphene oxide membrane prepared by solution casting for the application in VRFB. The study showed that increasing the content of incorporated graphene oxide improved mechanical and thermal stability of the membrane, while the permeation of VO^{2+} is reduced. The incorporation of graphene oxide nanosheets in

the membrane resulted in the formation of a barrier that effectively hindered the transfer of vanadium species across the membrane (figure 32).

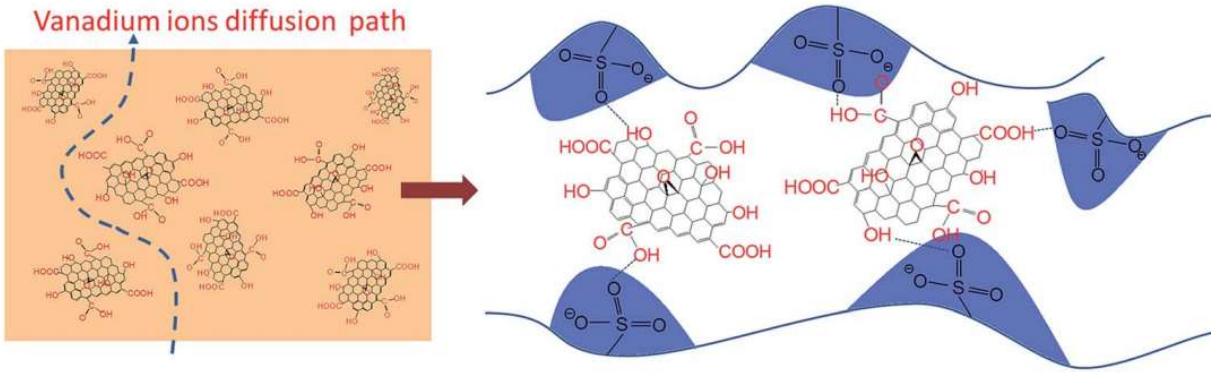

Figure 32. Proposed mechanism of vanadium ion migration in SPEEK/ graphene oxide composite membrane [167].

The membranes performances were evaluated in a VRFB cycling experiment. The cell assembled with the SPEEK/ graphene oxide membrane demonstrated an improved performance and higher efficiencies, compared to a commercial proton exchange membrane (Nafion® N 117). To enhance the long-term cycle stability, SPEEK/GO membrane was incorporated into the pores of PTFE based porous sheet resulting in a pore-filled type IEM. The cell assembled with the SPEEK/ graphene oxide -PTFE membrane exhibited high coulombic efficiency (99%) almost constant for over 1200 cycles with relatively low-capacity losses [167]. The effect of incorporated graphene oxide nanosheets on the membrane properties such as proton conductivity, permeability, swelling ration and single battery performance (in VRFB) was also studied for polysulfone - polyvinylpyrrolidone (PSF-PVP) composite membranes [168]. In previous work of Wu Chunxiao *et al.* [169] a novel PSF – PVP membrane was proposed. PSF served as a mechanical reinforcement, while PVP was providing proton conductivity. The composite membrane with GO nanosheets exhibited improved ion selectivity and mechanical stability, compared to the PSF-PVP without nanofillers. The charge-discharge experiments in VRFB cell showed a significantly lower rate of self-discharge (figure 31 a) using the PSF-PVP/ graphene oxide membrane as well as improved coulombic and energy efficiency (figure 33 b).

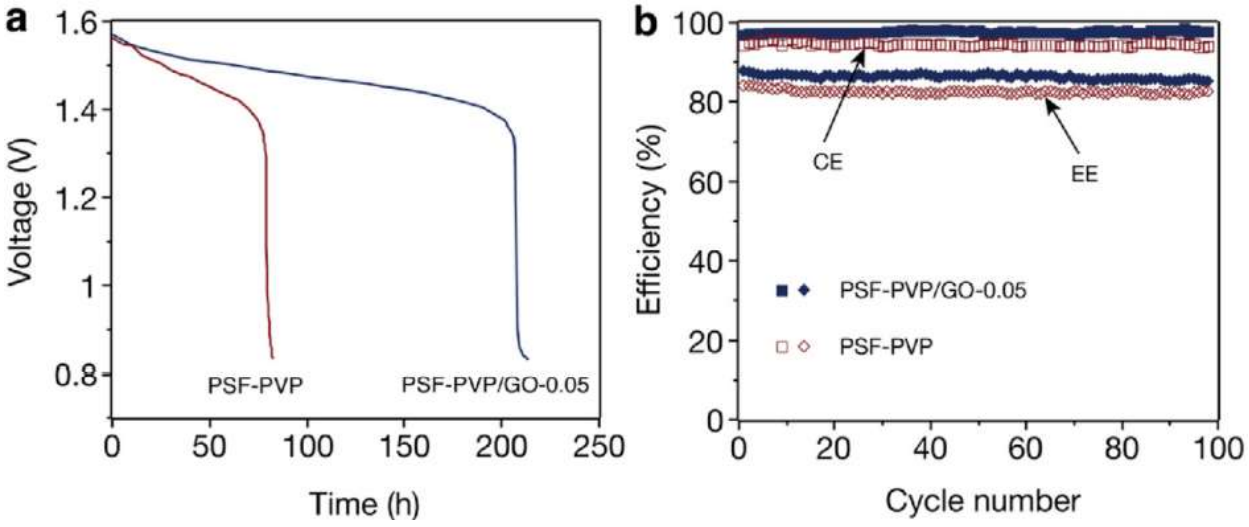

Figure 33.a) Self discharge experiment: open-circuit voltage in function of time and b) battery cycle performance of PSF-PVP/graphene oxide (GO) membrane in comparison to the pristine PVP-PSF membrane (CE: coulombic efficiency, EE: energy efficiency) [169].

The graphene oxide based nanofillers can also undergo chemical modification allowing to tune the properties of the material after their incorporation. In the work of G. Shukla and V.K. Shahi [170] the nanosheets of graphene oxide were alkylated and bonded to poly(ether sulfone) by 1,4-diazabicyclo[2,2,2]octane (DABCO). The resulting ionomer possessed a high number of amino, functional groups. Therefore, the membrane exhibits excellent ion conductivity. In parallel, the incorporation of quaternized graphene oxide led to the formation of ion pathway because of phase separation between hydrophobic and hydrophilic part of the membrane. In addition, the presented AEMs exhibited improved chemical stability in acidic and oxidative condition, owing to the resulting steric hindrance in the membrane, which limits the attack of oxidative species. The results of charge-discharge experiment carried out in VRFB indicated good performance of the membrane since at 60 $mA.cm^{-2}$ the cell with the composite membrane achieved higher efficiencies (coulombic (98.06%), energy (76.4%), and voltage (78.0%)) than those for Nafion® N 117 membrane.

1.4. Conclusions and positioning of the thesis

The presented literature study describes comprehensive list of methods for fabrication ion exchange membranes and porous membranes as well as an extensive comparison of different chemistries and material that are used to obtain IEMs. Those methods range from solvent casting of a functional material, commercially available alone or together with a second polymer to form a blend membrane or well-design, complex synthetic routes leading to a multi-block ionomer of with organized structure with hydrophilic and hydrophobic domains. The most commonly used membrane, particularly in RFBs, are in a form of dense, self-supported membranes. In VRFBs, the chemical stability remains as a very challenging issue due to the highly acidic (2 – 3 M sulfuric acid) and oxidative electrolyte (1.5 – 2 M concentration of V^{2+} in case of charged negative electrolyte). Thus, the benchmark membranes such as Nafion® of Fumasep® are prepared out of fluorinated polymers. As a result, the cost of IEMs suitable for VRFBs remains high and impedes further widespread use of this technology. In order to overcome this limitation, many efforts were taken towards the development of a lower cost IEM by changing the membrane structure into a heterogeneous one – a composite IEM. Recently, there is a growing scientific interest in this type of membranes, which are considered as a flexible platform that can allows reaching the trade-off between material/fabrication cost and the membrane's performance.

Considering the literature study, it can be concluded that wide variety of methods and synthetic procedures for the preparation of IEMs has been reported. During designing and preparing of a suitable membrane for the application in RFBs, the specific requirements of the IEM have to be considered. Those are related to the role of the membrane in RFBs: separation of the redox active species and in parallel, permeation of the balancing, charge carrying ions. Another important criterion is the dimensional and chemical stability of the membrane. Lastly, the membrane should be available at relatively low cost in order to diminish the total cost of RFB stack to boost their commercialization. Therefore, this thesis presents a composite AEM prepared in an industrially oriented process consisting of blade-coating and in-situ radical polymerization (UV-curing). Both of

these techniques allow for facile possible future scaling up of the membrane. The membranes were prepared by applying a layer of UV-curable mixture of ionomer's precursors on top of a mechanically robust porous substrate. This allowed broadening the range of possible ion-exchange polymers to those that do not exhibit filmogenic properties and lack mechanical durability. Depending on the ion-exchange layer formulation different approaches are described in this thesis showing the evolution of the membrane in terms of improving ion-transport properties of the composite membranes, long-term performance in VRFB and chemical stability.

Chapter 2 – Material and methods

2.1. Materials

The reagents used for the fabrication of ion-exchange coating layers and their suppliers' details are listed in Table 2. PVC-Silica porous substrates with median pore size 80 nm, volume porosity 63.7 %, and an average thickness of 600 μm were produced internally at Amer-Sil SA, Luxembourg. Commercially available homogeneous IEMs – Fumasep® FAP 450 – AEM (Fumatech GmbH, Germany) and Nafion® N 115 - CEM (Chemours, USA) - were purchased at Fuel Cell Store Inc., USA and used for performance comparison. *N,N*-Diallylpiperidinium chloride (DAPCl) was kindly provided by Misgina Tilahun Tsehaye (University of Grenoble, aboratoire d'Electrochimie et de Physicochimie des Matériaux et des Interfaces, synthesis described by Tilahun M.T. *et al* [171]

Table 2. Chemical reagents, acronyms and supplier details.

Name	Acronym	Supplier
(Vinylbenzyl)trimethylammonium chloride	VBTC	Merck (Sigma Aldrich Chemical Co
Allyl bromide		Alfa Aesar
Allyl chloride		Alfa Aesar
Biphenyl peroxide	BPO	Merck (Sigma Aldrich Chemical Co)
Chlorobenzene	PhCl	Merck (Sigma Aldrich Chemical Co)
Diphenyl(2,4,6-trimethyl benzoyl)phosphine oxide	TPO	Hock chemicals GmbH
Hexafunctional polyester acrylate resin - Ebecryl 830	EBE830	Allnex B.V.
Hydroxy-2-methyl-1-phenylpropanone	Omnirad 1173	IGM Resins B.V.
Irgacure® 500 (50 % 1-Hydroxy-cyclohexyl-phenyl-ketone, 50 % Benzophenone)	I500	Ciba Specialty Chemicals
N,N'-Methylenebis(acrylamide)	MBAAM	Merck (Sigma Aldrich Chemical Co)
N,N-dimethylacetamide	DMAc	Merck (Sigma Aldrich Chemical Co)
N-[3-(Dimethylamino)propyl]methacrylamide	DMEA	Merck (Sigma Aldrich Chemical Co)
N-allylpiperidine		Merck (Sigma Aldrich Chemical Co

N-bromosuccinimide	NBS	Merck (Sigma Aldrich Chemical Co)
N-Hydroxyethyl acrylamide	HEAA	Merck (Sigma Aldrich Chemical Co)
Poly(2,6-dimethyl-1,4-phenylene oxide) (20 kDa, polydyspersity~2.5)	PPO	PolySciences, Inc
Poly(acrylic acid) (1250 kDa)	PAA	Merck (Sigma Aldrich Chemical Co)
Poly(vinyl pyrrolidone) (50 kDa)	PVP	BTC Chemical Distribution

2.2. Synthesis of polymers

2.2.1. Bromination of poly(2,6-dimethyl-1,4-phenylene oxide)

The bromination reaction was adapted from the protocol reported by Willdorf-Cohen e*t al.* [112]. PPO (15.0 g, 125 mmol structural units) was slowly stirred and heated up to 136 °C in 300 mL of chlorobenzene until it was dissolved. Then, BPO (1.6 g, 6.6 mmol) and NBS (16.7 g, 94 mmol) were added to the solution that was stirred at reflux for another 5 h. After that, the reaction mixture was cooled down to room temperature. The product was precipitated by pouring it into a 5-fold excess of methanol and stirred for 24 h. The brominated PPO (Br-PPO) was filtered and washed several times with methanol. To eliminate the residual impurities, the polymer was reprecipitated from chlorobenzene/methanol. The product in a form of white powder, was dried under vacuum at 50 °C for 24 h. ^{1}H NMR spectroscopy (Bruker Avance 400 spectrometer) confirmed that 25% of the methylated groups were brominated: (400 Hz, DMSO), δ (ppm): 2.09 (s, 9H), 4.34 (s, 2H), 6.47-6.452 (d, 2H), 6.67-6.71 (m, 2H) (figure 34). The yield of the reaction was 72%, the mass of collected polymer: 14.4 g.

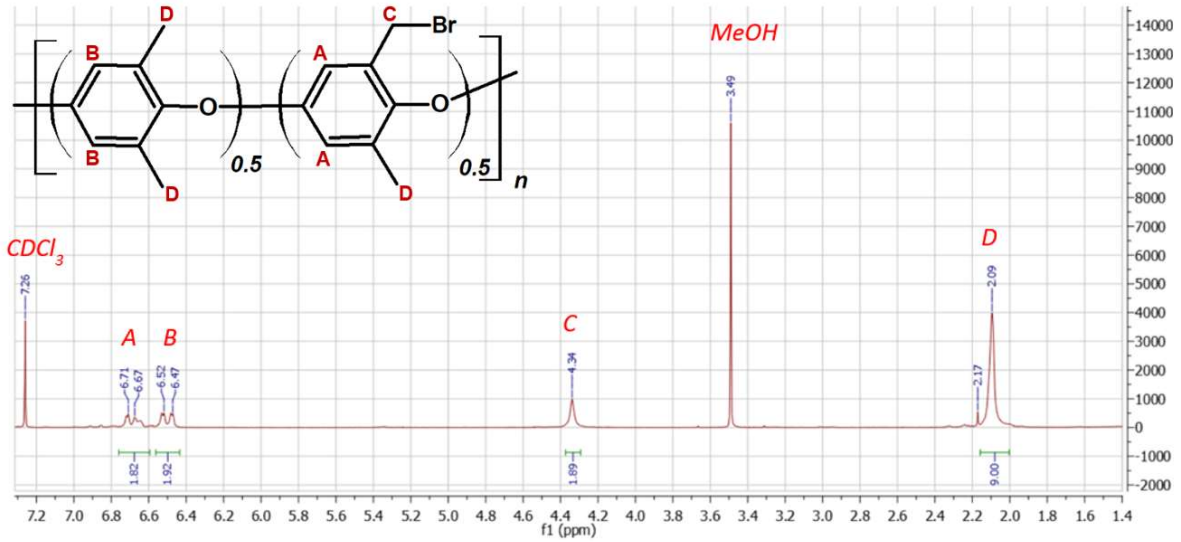

Figure 34. ^{1}H NMR spectrum of brominated PPO (Bruker Avance 400 spectrometer).

2.2.2. Synthesis of *N*-vinyl imidazole functionalized PPO (VIMPPO)

N-vinyl imidazole (10.2 mL, 112 mmol) was added dropwise to the solution of Br-PPO (12 g, ca. 37 mmol of brominated structural units) in 300 mL of *N, N*-dimethylacetamide. The reaction was stirred at 30 °C for 48 h. The product was then precipitated by pouring into a 5-fold excess of diethyl ether and stirred overnight. The polymer was recovered by filtration and washed several times with diethyl ether. The powder was dried under a vacuum for 24 h at 30 °C. The substitution of $-CH_2Br$ groups with *N*-vinyl imidazole was complete as proven with ^{1}H NMR spectrum: (400 Hz, DMSO), δ (ppm): 2.06 (m, 9H), 5.37(m, 3H), 5.91 (t, 1H), 6.47 (d, 2H), 6.72 (s, 1H), 6.93 (m, 1H), 7.22-7.33 (m, 2H), 7.77 -7.98 (m, 1H), 8.11-8.18 (m, 1H) (figure 35). The yield of the reaction reached 88% (mass: 13.5 g)

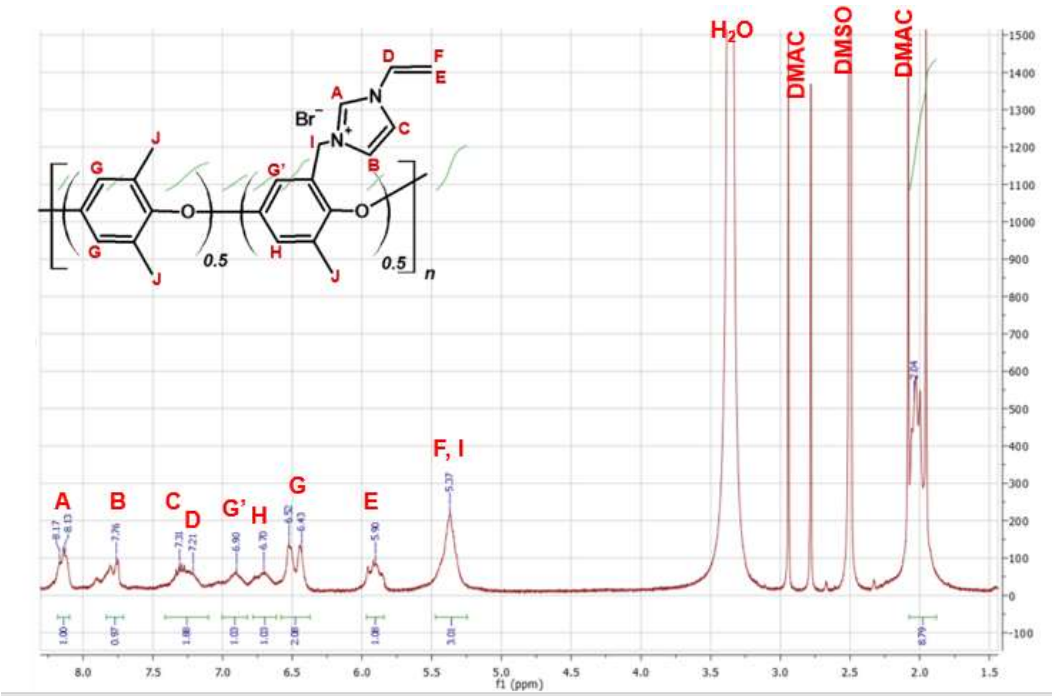

Figure 35. ^{1}H NMR Spectra of *N*-vinylimidazolium PPO (VIMPPO) (Bruker Avance 400 spectrometer).

2.3. Methods

2.3.1. Fabrication

The fabrication process of the hierarchical membranes is limited to three steps in which low-cost reagents are formulated, applied on the substrate and rapidly cured under UV light (figure 36).

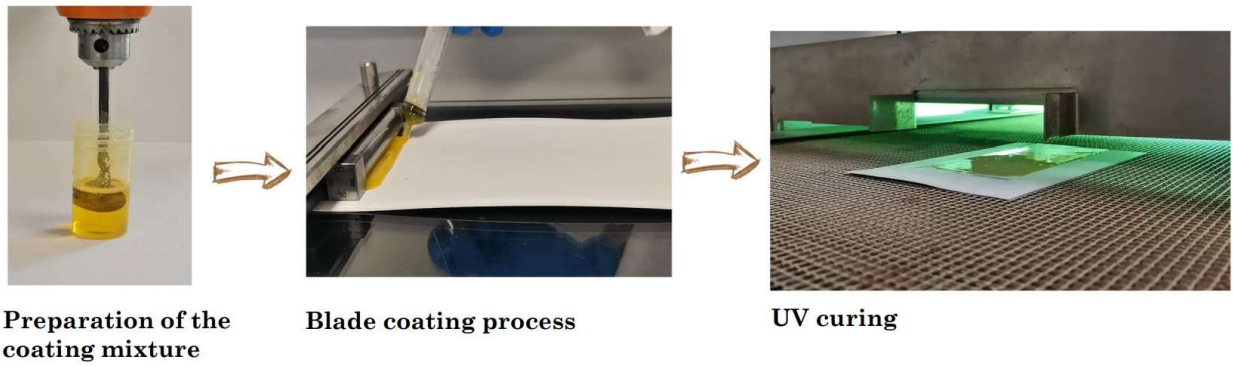

Figure 36. Representative images of the fabrication's steps: mixing the precursors (left), applying the mixture using blade coating technique (middle) and exposure of the coated substrate to UV irradiation.

To prepare the ion exchange coating formulation, the liquid precursors for anion-exchange polymer were mixed together and all the solid-state reagents were dissolved either in the solution of reactive monomers and sonicated at moderate temperature (40 °C, 1 - 3 hour). In the case of using VIMPPO, the polymer was firstly dissolved in small amount of methanol (60 % concentration solution) and then added to the remaining monomers. In case of low viscosity formulation, 0.5-1 wt. % of rheology modifier such as poly(acrylic acid) (PAA) was added. Having a highly viscous precursors mixture was particularly desired since such mixtures do not impregnate into the porous substrate. Therefore, a layer only on top of the substrate could be obtained with limited penetration into the pore of substrate. The uncured formulation was applied on the porous substrate by means of blade coating using an applicator with gap of 60 µm and an automatic driver (BYK GmbH, Germany). In the final step the coating was cured (by radical polymerization (radical curing) under UV irradiation (UV conveyor Jenton International Ltd, UK) equipped with a 2000 W Fe doped Hg UV lamp (365 nm). The curing step took 1 – 1.5 min and was performed under no inert gas at room temperature. Figure 35 represents schematic curing step performed for the composite membranes fabricated using acrylamides and PVP (chapter 37).

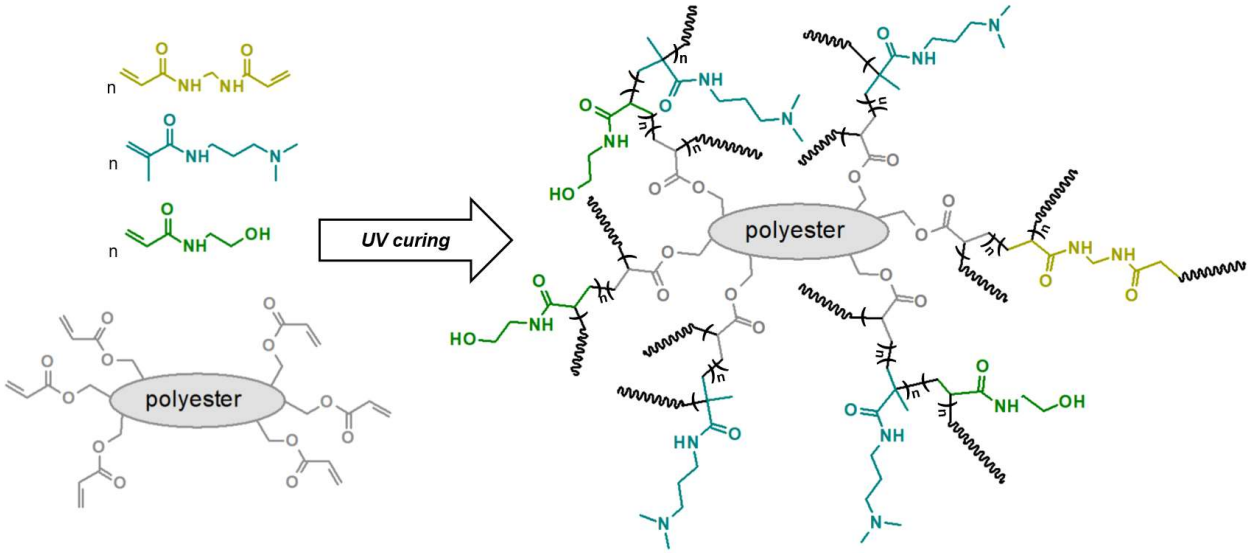

Figure 37. Schematic depiction of the UV curing step performed for a formulation based on acrylamides and acrylic oligomer (acrylated polyester).

2.3.2. Morphology characterization

Surface and cross-section morphologies of the fabricated membranes were investigated using a scanning electron microscopy SEM (JSM IT500HR, JEOL, Japan) coupled with energy-dispersive X-ray spectroscopy (EDS, SDD Ultim Max 170 Standard, Oxford Instruments, UK; software – AzrecLive). EDS was used to assess the elemental composition of the coating surface and to examine the cross-section of the composite membranes with particular focus on the interphase between the anion-exchange coating and the porous support. To avoid deformation of the membranes, structure the samples were cut in in liquid nitrogen and coated with approximately 5 nm of Au on their surface.

2.3.3. Ionic transport properties: water uptake, area-specific resistivity, ion-exchange capacity and permeability

2.3.3.1. Water uptake

The water uptake (WU) of the anion-exchange layers was determined as previously reported [172,173] according to Equation (1):

$$WU = \frac{W_W - W_D}{W_D} \cdot 100\% \quad (1)$$

Where W_W and W_D represent the mass of the layer under wet and dry conditions, respectively. It should be noted, that for this test anion-exchange layers were coated on poly(tetrafluoroethylene) (PTFE) sheets and UV cured, without a porous substrate to avoid the contribution of the substrate to the water sorption. Freshly prepared anion-exchange films were immersed in deionized water for 24 h. Before measurement, the excess water on the film surface was wiped off using absorbent paper.

2.3.3.2. Area-specific resistance

The area-specific resistance (ASR) of the membranes was measured in a standard 1 M HCl aqueous solution. The acidic environment was selected for consistency with the later use of the membrane in acidic VRFB electrolyte. The difference between sulfuric and hydrochloric acid conductivity may manifest in exact values of ASR but is not expected to impact the classification of membranes from most to

least conductive. The current was driven from 0 to 1 A (polarization curves) while recording the cross-membrane voltage (scan rate 10 mA.s^{-1}), using an Origaflex 05A (Origalys SAS, France) potentiostat. A custom-made cell (figure 38) with the geometric active surface area (A) of the membrane of 19.63 cm^2 was used. Before the test, membranes were equilibrated in the electrolyte solution for 24 h. The ASR of the membrane was determined as the difference between the cell's resistance with and without the membrane ($R_{with\ membrane}$, $R_{without\ membrane,\ respectively}$), following equation (2):

$$ASR = (R_{wit\ \ membrane} - R_{without\ membrane}) \cdot A \qquad (2)$$

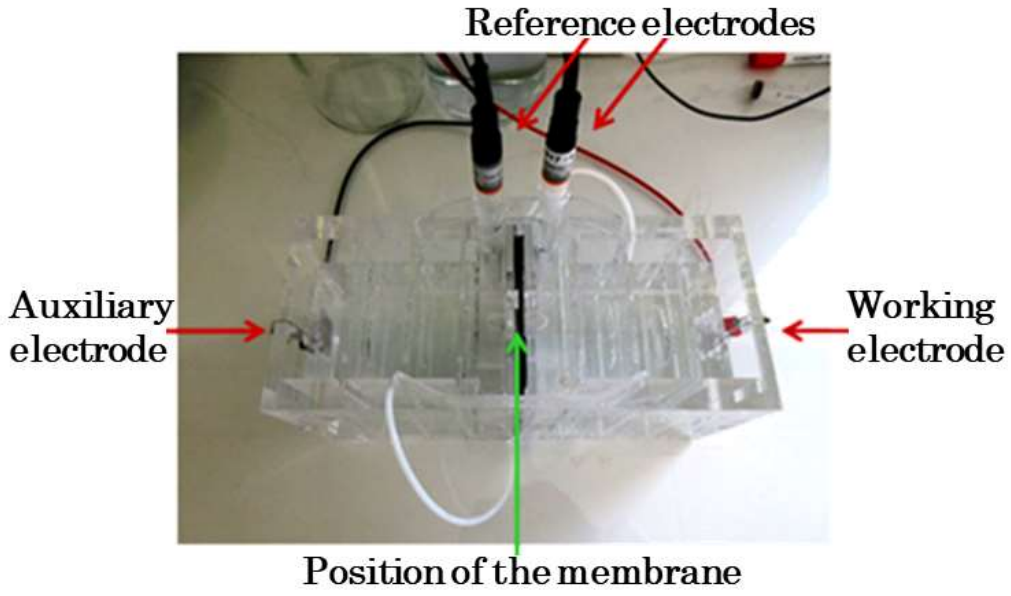

Figure 38. Custom-made cell used for measuring area-specific resistivity of the membranes.

2.3.3.3. Permeability to vanadium species

In VRFB one of the key roles of the IEM is to prevent the crossover of vanadium species such as VO_2^+, VO^{2+}, V^{2+} and V^{3+} between the positive and negative electrolyte. In literature, VO^{2+} is commonly used as a model, stable vanadium cation allowing to assess the permeability of membrane in an ex-situ experiment and thus, gain indication of the membrane's performance in terms of self-discharge and coulombic efficiency in later RFB cell operation [173,174].

The permeability of vanadium ions (VO^{2+}) across the membrane was observed using a diffusion cell. The cell was divided into two compartments (half cells) by the membrane (active area 19.63 cm^2). One of the half-cells (feeding) was filled with 200 mL of 0.15 M vanadyl sulphate ($VOSO_4$) in 3 M H_2SO_4. The other half-cell (receiving) contained 200 mL of 0.15 M magnesium sulphate ($MgSO_4$) in 3 M H_2SO_4 to compensate for osmotic pressure. The number of vanadium ions (VO^{2+}) that permeated across the membrane into the receiving solution was monitored over time by recording UV-vis spectra (Thermo Scientific™ Evolution 60S UV-visible spectrophotometer).

2.3.4. Performance testing in VRFB cell

2.3.4.1. Charge-discharge experiments

For cycling performance testing, the VRFB single cell was assembled with two pieces of thermally activated carbon felt electrodes (48 h at 400 °C, 50 mm × 40 mm × 4.6 mm). 60 mL of commercial electrolyte was used for anolyte and the same volume for catholyte (120 ml in total, vanadium electrolyte solution, Gesellschaft für Elektrometallurgie GmbH, Nürnberg, Germany containing 0.8 M VOSO4/0.8 M $V_2(SO_4)_3$ in 2 M H_2SO_4 and 0.05 M H_3PO_4) were circulated at the flow rate of 40 $mL.min^{-1}$. The negative electrolyte was kept under nitrogen to prevent undesired oxidation of V^{2+}. The cycling tests were carried out using Origalys potentiostat, at constant current densities of 20 $mA.cm^{-2}$, 50 $mA.cm^{-2}$ and 80 $mA.cm^{-2}$. The upper and lower limits of the charge/discharge voltage were set at 1.75 and 0.80 V, respectively. The coulombic efficiency (CE), energy efficiency (EE) and voltage efficiency (VE) of the membrane were calculated based on equation (3), (4) and (5):

$$CE(\%) = \frac{\int I_d \, dt}{\int I_c \, dt} \cdot 100\ \% \tag{3}$$

$$EE(\%) = \frac{\int V_d \, I_d \, dt}{\int V_c I_c \, dt} \cdot 100\ \% \tag{4}$$

$$VE(\%) = \frac{EE}{CE} \cdot 100\ \% \tag{5}$$

Where I_d and I_c stand for the discharging and charging current, respectively, while V_d and V_c are discharging and charging voltages.

2.3.4.2. Self-discharge experiment

To observe the crossover of vanadium species in an RFB device, open-circuit voltage (OCV) of the charged VRFB cell (after a complete charge up to 1.7 V) was observed until the voltage of the cell decreased below 0.8 V. The cell was filled with a total amount of 20 mL of vanadium electrolyte, recirculated with a flow rate of 40 $mL.min^{-1}$. The volume of electrolyte was reduced compared to cycling experiments in order to limit the batteries electrical capacity and obtain the discharge results in a shorter period of time. The drop of the OCV of the cell was directly related to the diffusion of the vanadium ions at various oxidation states across the membrane separating the two half-cells resulting in the self-discharge reactions.

2.3.4.3. Ex-situ chemical stability in VO_2^+

The chemical stability of the membrane was evaluated by immersing a specimen (3 cm by 0.5 cm, mass of the samples: VIMPPO_10% - 0.076, VIMPPO_15% - 0.081 g, VIMP-PO_20% - 0.079 g) in 8 ml of solution of vanadium (VO_2^+) in sulfuric acid at room temperature. A commercial vanadium electrolyte (Gesellschaft für Elektrometallurgie GmbH, Nürnberg, Germany containing 0.8 M $VOSO_4$/0.8 M $V_2(SO_4)_3$ in 2 M H_2SO_4 and 0.05 M H_3PO_4) was used to obtain the solution of VO_2^+ by charging it in the VRFB cell to 1.7 V and holding the voltage until the current dropped down to 10 mA. After that, the catholyte was used as a source of oxidative species for testing the stability of the membranes. Before the immersion, the membranes were washed in deionized water to remove the possibly remaining unreacted initiator or solvent. The VO^{2+} cations resulting from VO_2^+ reduction accompanying membrane oxidative degradation were detected using UV-vis spectroscopy. After the chemical stability tests, the cross-sections of the membranes were observed under SEM (JEOL IT500HR).

The next three chapters of the thesis describe the different concepts of the composite AEM fabricated and studied for the use in redox flow batteries. Depending on the chemistry of ion-exchange coating, three approaches can be distinguished:

- Composite anion exchange membranes fabricated by coating and UV crosslinking of PVP/ acrylamide layer on top of porous substrate (chapter 3)
- Composite anion exchange membrane fabricated by UV curing of polyacrylamides and poly(2,6-dimethyl-1,4-phenylene oxide) modified with *N*-vinylimidazole (VIMPPO) (chapter 4)
- Photocured VIMPPO-based anion exchange composite membranes: Study of the spacing monomer nature on the properties of the AEMs (chapter 5).

Chapter 3. Composite anion exchange membranes fabricated by coating and UV crosslinking of PVP/ acrylamide layer on top of porous substrate

3.1. Formulation concept

The anion exchange coatings were fabricated using a water-soluble polymer – poly(vinyl pyrrolidone) (PVP). PVP is a commodity reagent, widely used as a hydrophilic polymer in the preparation and modification of filtration membranes [175,176] or as a precursor for ion exchange membranes fabrication. In recent works, membrane containing PVP were positively tested for the application in VRFBs [169,177]. In highly acidic conditions the pyrrolidone segments can be protonated, facilitating ion conductivity and reducing vanadium permeation due to a positive charge [178]. In this study, PVP was immobilized in a densely crosslinked matrix to create a semi-interpenetrating polymer network (sIPN). Radically reactive anion exchange precursors were used to form the sIPN matrix in order to contribute to the ion transport properties of the coating layer. The crosslinked matrix allowed to control the swelling of PVP while keeping the coating hydrophilic and conductive. Figure 39 qualitatively illustrates the structure of the coating layer (figure 39a) and a fragment of possibly obtained crosslinked matrix (figure 39b).

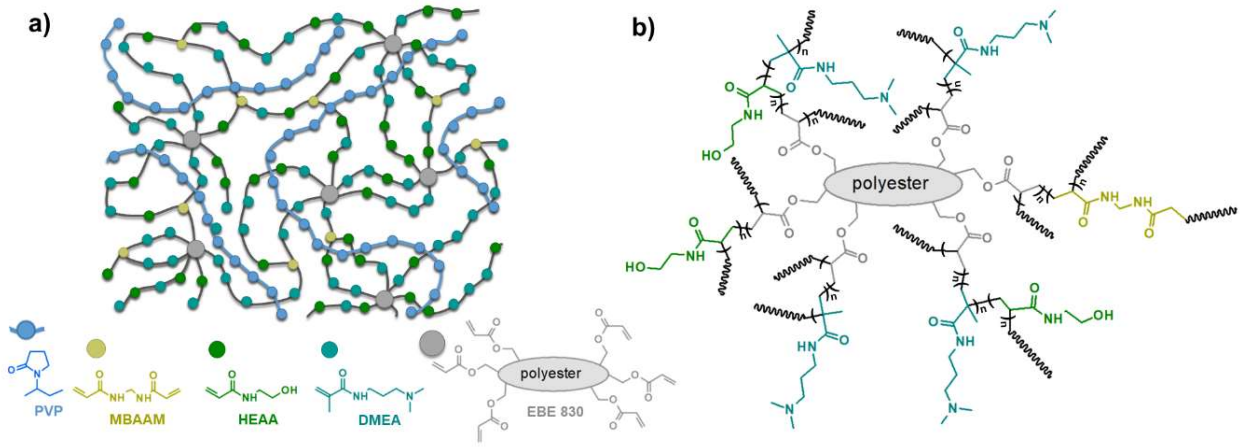

Figure 39. (**a**) A diagrammatic depiction of the obtained sIPN layer of the anion exchange membrane and (**b**) a fragment of UV-cured matrix with the chemical structures of the used compounds.

Membranes with different PVP/matrix ratios were fabricated in order to investigate the effect of the PVP content on the membrane ion transport properties and performance in vanadium redox flow batteries (VRFBs).

3.2. Fabrication and morphology study of the PVP/acrylamide-based composite AEM

Ion exchange layers were successfully fabricated on top of the porous PVC-Silica substrate with PVP content in the coating layer ranging from 6 wt.% up to 16 wt. % (Table 3).

Table 3. Ratio of the compounds used in individual formulation.

	PVP [g]	DMEA [g]	HEAA [g]	MBAAM [g]	EBE830 [g]	I500 [g]
PVP_6%	0.85	6.3	3	0.75	2.2	0.4
PVP_8%	1.1	6.3	3	0.75	2.2	0.4
PVP_11%	1.6	6.2	3	0.75	2.2	0.4
PVP_14%	2.1	6.3	3	0.75	2.3	0.4
PVP_16%	2.5	6.3	3	0.75	2.4	0.4

The water-soluble PVP was immobilized in a UV-cured polymeric matrix formulated of monomeric acrylamides and acrylate resin. Upon curing, the obtained polymer adopts sIPN crosslinked structure due to the use of bifunctional and hexafunctional radically reactive compounds (MBAAM and MBAAM). The UV cured matrix was dense enough to hold up to 16 wt.% of PVP, which otherwise would be soluble in water. Membranes with greater content of PVP were not obtained as the coating dissolved or formed gel flakes in contact with water. Membranes with a PVP content below 6 wt.% could not be prepared as the viscosity of the formulation became too low, and it would soak into the porous substrate before curing.

The dimensional stability of the AEMs was granted by the porous substrate that served as a mechanical reinforcement. The mechanical properties such as tensile

strength are in significant majority provided by the substrate and only a minor contribution of the coating layer can be observed (table 4).

Table 4. Mechanical properties of the composite anion-exchange membrane (wet form) and uncoated porous separator (wet form): tensile strength test.

	Maximum force stress [N]	
	Sample 1	Sample 2
Substrate	33.15	32.67
PVP_8% (coated membrane)	35.13	34.89
PVP_14% (coated membrane)	35.96	36.34

The role of the PVP in the coating layer was to secure high hydrophilicity of the layer, proper viscosity that allows coating the porous substrate without impregnating the substrate and finally contribute to the ion-exchange capacity in acidic media (such as VRFB electrolyte). Fourier Transform Infrared Spectroscopy (FTIR) spectra recorded for PVP dissolved PVP dissolved in 2 M sulfuric acid demonstrated a noticeable peak at 1045 cm^{-1} indicating possible protonation of pyrrolidone segments (figure 40)

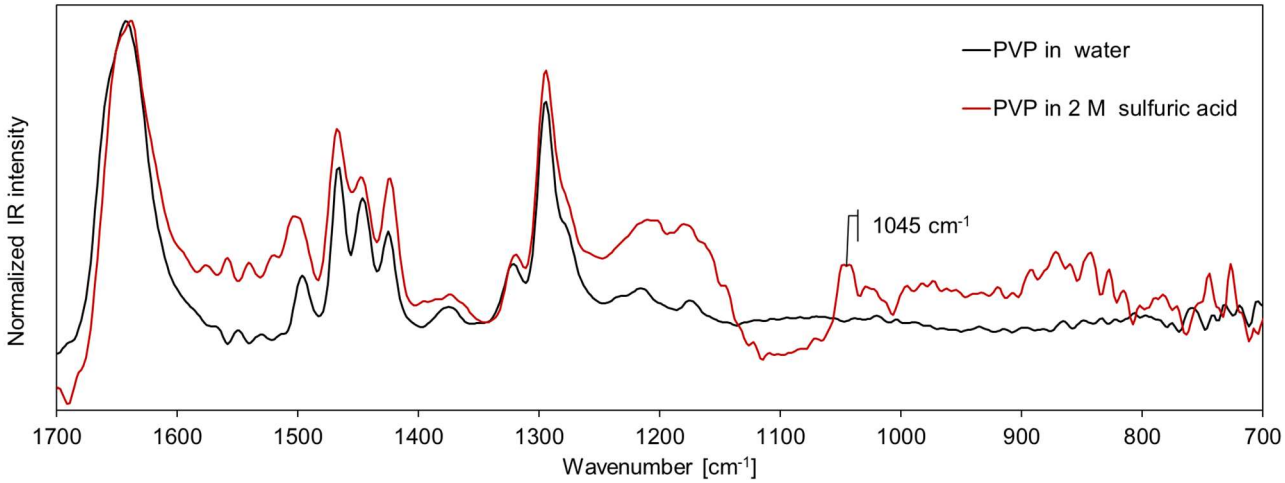

Figure 40. FTIR spectra recorded for PVP dissolved in distilled water (black curve) and PVP dissolved in 2 M sulfuric acid (red curve).

The fabricated membranes were examined under scanning electron microscope (SEM), as shown in figure 41a. The micrographs show that the coating is intact and smooth (no cracks and defects, no visible signs of strain). The coating was homogeneous in structure and in composition as proven by energy-dispersive X-ray spectroscopy (EDS) data (figure 41b). This confirms that the formulations were brought to a proper solution state for coating, and the curing process did not lead to a phase separation of the components.

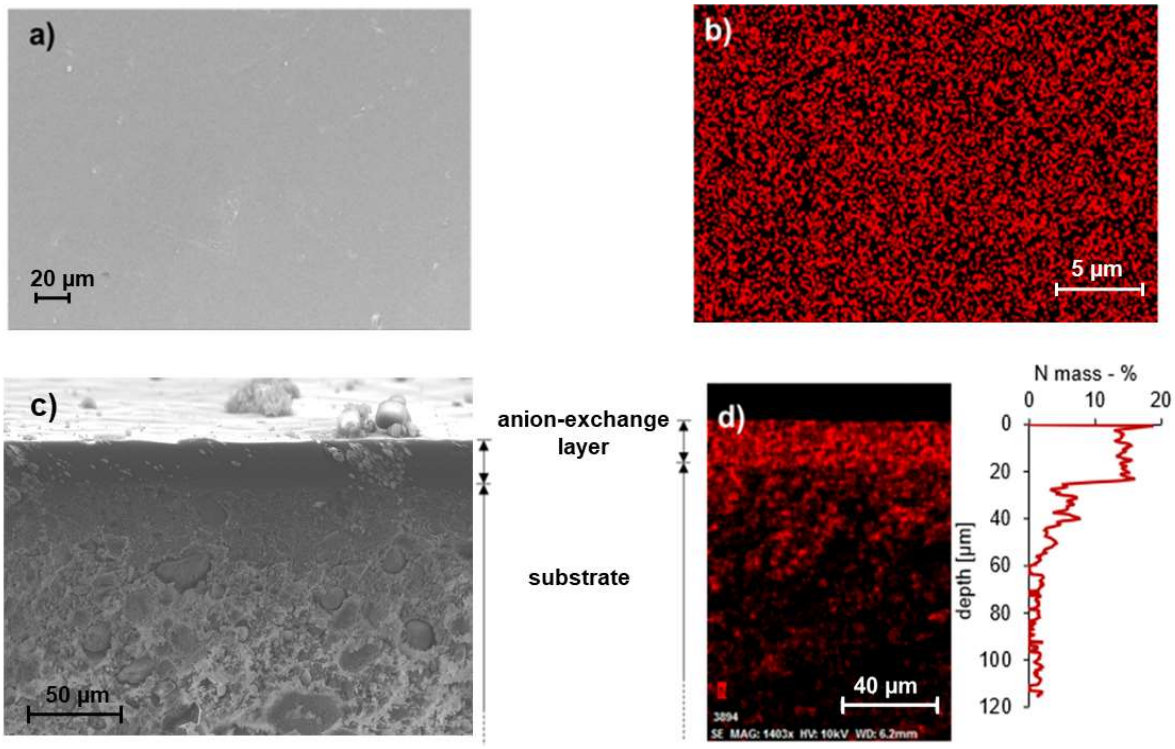

Figure 41. SEM/EDS micrographs presenting the structure of the composite AEM (PVP_8%): (**a**) anion exchange coating surface microscopy highlighting the coating continuity, (**b**) the uniformity in the nitrogen distribution is proven by the surface EDS map. (**c**) cross-section microscopy showing the hierarchical structure of the membrane: the ion exchange coating can be identified as the darker layer on top of the porous substrate. (**d**) cross section nitrogen EDS map and line scan confirming limited penetration of the anion exchange coating formulation in the porous substrate.

Cross-sections of the membrane were also observed under a SEM (figure 41c). The inter-face between the coating and substrate was clearly identifiable, indicating that the formulations had a high enough viscosity to prevent soaking into the pores of substrate before curing. EDS data (figure 38d) show a steep step in the line scan

and nitrogen is no longer detectable at 30 μm under the coating/substrate interface. This depth of penetration can be considered limited when compared to the thickness of the substrate (35 μm and 600 μm respectively). The average thickness of the anion exchange layer was found to be 35.4 μm with a standard deviation of 8.9 μm. Varying the content of PVP from 6 to 16 wt.% could potentially affect the viscosity and cure shrinkage of specific formulations that occurs during UV-curing step. The relatively high deviation in the coating thickness is attributed to the uneven surface of the substrate, originated by its fabrication process, and leading to local differences in the film thickness.

3.3. Characterization of the PVP/acrylamide-based composite AEM

3.3.1. Area-specific resistivity

Figure 42 reports the area-specific resistance (ASR) of the composite membranes as a function of the PVP content in the coating layer. In the plot, the ASR value for FAP 450 (black line – 0.56 $\Omega.cm^{-2}$) is marked as a reference point for a commercially available anion exchange membrane. The value recorded for a bare (not coated) substrate is also reported (grey line – 0.35 $\Omega.cm^{-2}$) to illustrate the effective contribution of the coating to the total membrane resistivity. A lower content of PVP in the coating layer caused a higher ASR of the membrane. A significant increase of the ASR can be observed when the PVP content falls below 8 wt.% (from 0.89 $\Omega.cm^2$ to 1.99 $\Omega.cm^2$), while at higher polymer contents changes are less steep. This can be understood as at 6 wt.% PVP the water uptake of the coating is only 56 % compared to 73 % at 8 wt.% of PVP. At low PVP contents the densely crosslinked matrix limits the swelling of the functional coating, resulting in a greater ASR. The water uptake of the coating increases with the growing content of PVP, providing for easier ion transport. Membranes with 14 wt.% and higher content of PVP exhibit low ASR – comparable to the commercial reference FAP 450.

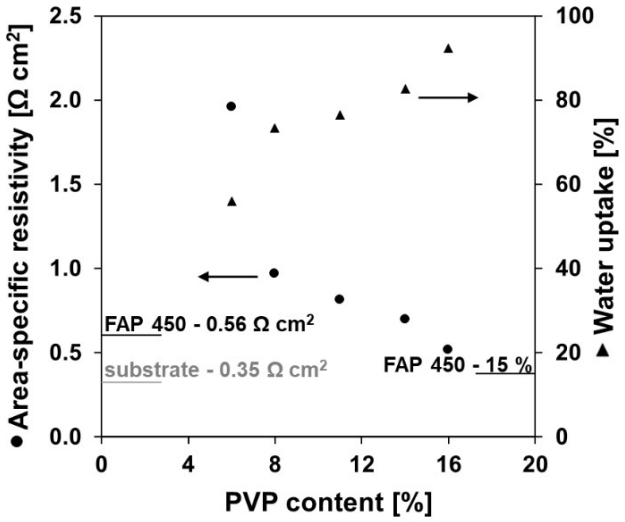

Figure 42. Area-specific resistance (1 M HCl, scan rate 10 mA.s^{-1}) and anion exchange coating water uptake of the fabricated membranes. Values for a commercial reference (FAP 450) and the bare substate are indicated with lines in the plot.

3.3.2. Permeability to vanadium ions

The composite anion exchange membranes were proven to be effective in slowing down the transport of VO^{2+} ions. Figure 40 pictures the diffusion test cells for the sample PVP_14%, PVP_8% and the commercial reference FAP 450, after 42 hours from the beginning of the experiment. Permeation of vanadium ions through the membrane can be noticed by the change of colour in the receiving solution and confirmed by the UV-vis spectra. To obtain a more quantitative estimate of the diffusion rate and compare the different samples, the UV absorbance at 775 nm proportional to the VO^{2+} concentration in the receiving cell, was measured at regular time intervals.

Figure 43b reports the results of the experiment. All the points marked for the fabricated membranes fall between the data measured for FAP 450 (grey points) (slowest diffusion – lowest slope) and the bare separator (black points) (fastest diffusion – highest slope). The transport of VO^{2+} ions was observed to be slower for the membranes with a lower content of PVP. The samples containing 6 % and 8 % of PVP showed the slowest diffusion rates, approaching the one of FAP 450. This can be explained by the higher cross-linking density and content of amine rich matrix which in acidic media can become protonated increasing ion exchange capacity. In parallel, higher PVP contents lead to a gradually faster permeation of

VO^{2+} ions, as a result of less densely crosslinked structure of the sIPN-type coating layer thus, high water uptake.

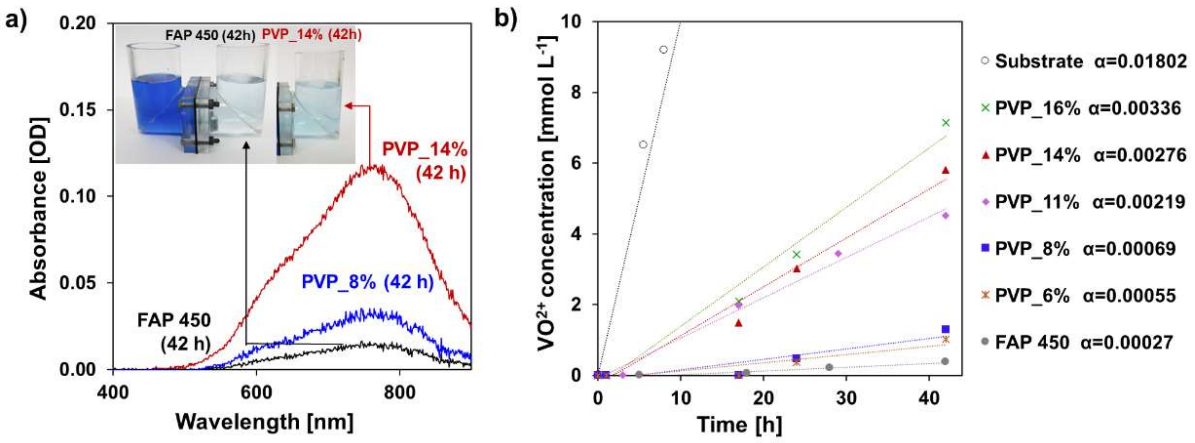

Figure 43. (**a**) UV-vis spectra of receiving solutions at 42 h from the beginning of the permeability test (PVP_14%, PVP 8% and FAP 450), the picture inset shows the permeability test cells at the time of sampling; (**b**) anion exchange membranes permeability test results – VO^{2+} concentration vs time, the α coefficients are calculated as the slopes of vanadium concentration curve as a function of time.

Self-discharge curves were recorded for the samples cycled in the RFB cell (figure 44). As a result of its lower vanadium permeability, the sample PVP_8% allowed for a longer charge retention compared to PVP_14%. The gap in the performance of the two samples was however found to be smaller than expected from the permeability data, probably due to the different vanadium species involved in this experiment and the oxidative character of the charged electrolyte to which the membranes were exposed in this experiment.

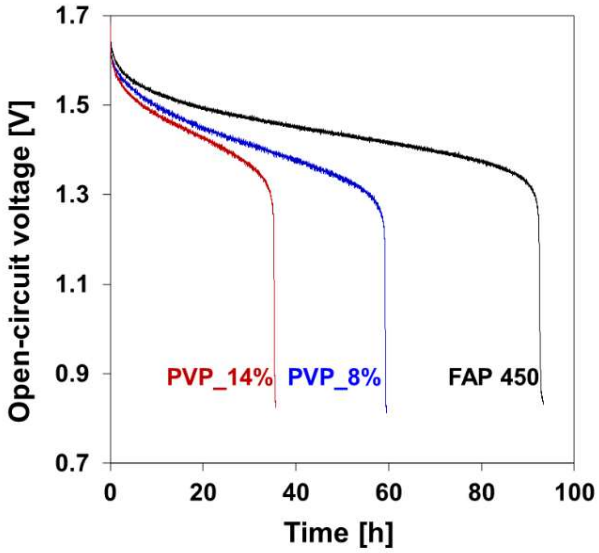

Figure 44. Open-circuit voltage as a function of time – self discharge curve recorded for FAP 450 and two composite membranes (PVP_14% and PVP_8%).

3.3.4. Stability in VO_2^+

Figure 45 reports the results of the ageing test in the V_2O_5 (VO_2^+) 2M H_2SO_4 solution. Diluted samples of the ageing solutions for membrane samples after 1000 h are pictured in figure 45a. The change of colour (from yellow to green), noticeable for all the hierarchical membrane samples, indicates a change in the oxidation state of the vanadium ions in the solution and thus, degradation of the ion exchange coating layers. This can be further confirmed by the appearance of an absorbance peak at 775 nm in the UV-vis spectrum, typical of VO^{2+} species. Individual tests performed for each of the coating components (PVP and the UV cured matrix) suggest that the crosslinked aminated matrix undergoes oxidation faster than PVP (figure 45b). This can be caused by the presence of methyl, hydroxide groups and tertiary amine moieties known to be prone to oxidation.

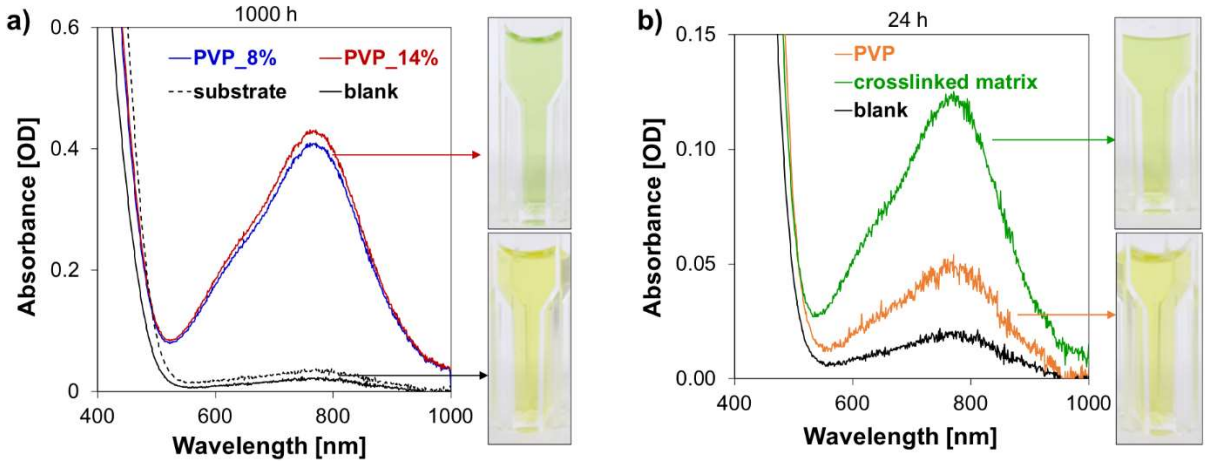

Figure 45. (**a**) UV-vis spectra of the ageing solutions for the fabricated membranes after 1000h of test, the substrate material is reported as reference. Oxidative degradation is observed for the PVP based hierarchical membranes. (**b**) UV-vis spectra of the ageing solutions for the coating components after 24h of test: the crosslinked matrix shows noticeably faster oxidation than PVP.

To improve the oxidative stability of the anion exchange coatings, the tertiary amino groups present in the functional coating matrix can be alkylated. The resulting positively charged quaternary ammonium groups are less susceptible to oxidation and more chemically stable [179]. As a simple proof of concept, 2 cm diameter round samples of coated PVP_14% were immersed in a solution of CH_3I (5%) in MeOH, mixed using magnetic stirrer for 48 h in order to allow complete alkylation of the tertiary amine groups present in the coating. After that, the membranes were rinsed with deionized water several times. In order to eliminate the excess of CH_3I used for quaternarization, the samples were left in deionized water overnight, then rinsed with deionized water. The samples were dried at 40 °C for 24 h and weighted. Then, the samples of a known coating mass were milled and immersed in 25 ml of 0.1 M $NaNO_3$ solution to allow the exchange of counter ions. Potentiometric titration (0.02 M $AgNO_3$) was used in order to determine the equivalent point and the amount of I^- in the solution. The degree of quaternarization was calculated using the following equation:

$$Nq = \frac{V_{AgNO_3} \cdot C_{AgNO_3}}{N_t \cdot 10} \ [\%]$$

V_{AgNO_3} – volume of used $AgNO_3$ to reach equivalent point [mL]

C_{AgNO_3} - concentration of $AgNO_3$ [mol·L^{-1}]

N_t – moles of tertiary amine groups in the coating [mol]

The degree of quaternarization was indicated as 60% when used 5% CH_3I in MeOH and 20% in case of 1% CH_3I in MeOH.

The quaternarized membranes showed improved chemical stability against oxidative degradation (figure 46).

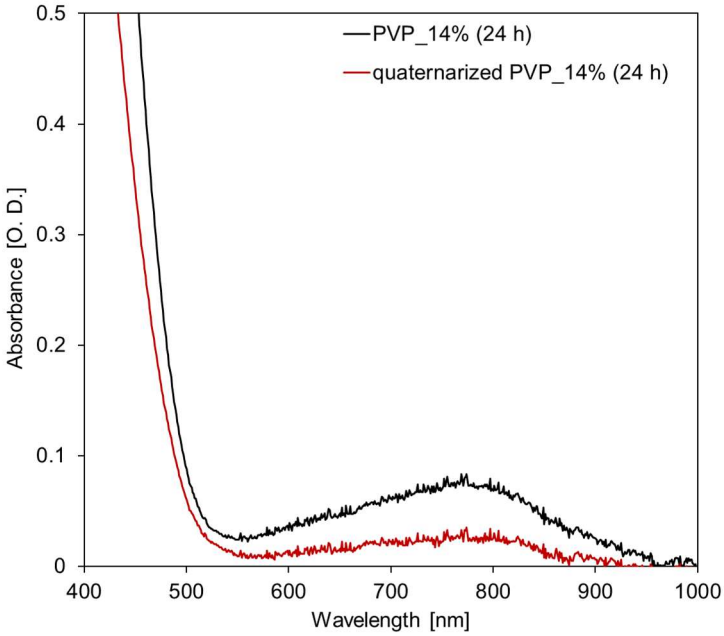

Figure 46. Comparison between UV-vis spectra recorded for the quaternarized membrane and the non-quaternarized one.

3.4. VRFB performance of PVP/acrylamide-based composite AEM

Selected membranes were tested in VRFB cycling experiments. Two membranes having an opposite combination of properties were studied: moderate ASR - low vanadium permeability (sample PVP_8%) and low ASR – moderate vanadium permeability (sample PVP_14%). Figure 47 reports the cycling curves obtained one of the composite membranes (PVP_8%) and the commercial reference. The first charge – electrolyte conditioning - was omitted because not relevant to further performance evaluation.

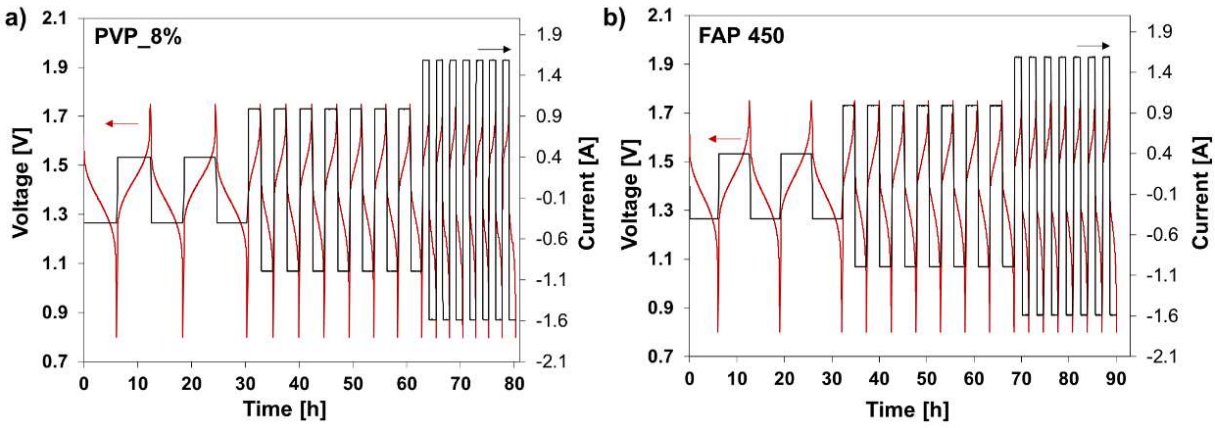

Figure 47. Cycling curves (90h) of the VRFB single cell (20 cm^2 of active area) assembled with PVP_8% (**a**) and FAP450 (**b**), cut off voltage: 0.80 and 1.75 V.

The data show that the composite membranes can be cycled in a VRFB with satisfactory results. Voltage, coulombic and energy efficiencies were computed for all the experiments. The results are shown in figure 48 as a function of current density. Benchmark data obtained for the commercial membrane FAP 450 are reported in grey for comparison.

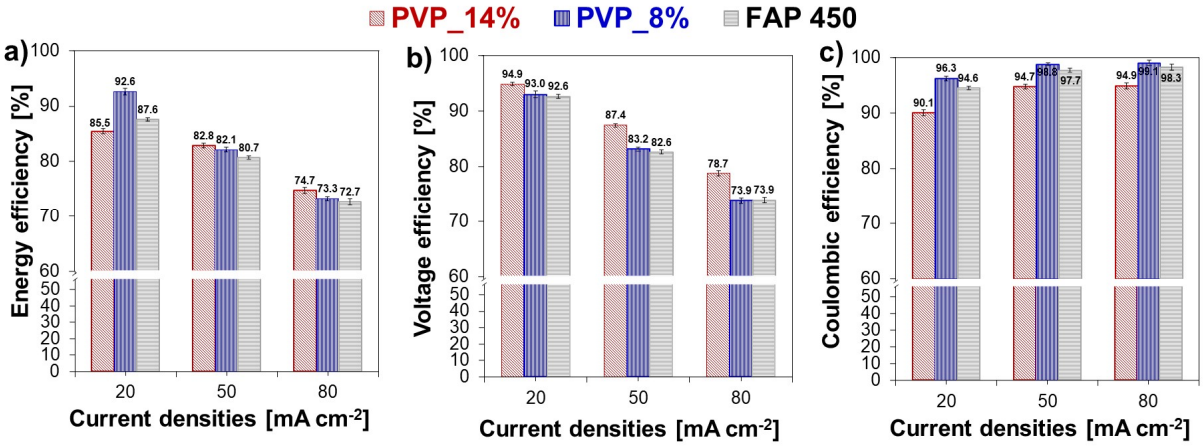

Figure 48. Energy (**a**), voltage (**b**) and coulombic efficiency (**c**) of the VRFB single cell assembled with FAP 450 and the fabricated hierarchical membranes prepared with 8 and 14 wt.% of PVP at different current densities.

At 20 $mA.cm^{-2}$, the membrane PVP_8% allows to reach a higher energy efficiency than PVP_14% (89.5 % in comparison to 85.5 %) owing to its excellent coulombic efficiency granted by lower cation permeability. This result could be expected from the data obtained in permeability tests (figure 43) and self-discharge

experiment (figure 44). At higher current densities - 50 mA.cm^{-2} and 80 mA.cm^{-2}- ohmic losses at the membrane become more significant and their effect noticeable in the voltage efficiency data (figure 48b). The voltage efficiency becomes thus the dominant contribution in the overall energy efficiency, resulting in higher values for the more conductive PVP_14% sample (energy efficiency: 74.7 % at 80 mA.cm^{-2}). At these high current densities, the low ASR of the membrane compensates its lower selectivity, leading to the highest energy efficiency. Experiments at higher current densities were not performed because of the steep decay in efficiency observed already at 80 mA.cm^{-2}. This is considered to be a cell limitation, present both for the proposed hierarchical membranes and the thin foil commercial membrane. The hierarchical membranes allowed reaching energy efficiency values in line with the commercial reference. In a more detailed analysis of voltage and coulombic efficiency results, some discrepancies in comparison with the pre cycling characterization are noticeable. The FAP450 membrane showed lowest ASR and lowest vanadium permeability in the pre-cycling testing. This allowed expecting it to be the best performing membrane in cell testing throughout the entire current density range explored. In fact, the performance gap between hierarchical coated membranes and FAP450 was not noticeable. PVP coated membranes were found to perform particularly good at higher current densities (figure 48a). This difference in the quantitative results between pre-cycling characterization and actual cycling experiments can be pointed to the different vanadium species and the different role of electromigration phenomena in the two types of experiments. Moreover, the internal resistivity of the RFB cell measured before every charging step was slightly decreasing upon the end of the cycling experiments in the case of the composite AEMs: 64 – 60 Ω, 82 – 73 Ω for PVP_14% and PVP_8%, respectively, while for the commercial membrane FAP 450 the internal resistivity slightly increases toward the end of cycling tests, from 63 to 65 Ω. The decrease of internal resistivity can be attributed to the degradation of the anion-exchange layer of the composite membrane. However, samples of the cycled membrane studied under SEM microscope still possessed a clearly visible, continuous coating layer (figure 49).

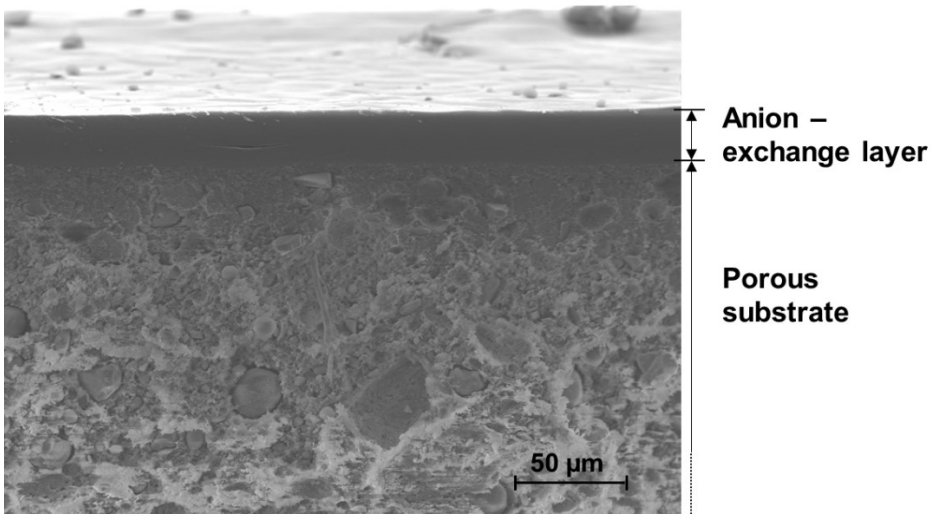

Figure 49. Cross-section SEM image showing the hierarchical structure of the membrane PVP_14%: the ion exchange coating can be identified on top of the porous substrate,

3.5. Conclusions

Anion exchange coatings based on water-soluble poly(vinylpyrrolidone) immobilized in an aminated crosslinked matrix have been formulated and deposited onto a porous substrate. This work can be considered a proof of concept for the use of PVP based composite anion exchange membranes in vanadium redox flow batteries.

The hierarchical structure of the membranes was confirmed by SEM observation and EDS analyses. Such membranes presented RFB testing performance well equivalent to commercial homogeneous ion exchange membranes, resulting from comparable ASR and vanadium permeability. These properties were proven to be easily tuneable by changing the PVP/matrix ratio in the ion exchange coating. Coatings with higher PVP content were found to have a lower ASR resulting in better VRFB performance at high current density (80 $mA.cm^{-2}$). For the sample PVP_14%, energy efficiency values of 74.7 % were calculated, higher than the value of 72.7 % obtained for the commercial reference FAP 450. On the other hand, a low PVP/matrix ratio enabled a lower VO^{2+} permeability at the cost of a higher resistivity. In VRFB cycling, this resulted in higher energy efficiency at low current

density (89.5 % for PVP_8% vs. 87.6 % for FAP450 at 20 mA.cm^{-2}) while in higher current regimes this membrane showed lower energy efficiency than PVP_14%, but still better performance than FAP450. Moreover, the sample PVP_8% showed the highest coulombic efficiency throughout all current density range. This feature can be seen as advantageous in view of long-term application in an industrial RFB.

Ageing tests in charged vanadium electrolyte (VO_2^+) showed hints of oxidative degradation of the functional coating, primarily related to the crosslinked polyacrylamide matrix. A simple quaternarization modification of the coating was proposed to mitigate this issue. Apart from VRFBs the fabricated membranes can be proposed for application in other RFBs with less harsh electrolytes all-iron and organic redox flow batteries.

All things considered, the proposed approach to membrane formulation and fabrication through blade coating and UV curing a radically reactive ionomer formulation can be seen as a flexible platform allowing for a facile membrane property tuning. This is seen as an advantage in electromembrane process design, by allowing to adjust the membrane properties to specific process parameters. The use of widely available precursors and simple processes in the membrane fabrication can make these materials available at a low cost, prevailing the development of ion exchange membrane-based energy storage technologies. However, the chemical stability in oxidative media still remained as a challenging issue that should be addressed in the next step of the research.

Chapter 4. Composite anion exchange membrane fabricated by UV curing of acrylamides and poly(2,6-dimethyl-1,4-phenylene oxide) modified with *N*-vinylimidazole (VIMPPO)

The membranes presented in **chapter 3** exhibited ionic transport properties comparable to the one of commercial membranes. However, in oxidative and highly acidic media the membrane underwent oxidative degradation. Moreover, the self-discharge experiment showed that such membranes are not able to prevent well the crossover of vanadium species. In order to mitigate the above-mentioned issue another type of formulation based on an ionomer that is chemically crosslinked with the matrix was studied. Vinyl imidazolium poly(phynelene oxide) was used as anion exchange polymer that also undergo crosslinking reactions with itself or with monomers reactive in radical polymerization. As a result, the coating layer possesses a structure of branched copolymer with crosslinked chains instead of the interpenetrating polymer network. Therefore, composite membrane with such structure of the coating layer were expected to exhibit better chemical stability, lower vanadium permeability and improved long-term cycle performance.

4.1. Formulation concept

In this concept composite AEMs were fabricated using an anion-exchange polymer vinyl imidazolium poly(phenylene oxide) (VIMPPO) reactive in UV-curing together with the low-cost acrylamide monomers (DMEA, HEAA, figure 50).

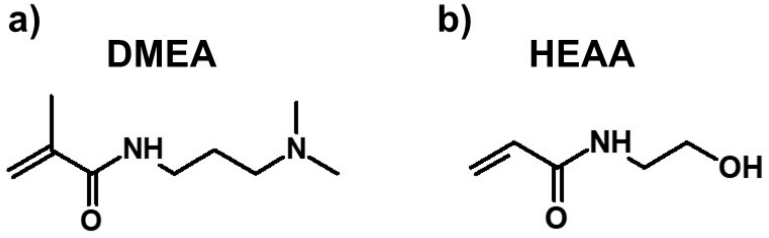

Figure 50. Chemical structure of the off-shelf available acrylamide monomers used for fabricating the ion-exchange coatings: (**a**) *N*-[3-(dimethylamino)propyl]methacrylamide (DMEA), (**b**) *N*-hydroxyethyl acrylamide (HEAA).

VIMPPO was synthesized in a simple two step synthetic procedure, starting from a poly(phenylene oxide) – a polymer that is available commercially in large quantities [180]. Due to the presence of a radical reactive vinyl bound attached to the imidazolium moiety, VIMPPO can be considered as a functional crosslinking agent. The use of speciality chemicals (such as functionalized PPO) in the ion-exchange coating formulation was kept at a minimum in order to minimize the material cost. Moreover, cheap reagents such as common, non-toxic acrylamide derivatives were used as the majority components in the coating formulation. In addition, the final properties of the ion-exchange membrane could be tuned in a wide range of conductivity and selectivity, by adjusting the composition of the mixture of photoreactive precursors, without the need of repeating dedicated ionomer synthesis for each specimen. The proposed anion-exchange layers could not be fabricated as self-supported films. The porous substrate was proposed as a reinforcement and carrier of the ionomer coating. This allowed for including a large share of low-cost, highly hydrophilic materials in the formulation, which would not allow reaching the integrity and dimensional stability required for a self-standing film.

To demonstrate the applicability of the new membranes and find the best performing composition, their performance was evaluated using a laboratory vanadium redox flow battery (VRFB) cell.

4.2. Synthesis of poly(2,6-dimethyl-1,4-phenylene oxide) modified with *N*-vinylimidazole (VIMPPO)

VIMPPO was obtained in a two-step synthesis, following the protocol described in the section 2.1. Materials and presented in figure 51. The aim was to obtain an ionomer with a high ion-exchange capacity, to guarantee excellent ionic conductivity and selectivity of the membrane. Therefore, in the first step, 50% of polymer structural units were brominated. In the quaternarization step, all benzyl bromide groups were successfully substituted with *N*-vinyl imidazole, resulting in an ionomer with a theoretical ion-exchange capacity of 2.4 mmol g^{-1} (^{1}H NMR data confirming the synthesis products are presented in figure 34 and 35). Crosslinked

VIMPPO self-supported membranes were reported in the works on fuel cells [181]. In this study, *N*-vinyl imidazole was selected for the functionalization of PPO, due to the presence of vinyl moiety, which allows VIMPPO to react with other radically reactive monomers in the process of UV curing. Effectively, VIMPPO is used to introduce positively charged groups and act as a crosslinker for the coating. In this way, it contributes to ionic conductivity and stability of the ionomer layer.

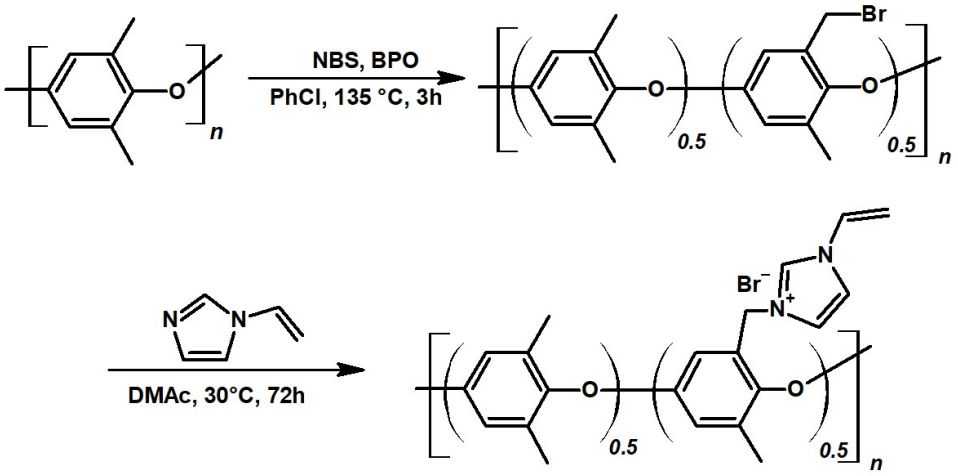

Figure 51. Synthetic route for obtaining the poly(2,6-dimethyl-1,4-phenylene oxide) modified with *N*-vinylimidazole (VIMPPO).

4.3. Fabrication and morphology study of the VIMPPO/acrylamides-based composite AEM

The VIMPPO obtained in the synthesis described above reached an excessively high cross-linking degree when UV-cured alone. Such coating layers were expected to exhibit remarkably low permeability of cations, at the cost of a low overall ionic conductivity. Unlike the state-of-the-art imidazolium PPO-based membranes [182,183], herein, the AEMs were obtained by diluting the VIMPPO with acrylamides, significantly diminishing the amount of needed ionomer, which could be seen as an economical benefit. Diminishing the content of VIMPPO in the coating to below 25 wt.% by introducing acrylamide derivative monomers in the formulation, led to a decreased cross-linking density caused by the incorporation of a large fraction of hydrophilic polyacrylamide in the resulting, cross-linked polymer. PAA (1 wt.%) serving as a rheology modifier was added to the solution of

DMEA and HEAA – two industrially available, safe and non-toxic acrylamide monomers (chemical structures presented in figure 50).
Composite AEMs prepared using different wt.% of VIMPPO in the coating layer were successfully fabricated by blade coating and UV-curing (details of each composition are presented in table 5). A membrane with a top anion exchange layer formed of the UV cured ionomer alone (sample VIMPPO_100%) was fabricated to compare the properties of VIMPPO/acrylamide copolymer with a neat VIMPPO.

Table **5**. The compositions of the formulations used for fabricating the ion exchange coatings.

	VIMPPO [g]	**DMEA [g]**	**HEAA [g]**	**PAA [g]**	**initiator [g]**
VIMPPO_10%	0.7	3.5	2.5	0.08	0.15
VIMPPO_12%	0.85	3.5	2.5	0.08	0.15
VIMPPO_15%	1.1	3.5	2.5	0.08	0.15
VIMPPO_17%	1.3	3.5	2.5	0.08	0.15
VIMPPO_20%	1.6	3.5	2.5	0.08	0.15
VIMPPO_25%	2.1	3.5	2.5	0.08	0.15
VIMPPO_100%	2.5	0	0	0	0.05

DMEA monomer has a tertiary amine group in its chemical structure. This weakly basic group ($-NR_2$) possesses a lone pair of electrons which becomes protonated in the acidic electrolyte of VRFB [184]. The resulting $-NR_2H^+$ moiety facilitates a labile proton, which can be transferred to another amine group participating in the Grotthus mechanism of proton hopping, contributing to the ionic conductivity [20]. Hence, the anion exchange membrane can also be considered to be a proton exchanger. Effectively, formulating VIMPPO in a mixture of acrylamide monomers enabled to control the trade-off between the cation permeability and the resistivity of the coating. The VIMPPO content ranged from 10 to 25 wt.% in the fabricated coatings.

VIMPPO/acrylamide copolymers were found to be highly hydrophilic in the studied range of formulations and would not be able to form self-supported membranes. The lowest content of VIMPPO providing sufficient cross-linking for obtaining a stable coating layer was 10 wt.%. The VIMPPO_10% sample reached water uptake values of 74%. During attempts to fabricate the membrane samples with VIMPPO content in the coating below 10 wt.%, the coating layers were found to be unstable in aqueous electrolyte and separated from the substrate in the form

of a soft gel. In such cases, crosslinking was found to be insufficient to secure the integrity of the ionomer film.

Taking the advantage of the dimensional and mechanical stability of the porous PVC-silica substrate, the anion exchange layers were kept at a maximum of 50 μm. The final thickness of the coating layer was determined by the gap of the blade applicator, the viscosity of the applied mixture and shrinkage occurring during the radical polymerization. Varying the content of VIMPPO (10–25 wt.%) could potentially affect the viscosity and cure shrinkage of specific formulations. The fabricated anion exchange layers had an overall average thickness in the range of 20–40 μm when cured and dried. Within one sheet of the membrane, thickness deviation due to the uneven surface of the substrate was present. As a result, the thickness of the coating layer could be locally different (minimum of 15 μm and a maximum of about 50 μm were noticed in the analyzed dataset). The non-uniform surface of the substrate additionally rich in the exposed grains of silica particles was found to be advantageous. Such surface provided for very good adhesion between the substrate and the polymeric coating. Other types of porous materials such as thin poly(ethylene) or poly(propylene) porous sheets (stretched foils) or cellophane membranes did not provide sufficient adhesion between the substrate and coating. When coating attempts were taken on such supports, the ionomer formulation would not distribute evenly during the coating, and despite curing, delaminate upon wetting and swelling. This was not an issue in the case of the PVC-Silica heterogeneous porous membrane used in this work. The use of thick PVC-silica substrate (0.6 mm) was not expected to cause substantial ion transport limitations, since the VRFB electrolyte is highly conductive (2 M H_2SO_4). In such an environment, effective current transport in electromigration is expected, even in areas inside the substrate that are free of convective transport. The same type of PVC-Silica separators were used before as porous separators in vanadium and copper RFBs [135,141].

SEM images and EDS analysis confirmed a hierarchical, layered, structure of the fabricated membrane, as illustrated with the cross-sections view and elemental map in figure 52 a, b. SEM image of the surface and corresponding elemental map are presented in figure 52 c, d.

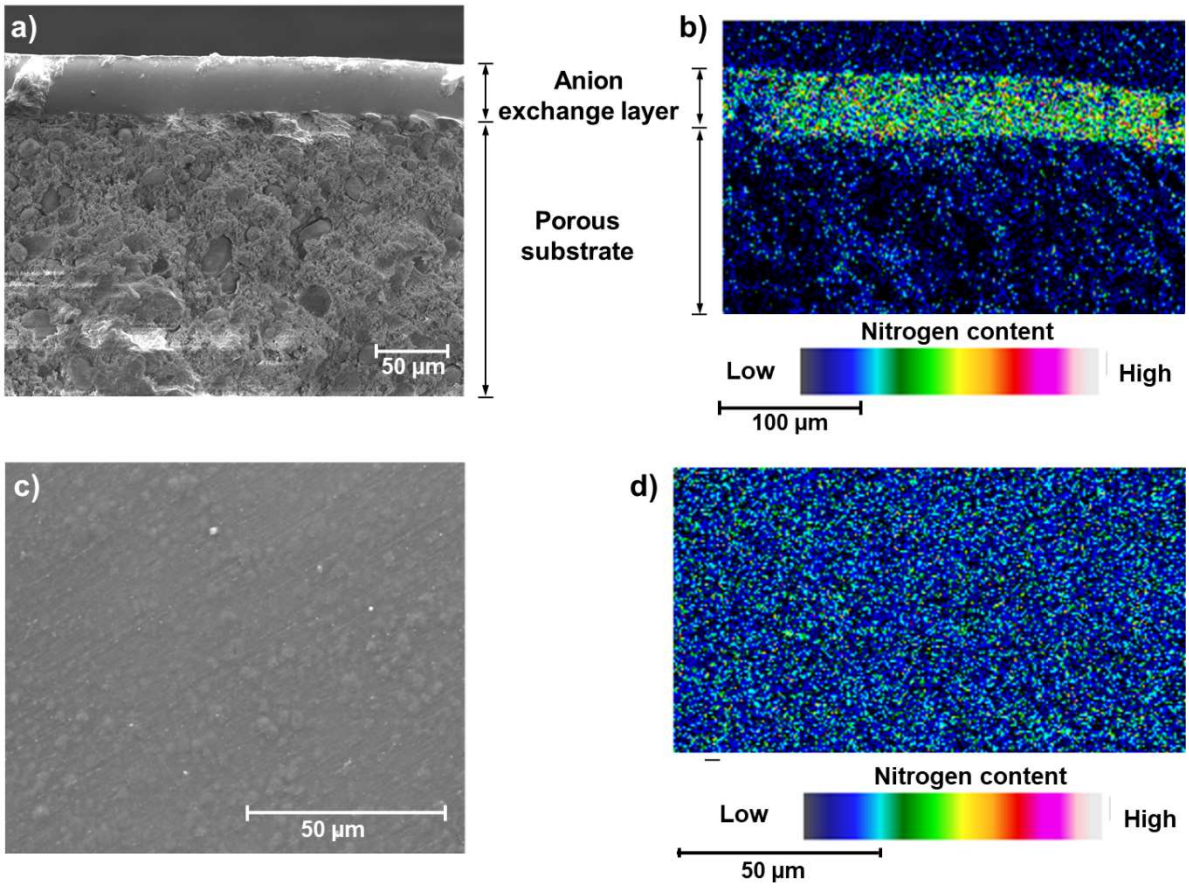

Figure 52. SEM/EDS micrographs showing the hierarchical structure of the coated composite membrane. (**a**) SEM cross-section image; (**b**) EDS Nitrogen map of the cross-section; (**c**) SEM surface image; (**d**) EDS Nitrogen map of the surface.

4.4. Characterization of the VIMPPO/acrylamides-based composite AEM

4.4.1. Area-Specific Resistivity (ASR) and Water Uptake (WU) of the Membranes

Figure 53 shows how the water uptake (WU) and the area-specific resistance (ASR) were changing, depending on the content of VIMPPO in the coating layer. The VIMPPO_100% membrane exhibited the highest ASR (1.4 $\Omega.cm^2$) and the lowest WU (20%) among the fabricated membranes, due to its densely cross-linked structure (values marked with blue arrows in figure 53). When the content of VIMPPO was reduced and the ionomer was used as a functional crosslinker for the formulation of polyacrylamides, the ion conductivity of the membrane was

significantly improved. The ASR value dropped from 1.4 Ω.cm² to 1.1 Ω.cm² at 25 wt.% of VIMPPO, and further down to 0.55 Ω.cm² at 10 wt.%.

The ASR trend following the diminishing content of VIMPPO in the coating is understandable. Formulations with the lower content of VIMPPO are expected to reach a lower density of cross-linking, allowing for a higher water uptake. The water uptake trend was also confirmed by the experimental data shown in figure 53.

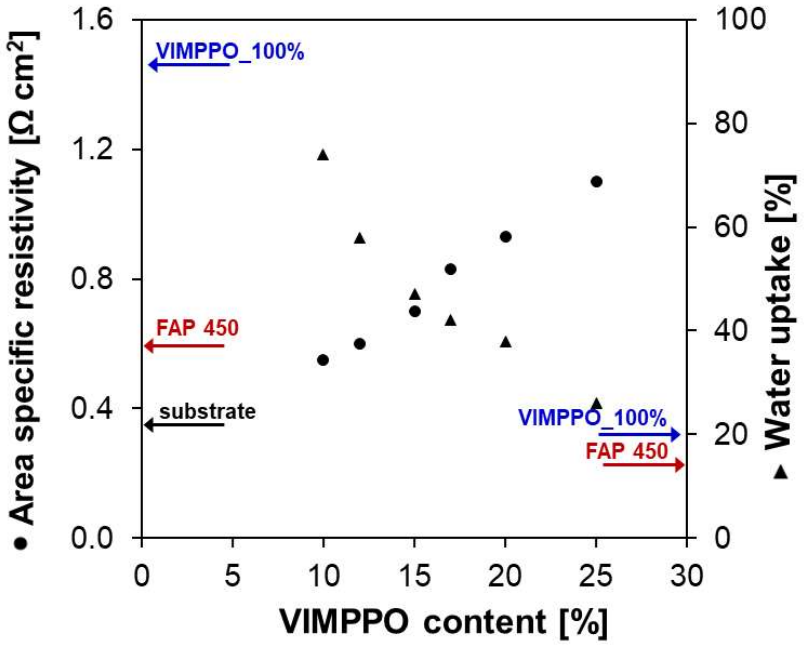

Figure 53. Area-specific resistance measured in 1 M HCl_{aq} at a current scan rate of 10 mA s^{-1} and water uptake of the membranes in a function of VIMPPO content in the anion-exchange coating.

Figure 53 allows comparing the resistivity and water uptake of the composite membranes, with results obtained for FAP 450, the commercial benchmark (WU—15%, ASR—0.58 Ω cm²; red arrows in figure 53).

In the case of the composite membranes, both the anion-exchange coating and the porous substrate contributed to the overall ASR of the membrane. To isolate these contributions, the ASR of the porous substrate was measured, giving 0.37 Ω.cm². This value could be subtracted from the ASR of the entire coated membrane reported in figure 50 to estimate the resistivity of the coating alone. For example, the ASR value of VIMPPO_10% membrane was 0.55 Ω.cm², out of which only 0.18 Ω.cm² was related to the coating after subtracting the ASR of the substrate. This value was remarkably below the ASR of the FAP 450 membrane. Two properties

of the coating layer could be seen as sources of this advantage in the ion conductivity. High water uptake of the VIMPPO_10% coating facilitated ion transport. In addition, the coating layer was only 20 μm thick, less than half of the thickness of the FAP 450 membrane (nominal thickness of 50 μm). A similar calculation could be computed for the VIMPPO_25% membrane; this coating contributed 0.73 $\Omega.cm^2$ to the overall membrane ASR. Its water uptake was 26%, closer to that of FAP 450. The above argumentation indicates that a further decrease of the resistivity of the composite membrane could be achieved by further optimizing the porous substrate.

4.4.2. Permeability to Vanadium Ions

The lowest permeability of the vanadium species (VO^{2+}) among all tested membranes was observed for the neat VIMPPO coating (VIMPPO_100% sample, grey circles in figure 54). High cross-linking density allowed neat VIMPPO to form an exceptionally effective barrier for cation transfer. When the cross-linking density was diminished by reducing the VIMPPO content in the coating to 20 wt.%, the coated membrane reached vanadium permeability matching that of FAP 450. At lower contents of VIMPPO, the permeation of vanadium through the corresponding membranes increased gradually. In the case of the lowest amount of VIMPPO (10 wt.%), the transfer of vanadium species through the membrane was still more than ten times slower, in comparison to a bare substrate. Slopes of the vanadium concentration in the receiving cell as function of time changed from $\alpha = 0.01902\ h^{-1}$ for the substrate to $\alpha = 0.0014\ h^{-1}$ for VIMPPO_10% and down to $\alpha = 0.00054\ h^{-1}$ for VIMPPO_25%.

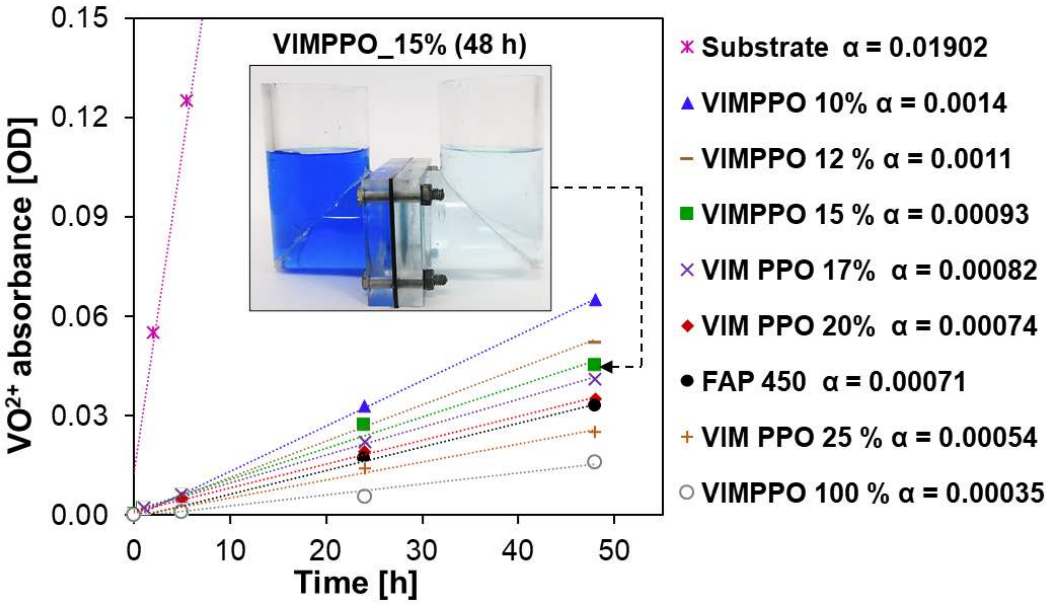

Figure 54. Changes in VO^{2+} absorbance (measured at 775 nm) recorded for the receiving solution over 48 h (initial solutions—receiving: 0.15 M $MgSO_4$ in 3 M H_2SO_4, donor: 0.15 M $VOSO_4$ in 3 M H_2SO_4). The picture inset presents the diffusion cell used for the permeability test assembled with VIMPPO_15% after 48 h of the experiment. Slopes of the absorbance curves (α in (h^{-1})) were calculated and used to quantify the permeation rate of vanadium cations.

Three composite membranes: VIMPPO_10%, _15%, and _20% were chosen for further study of vanadium crossover under the VRFB cell conditions. Self-discharge curves of a cell assembled with the three listed membranes and FAP 450 were recorded after an initial, complete charge. The experiments were performed with the minimal possible volume of electrolyte (10 mL in each of the two half cells, 20 mL total), in a test cell with 20 cm^2 of active area. The results are shown in figure 55. The curve obtained for FAP 450 was considered to be a reference value for interpretation. Among the composite membranes, VIMPPO_20% allowed for the slowest self-discharge; the cell retained charge for 79 h. Self-discharge of the cell with FAP 450 took 92 h. For membranes with a lower content of VIMPPO in the coating layer, 39 h and 28 h were recorded for VIMPPO_15% and VIMPPO_10%, respectively. The results of the self-discharge test come in a trend qualitatively matching VO^{2+} permeability experiments. The discrepancies between the relative self-discharge and results of the vanadium permeability experiments

could be explained by the migration of vanadium ions other than VO^{2+}. Indeed, cations such as VO_2^+ and V^{2+} play a significant role in the self-discharge process.

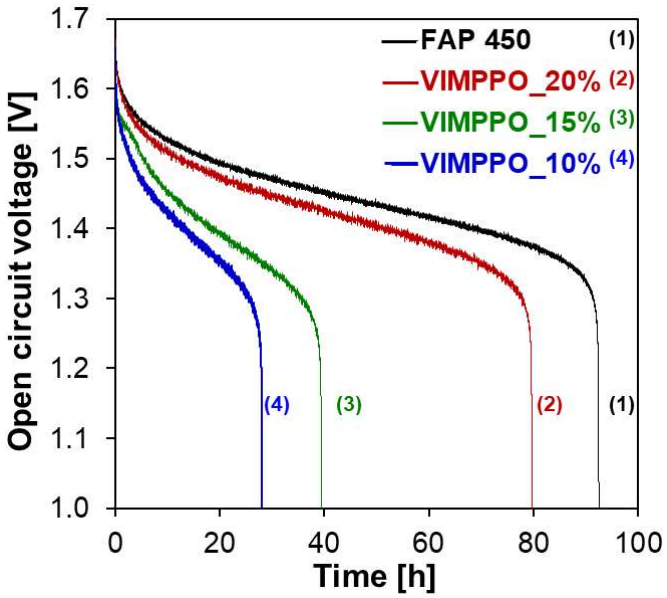

Figure 55. Open-circuit voltage as a function of time (self-discharge curves) recorded for FAP 450 and three composite membranes: VIMPPO_20%, VIMPPO_15%, and VIMPPO_10%.

4.4.3. Ex-Situ Chemical Stability in Vanadium (V) Electrolyte

The chemical stability in acidic and oxidative media was tested for 10, 15, and 25wt.% of VIMPPO in the coating layers. The membranes were placed in a 1.6 M solution of VO_2^+ in 2 M H_2SO_4 for over 1500 h. The results presented in figure 56a shows that the concentration of VO^{2+} was rising faster for the coatings with a lower content of VIMPPO (the UV spectra after 1500 h and 48 h are presented in figure 56a). Upon completing the 1500 h oxidation tests, the coatings were found to be intact. Figure 56b shows a cross-section image of the VIMPPO_15% membrane after the test.

The short-term stability test (48 h) conducted for individual components of the coating—cross-linked VIMPPO and polymerized acrylamides (VIMPPO free) demonstrated that no degradation occurred for VIMPPO, while oxidation took place for the polymerized acrylamides (relevant UV spectra are presented in figure 57b). The oxidation of polyacrylamide was likely to originate from the methyl and hydroxide groups present in *N*-[3-(dimethylamino)propyl]methacrylamide and *N*-

hydroxyethyl acrylamide. Future formulation optimalization will focus on the replacement of these components.

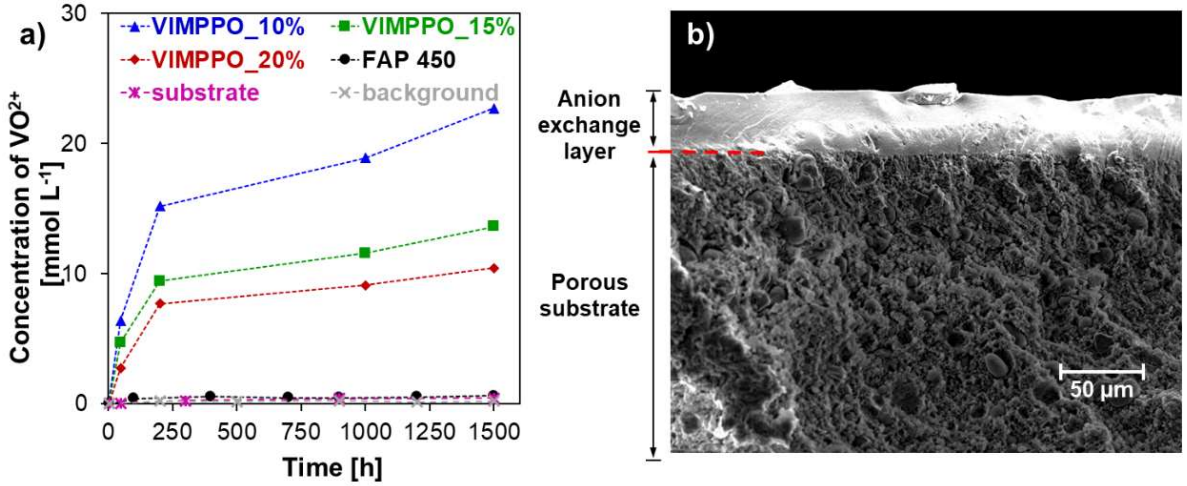

Figure 56. The results of oxidative stability test performed by the ageing membrane samples (VIMPPO_20%, VIMPPO_15%, VIMPPO_10%) in 1.6 M VO_2^+ in 2 M sulfuric acid solution. (**a**) Change in the concentration of VO^{2+} measured over 1500 h; and (**b**) SEM cross-section image of VIMPPO_15% after 1500 h of ageing.

Figure 56a demonstrates that the oxidation of the tested coated membranes happened mostly within the first 250-300 hours of the test. At longer times, the reactions were majorly slowed down or nearly stopped, especially in the case of the VIMPPO_15% and VIMPPO_20% membranes. The slower rate of degradation observed for the membranes with a higher amount of VIMPPO could be also attributed to the denser cross-linking. Such coatings also exhibited lower water uptake and swelled less. Therefore, the attack of oxidative species could be additionally impeded by steric hindrance.

The collected information gave sufficient grounds to propose the composite membranes for VRFB testing, considering that at least the formulations with a higher content of VIMPPO would sustain the prolonged exposure to the vanadium electrolyte.

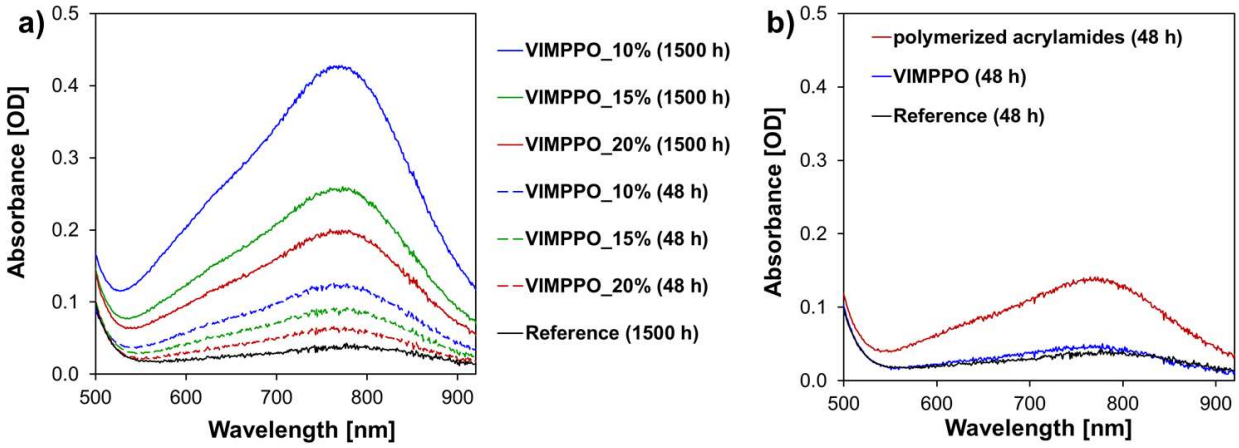

Figure 57. UV-vis spectra recorded for the ageing solution: (**a**) comparison between different composite membranes; (**b**) comparison of short-term results of stability test for different components of the coating layer: matrix UV-cured acrylamides, and VIMPPO cured alone.

4.5. VRFB performance of VIMPPO/acrylamides-based composite AEM

The RFB cycling test aimed at finding the trade-off between the opposite trends of the ASR and vanadium permeability of the membranes, which allowed for the highest energy efficiency of the RFB cell. Composite membranes with 10, 15, and 20 wt.% of VIMPPO content in the coating layer were selected for this experiment; FAP 450 and Nafion® N 115 served as performance benchmarks [185–188]

The charge–discharge tests were carried out at three current densities—20, 50 and 80 mA.cm^{-2}. Performance at a current density exceeding 80 mA.cm^{-2} was not studied, due to the RFB cell limitations, leading to a poor energy efficiency and a low effective cell capacity observed, even for the market-proven benchmarks. Exemplary charge–discharge curves recorded for the VRFB single-cell, assembled with a composite membrane, is presented in figure 58a. The cell showed stable cycling performance at all applied current densities over the experiment duration of 5 days, repeated twice without disassembling the cell and starting with a fresh electrolyte.

Figure 58b shows cell discharge capacities of the three listed membranes and commercial IEMs extracted from the charge–discharge curves. The coating layers of the composite membrane had a decisive role in affecting the charge retention in the battery. In the case of the two composite membranes with a higher content of crosslinking ionomer (VIMPPO_20% and VIMPPO_15%), the results of capacity retention followed the evolution of data obtained for FAP 450 and N 115. Using the VIMPPO_10%, membrane led to a steep loss of capacity at each applied current density. This was attributed to the significantly higher vanadium permeability through the insufficiently crosslinked structure of the VIMPPO_10% coating layer.

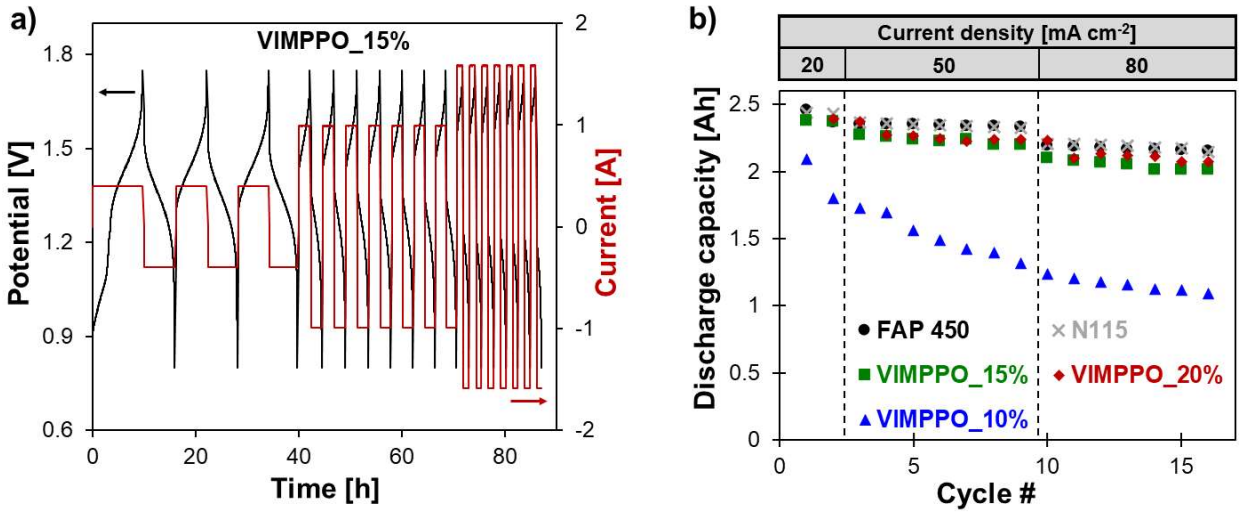

Figure 58. VRFB cycling performance data: (**a**) charge–discharge curve recorded for the VRFB single cell (Pinflowes, 20 cm^2 of active area) assembled with VIMPPO_15% at three current densities—20, 50, and 80 $mA.cm^{-2}$: and (**b**) discharge capacity for each tested membrane.

Figure 59 shows the cell efficiencies (energy, voltage, and coulombic) calculated for all cycling experiments (numerical data are presented in table 6). As is typical for RFB cells, the coulombic efficiency increased for all membranes, with increasing current density (figure 59c). An opposite trend was observed for voltage efficiency, figure 59b. Loss of voltage efficiency with the increasing current density—caused by ohmic losses—dominated the trend of energy efficiency, which also diminished with increasing current density (figure 59a). Among the coated membranes, VIMPPO_15% was seen as the best performing one, based on energy efficiency data presented in figure 59a. At low current density (20 $mA.cm^{-2}$), its result was matched by VIMPPO_20%. The energy efficiency of VIMPPO_15% at higher current density, closely followed the values recorded for N 115 and slightly surpassed the energy efficiency values of FAP 450 at the highest applied current (75.1% for VIMPPO_15% vs. 75.0% for N 115 vs. 73.0% for FAP 450, at 80 $mA.cm^{-2}$).

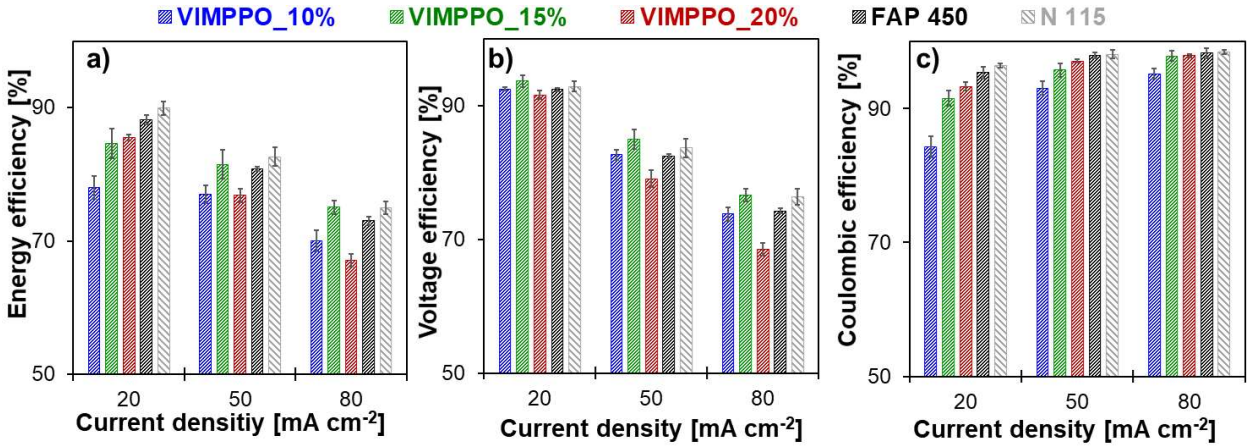

Figure 59. VRFB performances reached by the single-cells with the three tested composite membranes, FAP 450 and Nafion® N 115 cycled at 20, 50, and 80 mA.cm^{-2} - (**a**) energy efficiency, (**b**) voltage efficiency, and (**c**) coulombic efficiency.

Table 6. Performance of VRFB single cells (active area – 20 cm^2) assembled with different membranes.

current density [mA.cm^2]	VIMPPO_20%					
	Coulombic Efficiency$_{average}$ [%]	standard deviation	Voltage Efficiency$_{average}$ [%]	standard deviation	Energy Efficiency$_{average}$ [%]	standard deviation
20	93.3	0.6	91.7	0.6	85.5	0.4
50	97.1	0.3	79.1	1.2	76.8	1.1
80	97.9	0.3	68.5	1.0	67.1	0.9
	VIMPPO_15%					
20	91.5	1.2	93.7	0.9	84.7	3.2
50	95.8	1.0	85.0	1.4	81.5	2.2
80	97.9	0.8	76.7	0.9	75.1	1.0
	VIMPPO_10%					
20	84.3	1.6	92.5	0.3	78.0	1.7
50	93.1	1.0	82.7	0.8	77.0	1.4
80	95.2	0.8	73.8	1.0	70.0	1.6
	FAP 450					
20	95.4	0.9	92.5	0.3	88.2	0.7
50	97.9	0.4	82.5	0.3	80.8	0.3
80	98.3	0.7	74.3	0.4	73.0	0.6
	N115					
20	96.4	0.3	92.9	0.8	89.9	1.0
50	98.1	0.6	83.7	1.4	82.7	1.4
80	98.5	0.3	76.4	1.2	75.0	0.9

Trends observed for the energy efficiency were interpreted based on coulombic and voltage efficiencies data of the tested membranes; presented in figure 56b, c, together with the characterization discussed earlier.

Coulombic efficiencies achieved by the cells assembled with the tested membranes (figure 59c) was in line with the permeability data reported previously. The cell with the most densely cross-linked membrane (VIMPPO_20%), reached the highest coulombic efficiency among the other tested composite membranes (97.1% and 97.9% at 50 and 80 $mA.cm^{-2}$, respectively). The high coulombic efficiency was achieved at the cost of low voltage efficiency, caused by the highest ASR of VIMPPO_20% membranes. Therefore, the overall performance of the VIMPPO_20% membrane was suboptimal, particularly, at higher current density conditions, for which ohmic losses dominated the cell performance (energy efficiency - 76.8% and 67.1% at 50 and 80 $mA.cm^{-2}$, respectively). Diminishing the VIMPPO content in the coating layer led to a decreased coulombic efficiency - 93.3% for VIMPPO_20%, 91.5% for VIMPPO_15%, and 84.5% for VIMPPO_10% recorded at 20 $mA.cm^{-2}$ - current conditions at which coulombic losses were most pronounced. Therefore, higher permeation of vanadium species across the membrane was observed in the case of the less densely crosslinked membranes. This observation was in line with the permeability and self-discharge experiments.

The voltage efficiency trend of the three composite membranes was found in partial contrast to the ASR data reported earlier. ASR results correlated accurately to the content of VIMPPO in the coatings. However, despite the lowest resistivity, VIMPPO_10% did not allow us to reach proportionally high-voltage efficiencies during the RFB cycling experiments. This discrepancy is not completely understood but may have been caused by different conditions during the two experiments. ASR tests were performed in 1 M HCl with a short-lasting measurement that possibly did not include all concentration polarization effects that could build up over time, during the charge–discharge cycle in 2 M H_2SO_4. For the other two coated membranes, the results of voltage efficiency were in line with the ASR data. Undisputedly, the cell with VIMPPO_20% reached the lowest voltage efficiencies at all applied current densities (91.7%, 79.1%, and 68.5% for

20, 50, and 80 mA.cm^{-2}), resulting in a compromised energy efficiency, particularly at higher current densities. No transport limitations related to the porous substrate were manifested during the cycling experiments. The composite membranes - VIMPPO_15% and VIMPPO_10% reached voltage efficiencies comparable to the ones of the thin foil commercial IEMs. Thus, it can be concluded that the ionic transport properties of the composite membranes are controlled by the ionomer coating layer.

The cell assembled with the middle option membrane, VIMPPO_15%, reached the highest voltage efficiency values, given the unsatisfactory low voltage efficiency of VIMPPO_10%. Further it exhibited coulombic efficiencies in between the results of VIMPPO_10% and VIMPPO_20% membranes. When coulombic and voltage efficiency are combined into energy efficiency, VIMPPO_15% is considered to be the overall best performing membrane with comparable performance to the N 115 membrane, at the highest current density. The VIMPPO_15% membrane was also tested in a longer-term cycling experiment: cell was cycled exclusively at a current density of 80 mA.cm^{-2} for over 50 cycles. In this case, a stable operation was also recorded with energy efficiency in line with the above discussion (figure 60).

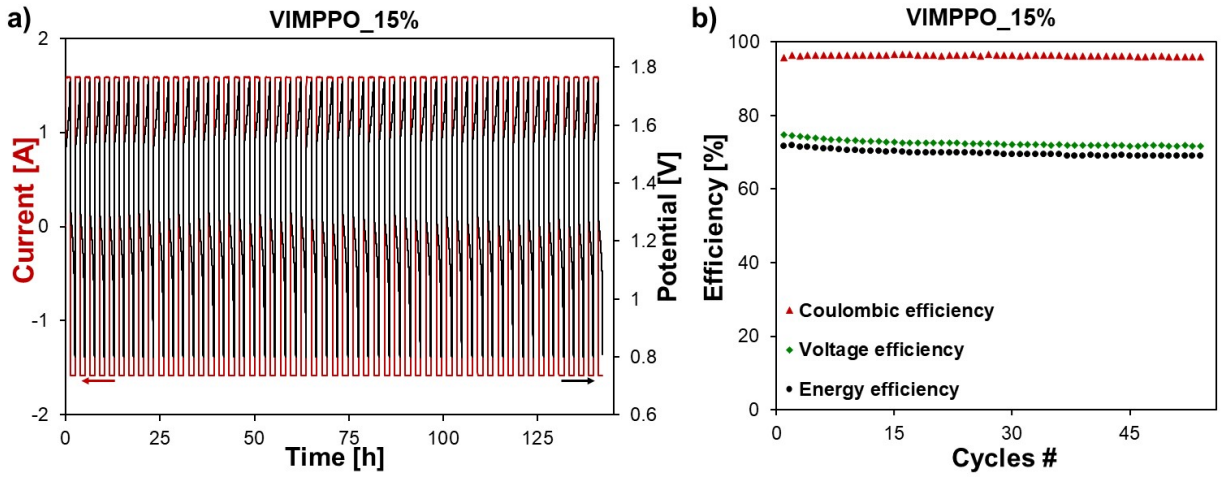

Figure 60. Cycling performance of the VRFB cell assembled with the membrane VIMPPO_15% - over 50 cycles at 80 mA.cm^{-2}: (**a**) charge-discharge curves recorded, (**b**) coulombic, voltage and energy efficiency of the cell.

4.6. Conclusions

The proposed composite hierarchical anion-exchange membranes were able to reach the low, area-specific resistance, and low cation (VO^{2+}) permeability, when formulated for the right level of crosslinking ionomer (VIMPPO). Compiling the characterization and RFB cell cycling results, VIMPPO_15% exhibited the optimal trade-off between the various properties determining the performance of a membrane in a VRFB cell. With 75.1% of energy efficiency at current density 80 $mA.cm^{-2}$, the VIMPPO_15% membrane closely matched the performance of the PFSA-based benchmark cation-exchange membrane N 115 (75.0%) and exceeded the performance of a commercial anion exchange membrane FAP 450 (73.0%). This was seen as an achievement, given that the coated membrane was fabricated in a straightforward manner and utilized in the majority (85 wt.%), low-value materials. Acrylamide monomers are readily available at the chemical reagent market and can be replaced with industrial commodity chemicals - DMAPAA™ or HEAA™ (KJ Chemicals Corporation, Japan). The proposed fabrication method, employing blade coating and UV curing steps, opens direct scale-up possibilities.

Despite the use of non-perfluorinated compounds, the chemical stability of the composite membranes was sufficient for their investigation. Indication of oxidation of the polymerized acrylamide was observed during the VO_2^+ ageing tests but in none of the experiments did the membrane display visible signs of degradation. Experimental data showed that other components of the formulation were less resistant to V(V) than the VIMPPO polymer itself. This aspect will require future attention and possible improvements of the membrane formulation.

This study shows that the ionic transport properties of the composite membrane can be conveniently controlled by changing the amount of VIMPPO used for the fabrication of the ion-exchange coating layer. Decreasing the content of VIMPPO in the coating, resulted in a lower density of crosslinking, and thus, higher water uptake, lower ASR, and higher cation permeability. In this way, the balance between coulombic efficiency and voltage efficiency of the cell could be controlled.

However, the chemical stability of the membrane stays not completely solved. As the ex-situ chemical stability tests indicated that the polyacrylamides are the

main source of oxidative degradation, work was focused on the preparation of the membrane without the use of acrylamide derivatives. This is described in the next chapter.

Chapter 5. Photocured VIMPPO-based anion exchange composite membranes: Study of the spacing monomer nature on the properties of the AEMs and their performance in VRFB

In this study the anion exchange layer was formulated without the use of acrylamide derivatives that were indicated as the source of oxidative degradation of the composite membranes, as described in chapter 2 and chapter 3. Instead, poly(2,6-dimethyl-1,4-phenylene oxide) modified with *N*-vinylimidazole (VIMPPO) was UV-cured with vinyl monomers that upon radical curing were able to loosen the structure of the resulting copolymer. Furthermore, to secure low area resistivity and high content of positively charged groups in the resulting ion exchange coating, the selected monomers possessed quaternary ammonium group.

5.1. Formulation concept

This section describes composite, anion exchange membranes consisting of a porous PVC-silica substrate and a thin layer of photocured vinyl imidazolium poly(phenylene oxide) (VIMPPO) based ionomer on top of it. However, VIMPPO cured alone exhibits too high area-specific resistivity for the application in RFBs due its excessive crosslinking density as described in section 4.2. To improve the ion-conductivity of the ionomer in this study, VIMPPO was formulated in combination with radically reactive monomers with quaternary ammonium moiety and vinyl groups: *N, N*-diallylpiperidinum chloride (DAPCl), (vinylbenzyl) trimethylammonium chloride (VBTC). Such monomers are capable of linear homopolymerization as well as can react with VIMPPO due to their reactivity in radical polymerization [171,189]. Therefore, the density of crosslinking in the resulting polymer layer was modified by the formation of molecular bridges built of VBTC or DAPCl units between the chains of VIMPPO polymer (chemical structures of each of the compounds are presented in figure 61).

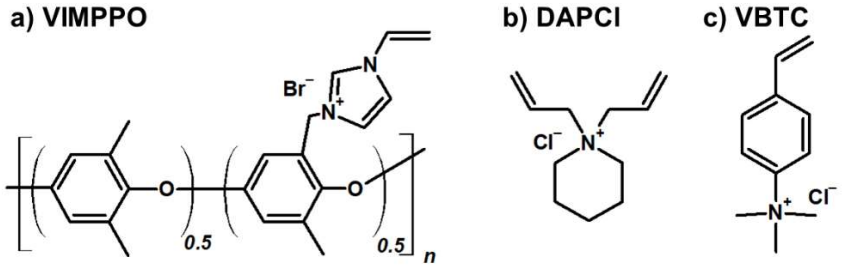

Figure 61. Chemical structures of the poly(2,6-dimethyl-1,4-phenylene oxide) modified with *N*-vinylimidazole – VIMPPO (**a**), *N, N*-diallylpiperidinum chloride – DAPCl (**b**), (Vinylbenzyl) trimethylammonium chloride – VBTC (**c**).

DAPCl and VBTC served as spacing monomers that can balance dimensional stability and simultaneously increase ion exchange capacity. Consequently, increasing the wt.% of those monomers in the coating formulation leads to larger spaces between the PPO backbone. DAPCl was selected owing to its stable quaternary ammonium group [190]. DAPCl was prepared via a two-step process by a nucleophilic substitution reaction as outlined in figure 62, as described in previous work of Tsehaye M. T.*et al.* [189].

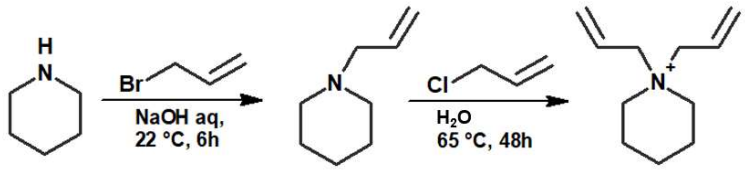

Figure 62. Synthetic procedure for DAPCl.

However, this molecule is not available off-shelves therefore, the commercially available monomer - VBTC was also studied to propose a membrane that can be a more suitable candidate for a potential, industrially oriented scale-up. Two series of membranes with different content of the monomer were fabricated, using the porous PVC-silica separator as support, the commercial product of Amer-sil. The substrate ensured dimensional stability regardless of the changes in the composition of the coating formulation. Thus, the ratio between the monomer and VIMPPO could be changed without restrains related to the need for mechanical properties of the ionomer.

5.2. Fabrication of the composite AEM with VIMPPO UV-cured with spacing monomers

To prepare the composite AEMs, VIMPPO, TPO and the selected monomer were dissolved in methanol. The mixture was sonicated at 40°C for 3 h until a brown, viscous solution was obtained. The wt.% of compounds used in each formulation is shown in table 7. The solution was cooled down to room temperature and applied on top of the porous separator using an automatic blade-coating frame applicator (60 μm gap, BYK GmbH, Germany). After the coating step, the applied mixture was exposed to UV irradiation for 2 min to perform UV initiated radical polymerization and cross-linking. The process was carried out using a conveyor and 2kW iron dopped mercury lamp (365 nm) (Jenton, UK).

Table 7. The composition of the anion exchange, photocured layers: wt.% of each used compound.

Sample	monomer	Content of VIM PPO [w/w %]	Content of monomer [w/w %]	Content of TPO [w/w %]
VIMPPO 100%	none	95	0	5
DAPCl 6%	DAPCl	90	6	4
DAPCl 17%		80	17	3
DAPCl 26%		71	26	3
DAPCl 37%		60	37	3
DAPCl 47%		50	47	3
VBTC 6%	VBTC	90	6	4
VBTC 17%		80	17	3
VBTC 26%		71	26	3
VBTC 37%		60	37	3
VBTC 47%		50	47	3
VBTC 60%		37	60	3

The composite membrane prepared using the monomers were compared to cured alone VIMPPO, coated on the same porous substrate – sample VIMPPO_100%.

The prepared membranes possessed a heterogeneous structure, consisting of two well-distinguishable layers: anion exchange coating (average thickness in the range of 20 – 30 μm) and porous substrate (600 μm), as shown in figure 63.

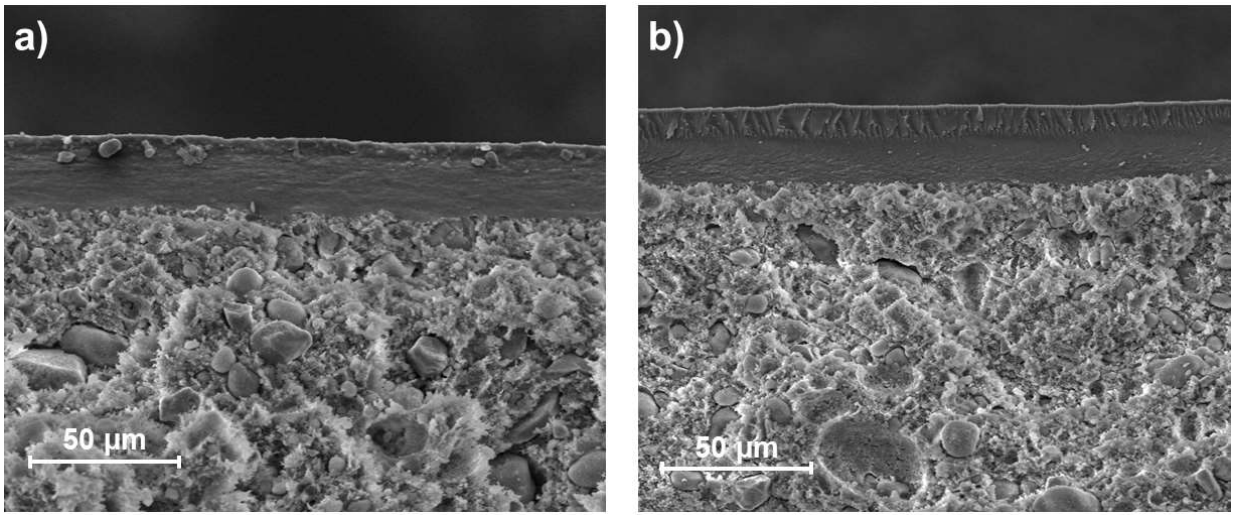

Figure 63. SEM images of cross-sections of the composite membranes with (**a**) 26 wt.% of DAPCl, (**b**) 48 wt.% of VBTC.

Table 8. EDS spectroscopy: content of different elements observed in the EDS spectra recorded for substrate and coating layer for samples: DAPCl 27%, VBTC 48%.

	DAPCl_27%		VBTC_48%	
	coating layer Mass [%]	substrate Mass [%]	coating layer Mass [%]	substrate Mass [%]
C	55.8	40.7	54.9	37.7
N	10.7	0.0	10.8	0.0
O	11.5	27.6	5.9	23.6
Cl	4.6	8.1	5.9	9.0
Br	6.9	0.0	5.9	0.0
Si	0.0	17.4	0.0	16.4
Au	10.1	8.3	14.6	16.3

EDS spectra recorded for the substrate and the coated layers indicated significant differences in the elemental composition between the two layers (table 8). No nitrogen or bromine was detected in the porous substrate, which may indicate that the coating layer was not impregnated inside the pores.

5.3. Characterization of the VIMPPO-based AEMs fabricated using spacing monomers.

5.3.1. Water uptake (WU), ion-exchange capacity (IEC), area specific resistivity (ASR) and permeability to VO^{2+}

The formation of molecular bridges between the VIMPPO chains resulted in the enhanced ability of the coating layer to absorb water (figure 64). VIMPPO cured alone exhibited relatively low WU values. The excessively crosslinked structure of VIMPPO_100% hindered the absorption of water, despite its high content of ionic groups and hydrophilic nature of the PPO backbone.

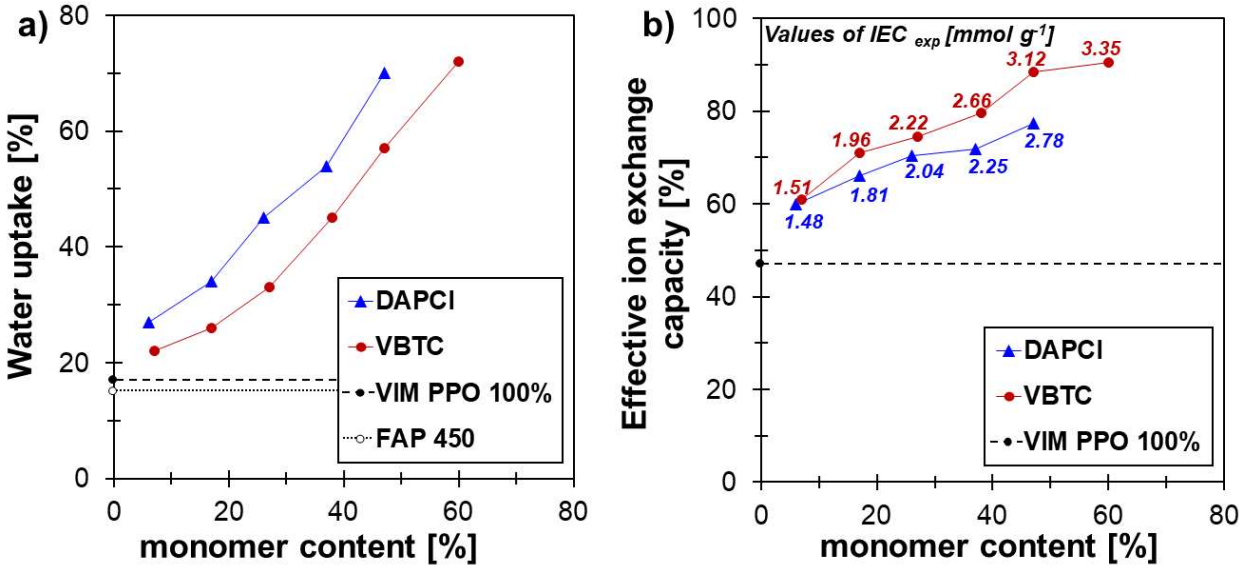

Figure 64. Changes in the properties of the membranes depending on the amount and type of used monomer: (**a**) water uptake in a function of monomer content, (**b**) effective ion exchange capacity in a function of monomer content.

With the increasing content of the spacing monomer, the WU of the resulting layers is gradually raising, reaching values up to 70 % for the membranes fabricated using DAPCl and 72 % for the ones prepared using VBTC. The loosened structure of the ionomer improved the accessibility of the vinyl imidazolium group by the counter-ions. VIMPPO cured alone exhibited only 50% of the theoretical ion exchange capacity (figure 61b) due to the steric hindrance caused by its densely cross-linked structure. The incorporation of spacing monomers increased the

effective ion-exchange capacity allowing to reach 77 % in the case of DAPCl and even 91 % using VBTC monomer.

The water uptake is well correlated with the crosslinking density of the ionomer, thus can be used as an indirect parameter that represents the influence of loosened structure on area-specific resistivity (ASR) and permeability to VO^{2+} (figure 65).

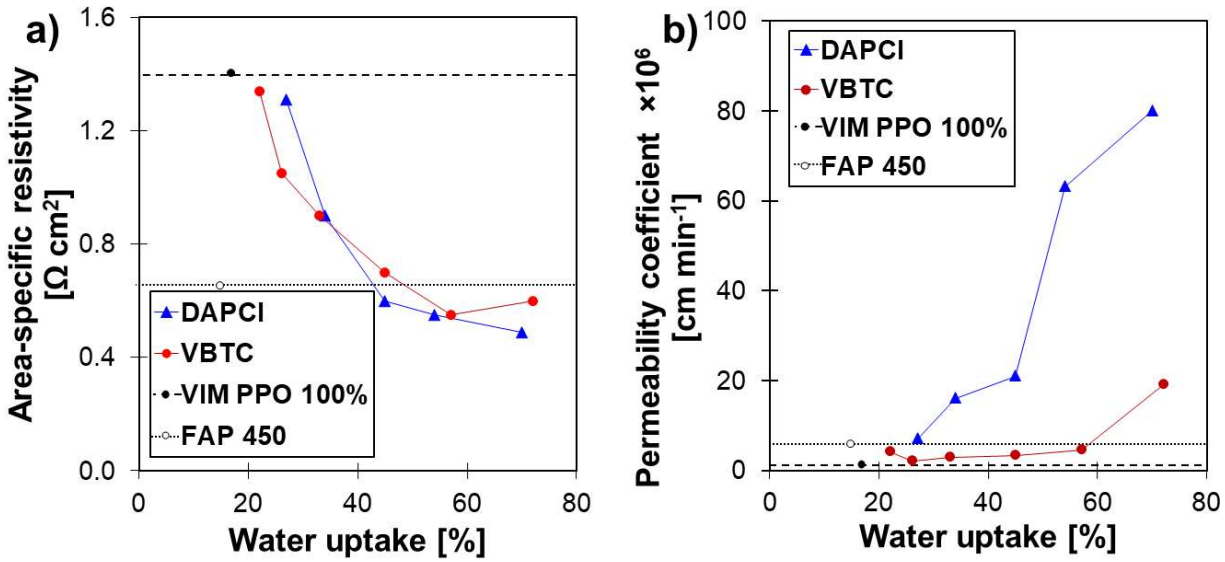

Figure 65. Ionic transport properties as a function of water uptake: (**a**) Area specific resistivity (measured in 1 M HCl_{aq} at current scan rate of 10 $mA.s^{-1}$), and (**b**) coefficients of VO^{2+} cations permeability.

Formulating VIMPPO with the spacing monomers diminished at least four times the resistivity of the composite membranes compared to the VIMPPO_100% sample (figure 65a), due to the substantial difference in the ionomer structure and water sorption properties. The composite membranes with WU higher than 40% exhibited ASR values comparable to the one of the commercial AEM – FAP 450 (0.55 – 0.7 $\Omega.cm^2$ versus 0.65 $\Omega.cm^2$). Further increase of WU resulted only in marginal changes of the membrane resistivity.

Figure 65b shows a strong correlation between water uptake and permeability of the membranes. In the case of the DAPCl monomer, the incorporation of only 7 wt.% of the monomer led to significantly higher permeability of the membrane. Further increase of the DAPCl content, resulted in dramatically faster VO^{2+} permeation, despite raising content of positively charged anion-exchange groups

in the ionomer and almost 80% of the effective IEC. Contrarily, the use of VBTC monomer did not significantly increase the permeability until the water uptake values for the coating layer exceeded 65%.

The two contradictory trends, i.e. decrease of ASR and increase of permeability as a function of water uptake, allowed determining the optimal range of WU in which the balance between ion selectivity and conductivity can be reached. In the range of 40 – 60 % of water uptake values, the composite membranes exhibited ionic-transport properties closely matching the one of benchmark AEM – FAP 450. Therefore, membranes: DAPCl_27% (WU 45%) and VBTC_48% (WU 57%), were selected for further performance testing chemical stability and applicability in the energy storage device – RFB.

5.3.2. Chemical stability in solution of VO_2^+ cations

Vanadium electrolyte is known to be a harsh environment due to the oxidative character of charged positive electrolyte (VO_2^+) and high acidity (1 – 3 M sulfuric acid). To evaluate the resistivity against oxidative degradation, four membranes samples were placed in a 1.6 M solution of VO_2^+ in 2 M sulfuric acid: DAPCl_27, VBTC_48 and VIMPPO_100%. The generation of VO^{2+} was the lowest in the case of the VIMPPO_100% membrane (figure 66) and the oxidation happened in the majority within the first 100 h. At longer times, no significant increase in VO^{2+} concentration in the solution with immersed VIMPPO_100% sample was observed. This can be due to the high crosslinking density of the ionomer. As a result, the ionic polymer absorbed less of the ageing solution, thus the number of oxidative species that can attack the polymer was limited.

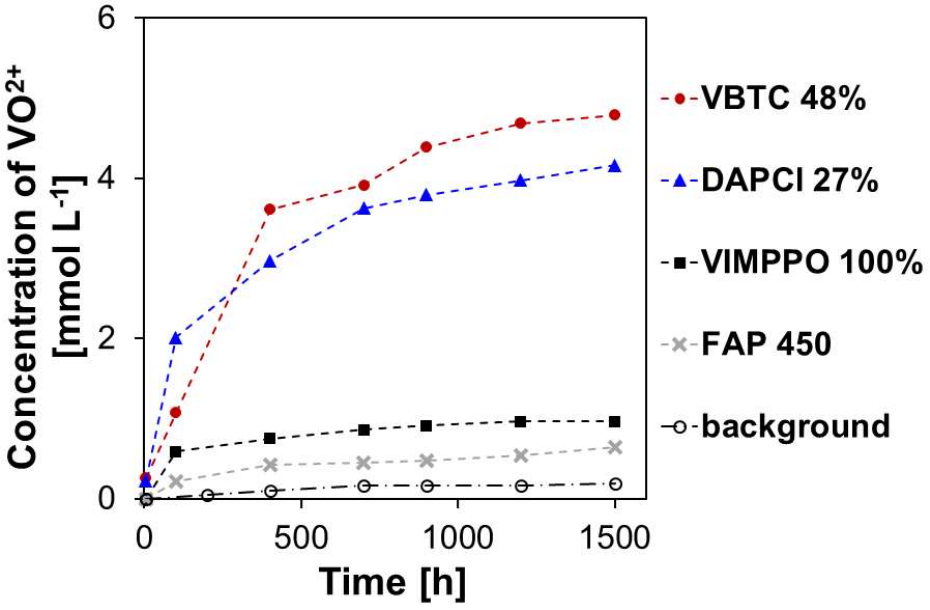

Figure 66. Concentration of VO^{2+} calculated based on the changes in the VO_2^+ absorbance intensity (775 nm) monitored over 1500 h.

Decreased crosslinking density of VIMPPO facilitated oxidative degradation. Membranes with the spacing monomers were oxidized mainly within 200 h after immersing in the ageing solution. After that, the reactions were significantly slowed down. In comparison to the membranes described in chapter 4, the membranes prepared without the acrylamide-based monomers exhibited improved chemical stability. After 1500 h of the exposure membranes to VO_2^+, the concentration of generated VO^{2+} ions is approximately twice lower in the case of membranes DAPCl_27% and VBTC_48% in comparison to the membrane VIMPPO_20% - the most chemically stable one among the membranes described in chapter 4 (figure 56a).

5.4. VRFB performance of VIMPPO-based composite AEM fabricated using spacing monomers

A single-cell was used to evaluate the performance of the composite membranes in an All-Vanadium redox flow battery cell. The cycling tests were carried out at three current densities: 20 (2 cycles), 50 (7 cycles) and 80 $mA.cm^{-2}$ (7 cycles) with 60 mL of vanadium electrolyte in each of the reservoirs. Therefore, the experiments lasted for c.a. 5 – 6 days and were repeated twice for each of the samples: membranes

VBTC_48% and DAPCL_27 % as the best-performing ones among the two studied series of the composite AEMs in terms of low ASR and low permeability.

The two listed membranes were compared to the commercial IEM (FAP 450, Nafion® N 115) and the VIMPPO_100% sample. Table 9 reports coulombic efficiency (CE), voltage efficiency (VE), and energy efficiency (EE) exhibited by the cells assembled with different membranes.

Table 9. Average coulombic (CE), voltage (VE) and energy efficiency (EE) of VBTC_48%, DAPCl_27%, VIMPPO_100% membranes and benchmark IEMs: FAP 450 and N115 tested at three different current densities: 20, 50 and 80 mA.cm^{-2}.

Current density	20 mA.cm^{-2}			50 mA.cm^{-2}			80 mA.cm^{-2}		
membrane	CE average [%]	VE average [%]	EE average [%]	CE average [%]	VE average [%]	EE average [%]	CE average [%]	VE average [%]	EE average [%]
FAP 450	95.4	92.5	88.2	97.9	82.5	80.8	98.3	74.3	73.0
N 115	96.4	92.9	89.9	98.1	83.7	82.6	98.5	76.4	75.0
VBTC 48%	95.6	94.4	90.2	98.3	86.8	85.3	98.4	78.7	77.4
DAPCl 27%	95.1	94.1	89.5	96.5	85.9	82.9	97.0	77.2	74.9
VIMPPO 100%	99.8	86.0	85.9	99.2	67.2	66.7	99.5	54.3	53.7

The cell with VIMPPO_100% membrane exhibited the worst overall cycling performance at all applied current density, EE: 85.9%, 66.7% and 53.7% at 20, 50 and 80 mA.cm^{-2}, respectively. The poor performance was caused by the excessive resistivity of VIMPPO_100%. Especially at higher current density, resulted in dramatic ohmic losses leading to low VE: 67.2% and 54.3% at 50 and 80 mA.cm^{-2}, respectively. Such poor voltage efficiency could not be compensated by the excellent CE, the highest among all tested membranes, above 99% at all applied current densities. Modifying the ionomer structure by the incorporation of spacing monomer significantly enhanced the performance of the composite membrane owing to the decreased resistivity. As a result, both VBTC_48% and DAPCl_27% reached higher voltage efficiency than in the case of the FAP 450 membrane and

N115. The VBTC_48% exhibited the best EE – 77.4% at 80 mA.cm^{-2}, 85.3 % at 50 mA.cm^{-2} and 90.2 % at 20 mA.cm^{-2}. The EE reached by the cell assembled with DAPCl_27% closely matched the performance of benchmark IEMs: DAPCl 27% - 74.9%, N115 - 75.0%, FAP 450 – 73.0% at 80 mA.cm^{-2}. However, the cell assembled with DAPCl_27% shown the lowest CE among all tested membranes due to unsatisfactory prevention of vanadium crossover. These results were found in good correlation with the data obtained from permeability experiments as well as in the discharge capacity (figure 67a). The VBTC_48% membrane allow for a good capacity retention in line with the benchmark membranes (N 115 and FAP 450). The ability to diminish the permeation of different vanadium species (VO_2^+, V_3^+, V_2^+, VO^{2+} across the membrane was studied in a self-discharge experiment using VRFB single cell. The open-circuit voltage of a charged cell mounted with the composite membranes and the commercial AEM (figure 67b) was monitored until it dropped down to 0.8 V.

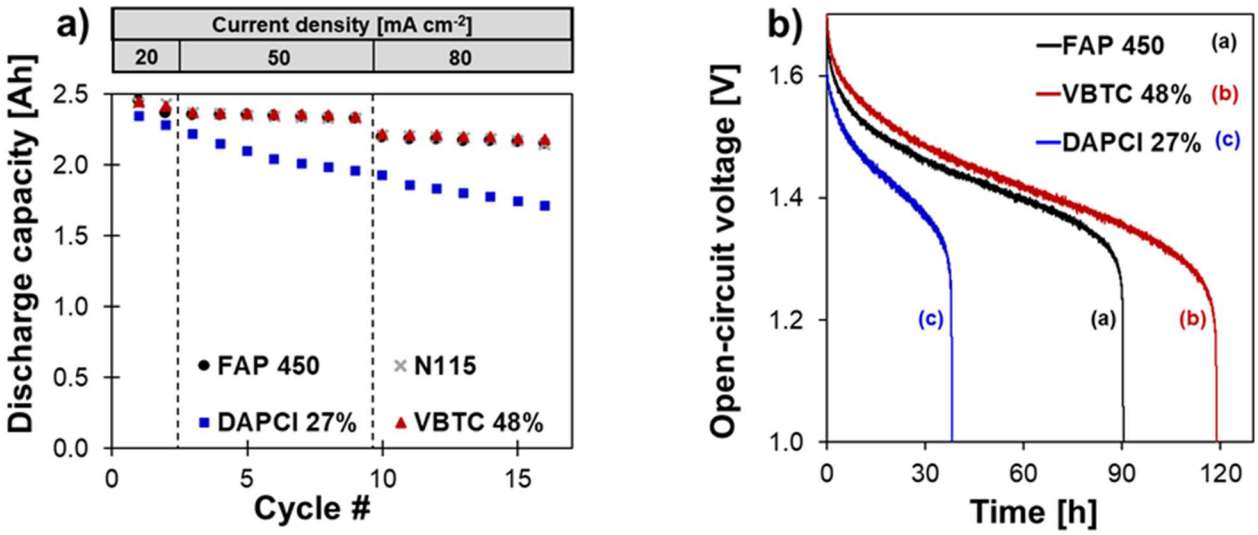

Figure 67. (**a**) Discharge capacity calculated for FAP 450, N 115, VBTC_48% and DAPCl_27% during the cycling experiments at three current densities: 20 mA.cm^{-2}, 50 mA.cm^{-2} and 80 mA.cm^{-2}. (**b**) Open-circuit voltage curves in function of time (self-discharge curves) recorded for FAP 450 and the composite membranes: VBTC_48% and DAPCl_27%.

VBTC_48% allowed for the longest self-discharge among the other tested membranes, being the only composite membrane that exceeded the results of FAP 450 membrane. In the case of VBTC_48%, the charge was retained for 119 h, while with FAP 450 for 92 h. DAPCl_27% membrane retained the cell charge for only 36

h. The shortest time of the self-discharge in the case of DAPCL_27% is in line with the result observed during permeability experiments and cycling performance (CE and discharge capacity).

Taking into account the cell performance, stability data and the results of the self-discharge experiments, the VBTC_48% membrane was considered as the optimum one that exhibited an excellent balance between ion conductivity, perm-selectivity and chemical stability. Therefore, this membrane was further investigated in a long-term performance test, 75 cycles at 50 mA.cm^{-2}. Figure 68 shows the performance of VBTC_48% during the long-term cycling experiment, compared to the commercial membrane FAP 450.

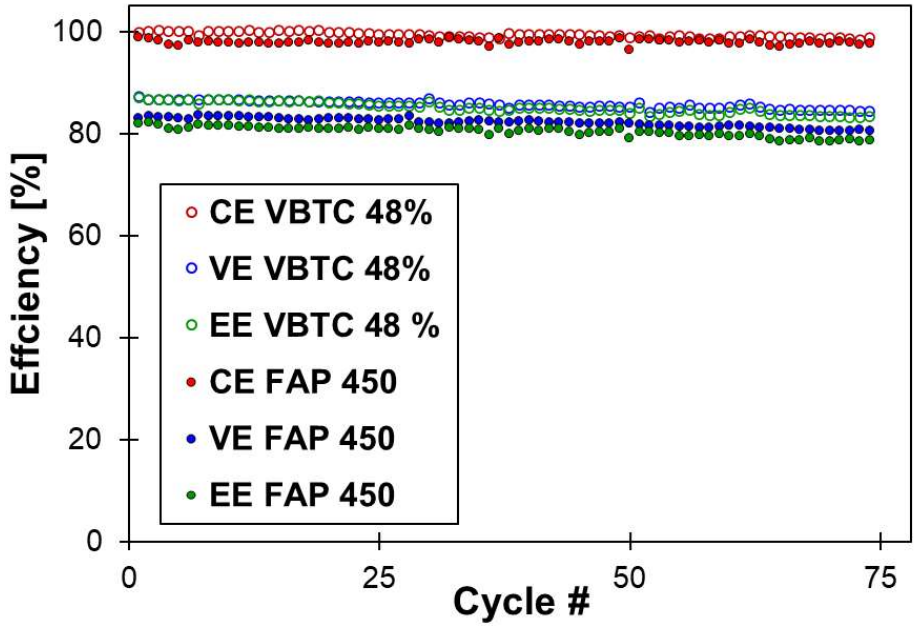

Figure 68. Efficiencies of the VRFB cell assembled with VBTC_48% and FAP 450 during 75 cycles at 50 mA.cm^{-2}, 70 mL in each of the electrolyte's tanks, CE-coulombic efficiency, VE-voltage efficiency, EE- energy efficiency.

The cell assembled with VBTC_48% exhibited improved cycling performance in comparison to the benchmark FAP 450 membrane. The composite membrane reached an average CE of 98.6% while the commercial AEM – 97.8%. The main enhancement of the membrane's performance is related to the VE: 85.6 % vs 82.0% for a cell with VBTC_48% and FAP 450, respectively. As a result, the overall average EE of the composite membrane is 4.2 %, higher in comparison to the benchmark membrane: 84.4% vs 80.2%.

5.5. Conclusions

Series of composite membranes with anion-exchange coatings based on VIMPPO and different content of the monomer (DAPCl or VBTC) in the coating layer were obtained in a straightforward process that involved blade coating and UV curing. The incorporation of UV-reactive monomer allowed to conveniently tune the resistivity and perm-selectivity of the composite membrane without the need for synthesis of an entirely new ionomer. Among the prepared composite membranes VBTC_48% exhibited the best ionic transport properties, exceeding the results of benchmark AEM. The performance tests carried out in a VRFB single-cell indicated that VBTC_48% membrane was the best performing membrane in terms of overall cell performance reaching an energy efficiency of 77.4% at 80 $mA.cm^{-2}$, which was higher than in the case of the commercial IEMs (N 115: 75.0 %, FAP 450: 73.0 %). In the self-discharge experiment, the VBTC_48% allowed retaining the cell charge for the longest time among the tested membranes, proving its low permeability to vanadium cations. The presented facile fabrication method and excellent performance make the VBTC_48% composite membrane a promising candidate for VRFB application.

Chapter 6. General conclusions and outlook

During this PhD project composite anion-exchange membranes (AEMs) have been prepared and characterized by adapting literature studies on porous membranes and ion-exchange polymer synthesis. Ion-transport properties such as water uptake, area specific resistance, permeability and ion-exchange capacity were characterized in order to find the relation between the chemical composition of the ion-exchange layer and membrane parameters. The performance of the AEMs in an energy storage device was tested in a vanadium redox flow battery (VRFB), since VRFBs are considered one of the most mature and studied flow batteries system. A commercial product of Amer-sil – PVC-silica porous separator (600 μm, median pore size – 83 nm, volume porosity 63.4 %) was used as a support for a layer of anion-exchange coating. Having a porous substrate as a mechanical reinforcement allow using ion-exchange materials that do not possess sufficient mechanical stability to form a self-standing membrane. Moreover, the ion-exchange layer can be a highly hydrophilic material thus, well ion-conductive because the dimensional stability of the entire membrane was secured by the porous substrate. As a result, the ion-exchange layer was formulated using low-cost monomer and polymers leading to low-cost material of the final AEM. The membranes were obtained in a simple fabrication process that consists of a blade coating step and UV-curing step. The fabrication methods are easily scalable as they are widely present in the coating industry including commodity sectors such as paper production, packaging, printing, etc., and often used in a roll-to-roll production set-up. Depending on the used chemical reagents for the ion-exchange layer, three types of the composite AEMs were studied. The optimal formulations for each type were found in the following membranes: PVP_8%, PVP_14%, VIMPPO_15% and VBTC_48%. The summary of their most characteristic properties and cycling performance is presented in table 10 and figure 69.

Table 10. Ion transport properties: water uptake (WU), area-specific resistivity (ASR), charge retention – results of the self-discharge experiment and cycling performance (coulombic and energy efficiency at 80 mA.cm^{-2}) of the composite AEMs: PVP_8%, PVP_14%, VIMPPO_20% and VBTC_48% compared with the one of commercial membrane FAP 450.

	WU [%]	ASR [mΩ cm^2]	Time of charge retention in the self-discharge experiment [h]	Cycling performance at 80 mA.cm^{-2}	
				Coulombic efficiency [%]	Energy efficiency [%]
PVP_8%	73	0.97	59	99.1	73.3
PVP_14%	83	0.71	35	94.9	74.7
VIMPPO_15%	47	0.69	39	97.9	75.1
VBTC_48%	57	0.55	119	98.4	77.4
Reference: FAP 450	*15*	*0.58*	*92*	*98.3*	*72.7*

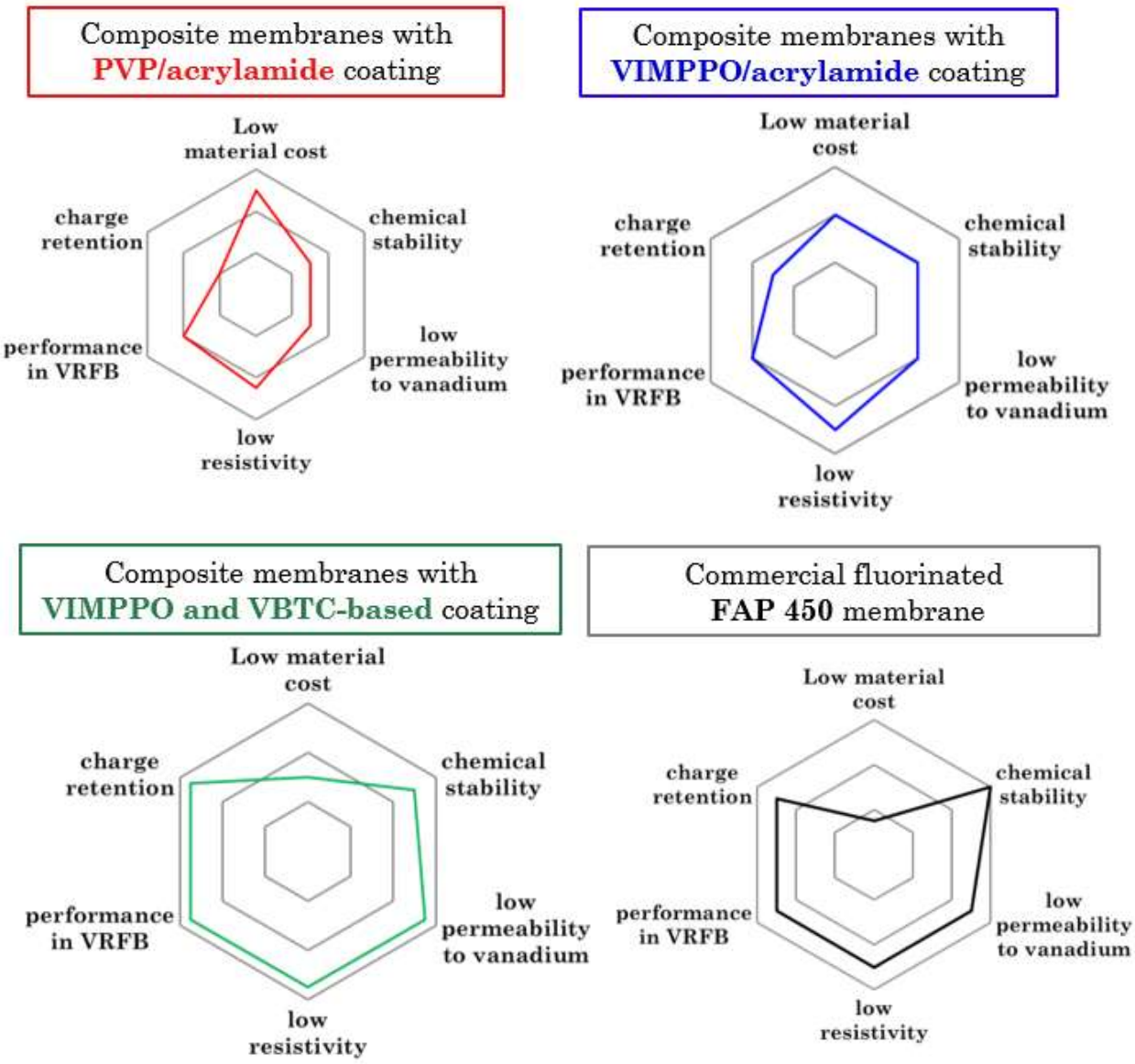

Figure 69. Comparison of the three types of composite AEMs and the commercial FAP 450.

Firstly, the anion-exchange layer was formulated using only low-cost, commodity reagents: PVP, acrylamide-based monomers and acrylated resin. The water-soluble PVP ensured high hydrophilicity of the coating layer and can potentially contribute to the ion-exchange capacity of the membrane. The pyrrolidone segments can undergo protonation in highly acidic media such as electrolyte in the vanadium redox flow batteries. To prevent PVP from dissolving in the aqueous electrolyte, the layer was formulated using UV-reactive monomers and crosslinking resin in order to immobilize the water-soluble polymer. The UV irradiation initiates radical polymerization of the precursors mixture that formed an interpenetrating polymer network with PVP densely entangled in its structure.

The ion-transport properties of the PVP/acrylamide-based membranes were tuned by changing the content of PVP. Membranes with 14 wt.% of PVP exhibited low area specific resistivity thus, excellent voltage efficiency – 78.7% at 80 mA.cm^{-2} on the cost of permeability to vanadium cations leading to a compromised coulombic efficiency 94.9%. The overall energy efficiency of such membrane matched the performance of a commercially available benchmarked AEM- FAP 450: 74.7% vs 72.7% for PVP_14% and FAP 450, respectively. The use of lower content of PVP – 8 wt.% led to lower voltage efficiency 73.9% and improved coulombic efficiency 99.1 and overall energy efficiency of 73.3% (efficiency values at 80 mA.cm^{-2}). However, the ex-situ stability tests in VO_2^+ indicate an oxidative degradation of the membrane. This affects the long-term membrane performance. Moreover, the self-discharge results of the VRFB cells mounted with the composite PVP-based membranes indicated a significant vanadium species crossover across the membranes leading to capacity decay and misbalanced electrolyte. In the second approach a vinyl imidazolium poly(phenylene oxide) (VIMPPO) polymer was synthesized and used as a anion-exchange polymer and a crosslinking agent. To minimize the material cost, the content of VIMPPO was kept at maximum 25 wt.% by crosslinking it with low-value acrylamide-based monomers. As a result, such membranes allowed reaching much lower vanadium permeability and low area specific resistivity. Membrane with 15 wt.% content of the VIMPPO in the coating layer enable to reach both high voltage efficiency and high coulombic efficiency (76.8%, 98.0% at 80 mA.cm^{-2}). The overall battery performance of a cell assembled with membrane VIMPPO_15% reached 75.2% of energy efficiency at 80 mA.cm^{-2}. The capacity retention trend followed the evolution of data obtained for commercial membranes (Fumasep® FAP 450 and Nafion® N 115). The long-term cycling experiment (50 cycles and 80 mA.cm^{-2}) showed stable cycling performance of the membrane. However, the ex-situ vanadium stability tests indicated signs of oxidative degradation. Moreover, the self-discharge experiment still indicated a significantly faster rate of the vanadium crossover than in the case of commercial FAP 450 (35 h in the case of VIMPPO_15% versus 92 h recorded for FAP 450). Therefore, in a third approach the anion-exchange layer was made with a majority of the VIMPPO ionomer. However, cured alone, VIMPPO exhibits excessive

crosslinking degree and thus, high area specific resistivity. The chemical structure of the VIMPPO was modified by formulating the polymer with monomers (DAPCl or VBTC) that upon UV curing can form a spacing bridge between the VIMPPO chains. The selected monomers also contributed to the ion-exchange capacity as they possess quaternary ammonium moieties. Thus, the resulting anion exchange layer possessed high crosslinking degree and exceptional ion exchange capacity, reaching the value of 3.2 $mmol.g^{-1}$. Such membrane exhibited remarkable low vanadium permeability and low area specific resistivity, exceeding the performance of commercial IEMs. The cycling tests carried out using the composite membrane VBTC_48% reached the best overall performance among all previously tested membranes: coulombic efficiency 98.5%, voltage efficiency 78.7 % and energy efficiency 77.4% at 80 $mA.cm^{-2}$. Moreover, the self-discharge experiment indicated that the VBTC_48% membrane shows improved capacity retention than in the case of commercial AEM. Long-term cycling experiments (75 cycles at 50 $mA.cm^{-2}$) demonstrated excellent, stable performance of the composite membrane and higher efficiencies of the cell in comparison to the cell with commercial membrane FAP 450. The results prove that the presented VIMPPO/VBTC composite AEMs can be considered as a well-performing alternative to the commercially available high-value ion exchange membranes.

However, despite the promising cycling performance of the proposed membrane and its improved chemical stability in comparison to the composite membranes prepared using acrylamide-based monomers, still the oxidative degradation of the membrane remains challenging. Thus, future research should focus on improving the membrane resistivity against oxidative environment. As a potential solution, we can propose the incorporation of low-value fluorinated polymers such as polyvinylidene fluoride as a part of the ion exchange layer.

Appendix – plasma deposited membranes

A.1. Introduction

Beside commonly known wet coating methods, another option to develop an anion-exchange coating is the use of plasma polymerization. In case of this technique, the polymerization is performed from gas phase so the polymeric layer is directly deposited on the substrate. This process allows modifying only the surface, not affecting the whole substrate. Therefore, the method appears to be a very promising way to coat the porous substrate since it does not allow the monomers to penetrate the substrate, thus there is no risk of blocking pores. Furthermore, under plasma polymerization conditions very thin layers of polymeric coatings can be easily formed. In this study, the aim was to deposit ultra-thin plasma polymeric layer on top of porous PVC-silica separator that would remain flexible. Therefore, three amino derivatives of silanes were selected: (3-Aminopropyl)triethoxysilane (**APTES**), *N*-[3-(Trimethoxysilyl)propyl]ethylenediamine (**DiAmSil**), *N*-1-(3-Trimethoxysilylpropyl)-diethyleneetriamine (**TriAmSil**). The chemical structure of the compounds is presented in figure 70.

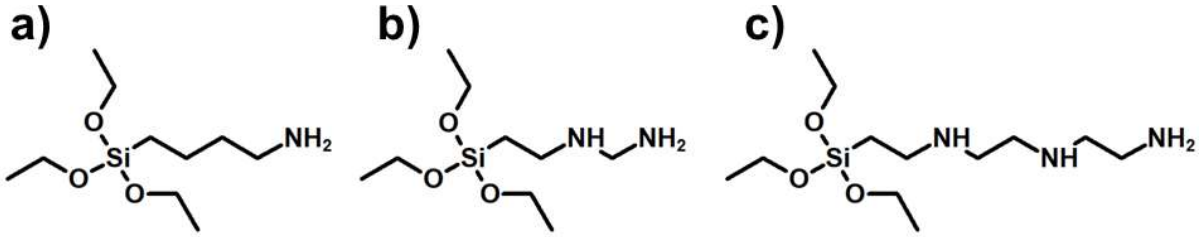

Figure 70. Chemical structure of (**a**) aminopropyl)triethoxysilane (**APTES**), (**b**) *N*-[3-(Trimethoxysilyl)propyl]ethylenediamine (**DiAmSil**) and (**c**) *N*-1-(3-Trimethoxysilylpropyl)diethyleneetriamine (**TriAmSil**).

A.2. Experimental – the setup for plasma treatment

The plasma deposited membranes were deposited using radiofrequency plasma. Samples of the PVC-silica separator (25 mm x 75 mm (± 1 mm)) were

placed in a quartz tube-reactor of the plasma setup in two different configurations. The setup was composed of a tubular quartz reactor, pumping unit, radiofrequency plasma generator, hydrogen, oxygen, argon and nitrogen circuits and a reservoir with the selected precursor (scheme presented in figure 71).

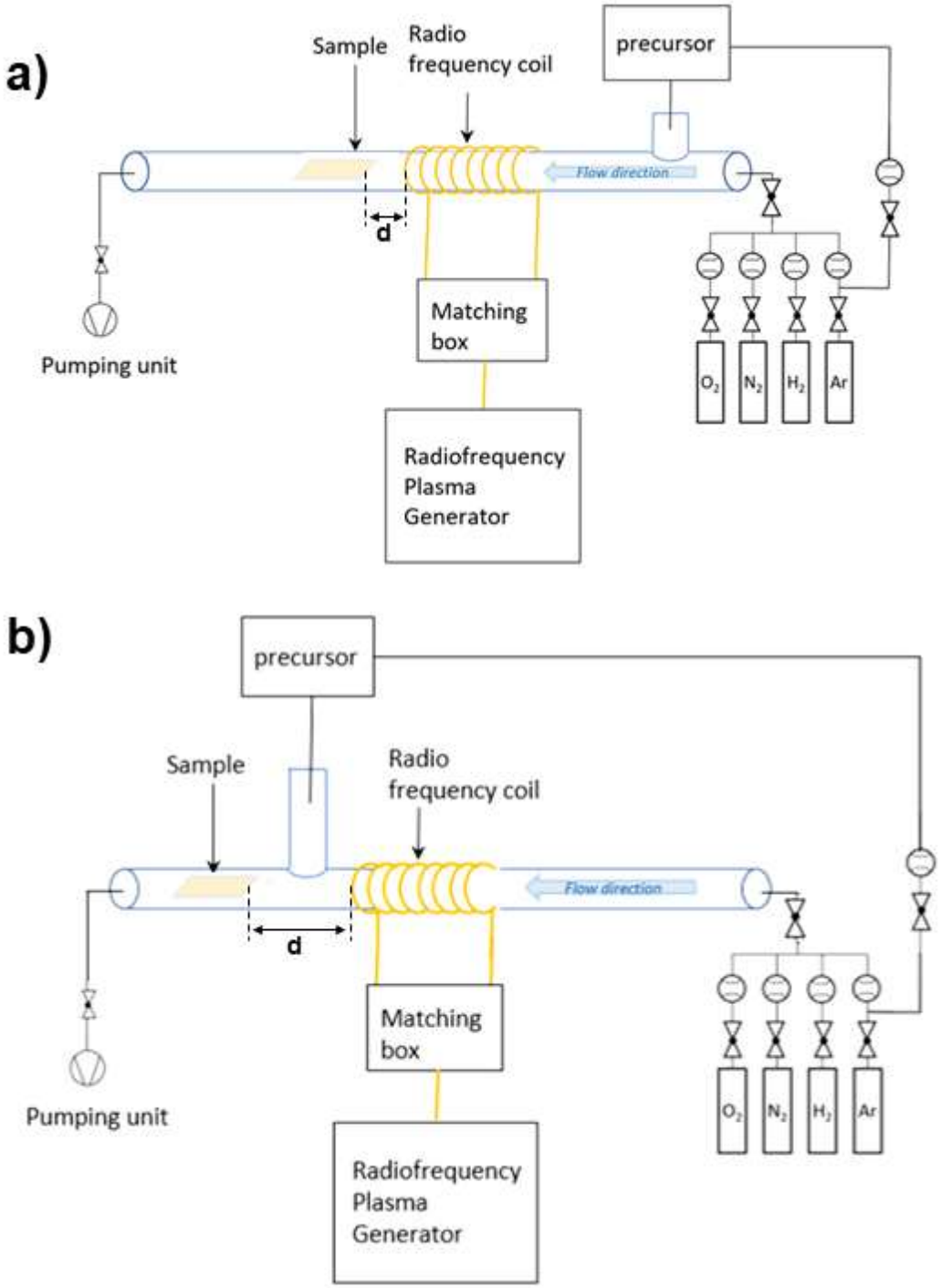

figure 71. Radiofrequency plasma setup in two configurations: (**a**) configuration I with the precursor's injection before radio frequency coil, (**b**) configuration II with the precursor's injection before radio frequency coil.

A.3. Deposition of APTES

The samples of porous separator were placed at different position: the distance between the edge of sample and the coil (d) was varied from 2 cm to c.a. 24 cm. The porous substrate was treated at low pressure (max 5 mbar) in Argon atmosphere or Argon/Nitrogen atmosphere. APTES was used as the simplest silane derivative to optimize conditions of the plasma experiments i.e. configuration of the plasma setup, input power of the plasma, composition of the plasma-atmosphere and the distance from the source of plasma. In the first step, two configurations were tested using APTES at argon atmosphere (0.3 slm). The precursor was heated at 90 °C. The deposition time was set at 60 min and the input RF power was fixed at 40 W. As a simple parameter that indicates the rate of deposition, the mass gain - ρ in $mg.cm^{-2}$ was used. Figure 72, shows that the mass of deposited material during plasma treatment is significantly higher in the case of putting the sample in configuration II than I.

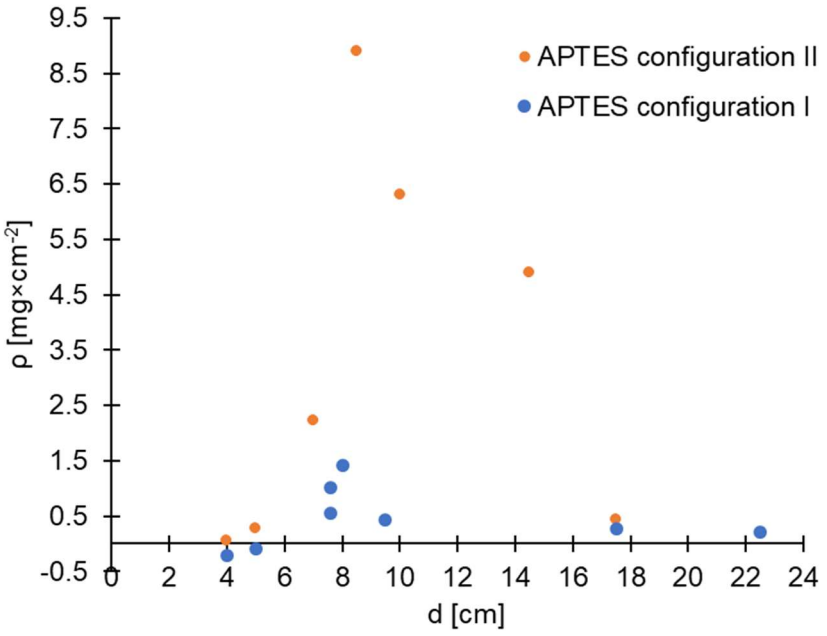

Figure 72. Mass gain (ρ) in a function of distance of the sample from the source of plasma (coil): comparison of two types of the plasma setup configuration.

Samples placed at distance of 8 cm form the coil in both configurations were observed under SEM with coupled energy-dispersive X-ray spectroscopy (EDS).

Figures 73 clearly indicates the difference between the untreated separator, the one treated with APTES in configuration I and configuration II.

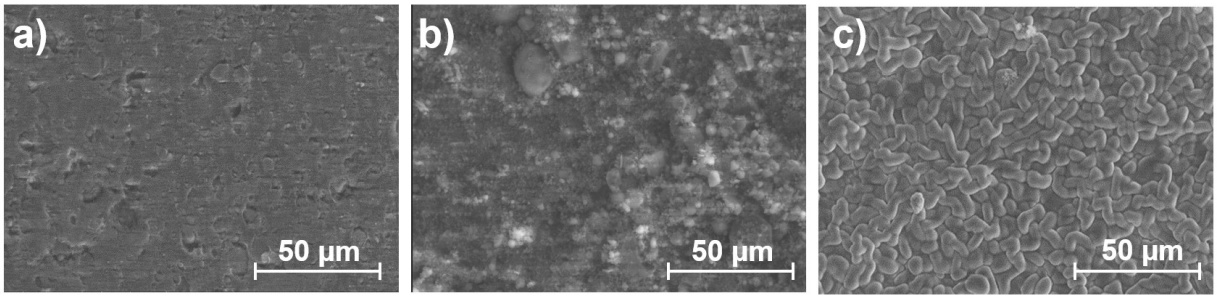

Figure 73. SEM surface images of the untreated sample (**a**), sample treated with APTES in configuration I (**b**) and sample treated with APTES in configuration II (**c**).

Samples treated in the configuration II possesses more uniformly deposited layer than in configuration I. Moreover, the EDX analysis (table 11) shows a higher deposition of Nitrogen containing group when the samples are treated in configuration II. In addition, almost no chloride is observed when the precursor is injected after the source of plasma. Thus, it can be concluded that the PVC-silica separator was completely covered with the new layer for plasma deposited material.

Table 11. EDX analysis of the surfaces of untreated separator, separator treated in configuration I and configuration II.

Sample	**C %**	**N %**	**O%**	**Si %**	**Cl%**
APTES Precursor before plasma	37.41	**7.18**	36.26	16.85	2.1
APTES Precursor in the afterglow	38.97	**11.55**	35.98	13.3	0.19
Untreated separator	28.9	**0**	37.86	21.05	11.92

In order to optimize the conditions of the plasma treatment samples were treated at different gas composition, different power and duration of the treatment (figure 74).

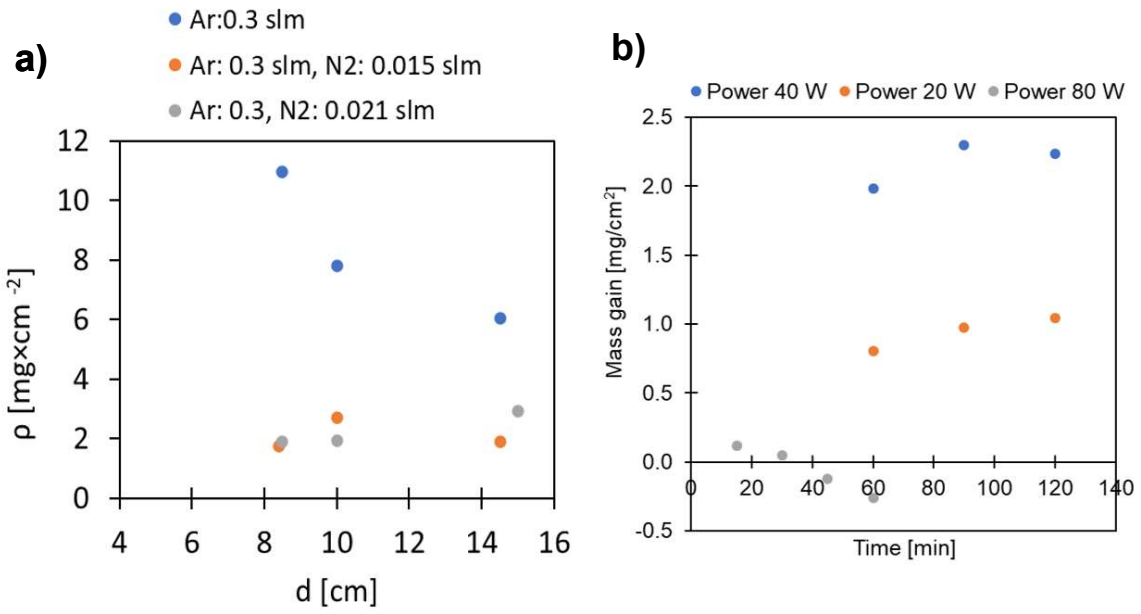

Figure 74. Mass gain ρ of the plasma treated samples at different conditions of the plasma experiment: (**a**) mass gain as a function of distance from the source plasma for different gas composition, (**b**) mass gain as a function of the treatment time for different RF power.

The highest mass deposition was observed when the sample was treated in the atmosphere of Argon (0.3 slm), a power of plasma of 40 W and when the duration of the experiment was set to 90 min. However, the samples were excessively brittle after the plasma treatments and some cracks on their surface were observed during SEM observation as showed in figure 75.

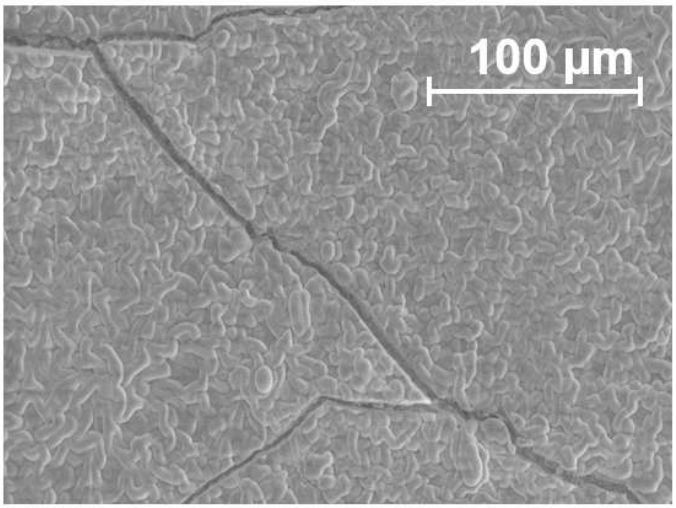

Figure 75. Surface SEM image of sample treated with APTES (power – 40 W, time – 90 min, configuration II).

Sample APT_90 was selected for further characterisation of its ionic-transport properties: permeability and resistivity.

A.4. Deposition of DiAmSil and TriAmSil

Following the results obtained using APTES precursor two other compounds were tested: DiAmSil and TriAmSil. Both of them were selected owing to the additional amine group that was expected to reduce the brittleness of the samples owing to the longer aliphatic chain with additional amine groups attached to the silicon atom. The precursors were heated at 90 °C and injected after the source of plasma (in the afterglow) – configuration II. The sample was inserted at 8 cm from the source of plasma. The precursors were deposited at 5-6 mbars in Argon atmosphere. The deposition of both precursors was much lower in comparison to the mass gain achieved using APTES (max. 1.2 $mg.cm^{-2}$ vs max. 10 $mg.cm^{-2}$ for APTES). The samples were less brittle. However, SEM images of their surfaces indicated that the deposition was not complete for TriAmSil (figure 76a) while the surface of sample treated with DiAmSil (figure 76b) had much different appearance than in the case of APTES.

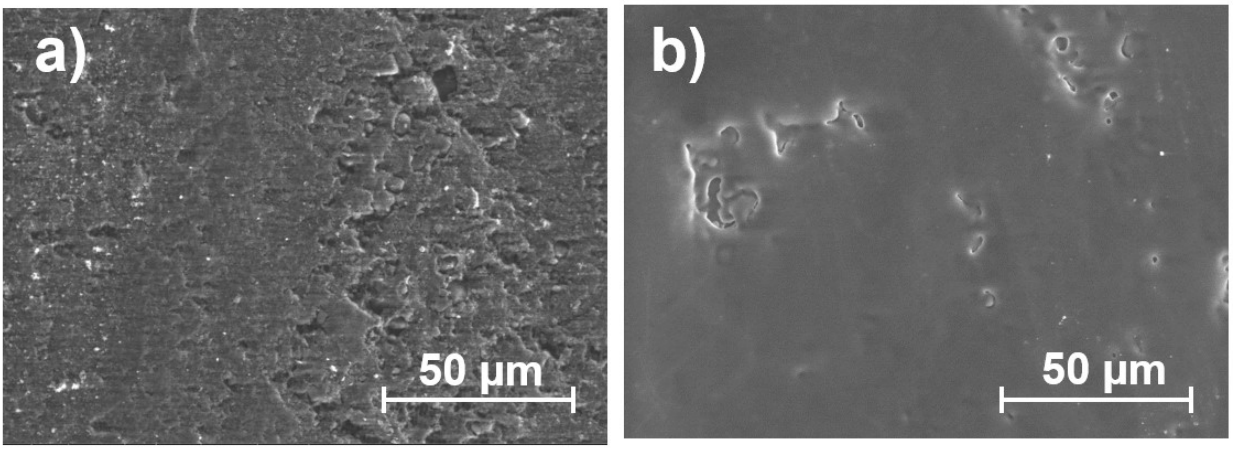

Figure 76. Surface SEM image of sample treated with TriAmSil (**a**) and DiAmSil (**b**) (power – 40 W, time – 90 min, configuration II).

A.5. Co-deposition of APTES and HMDSO

In order to improve the flexibility of the samples deposited using APTES, the aim was to deposit two precursors at the same time: APTES and hexamethyldisiloxane (HMDSO). HMDSO has been already studied by Joanna Rogińska [191]. Samples of porous PVC-Silica separator treated in radiofrequency plasma using HMDSO did not exhibit brittleness and possessed satisfactory mechanical properties. However, such samples were too resistive for the application in redox flow batteries, as the pores of substrate were completely blocked and not permeable to any ions. The plasma setup was modified in order to allow the injection of two precursors at once in the afterglow as presented in figure 77.

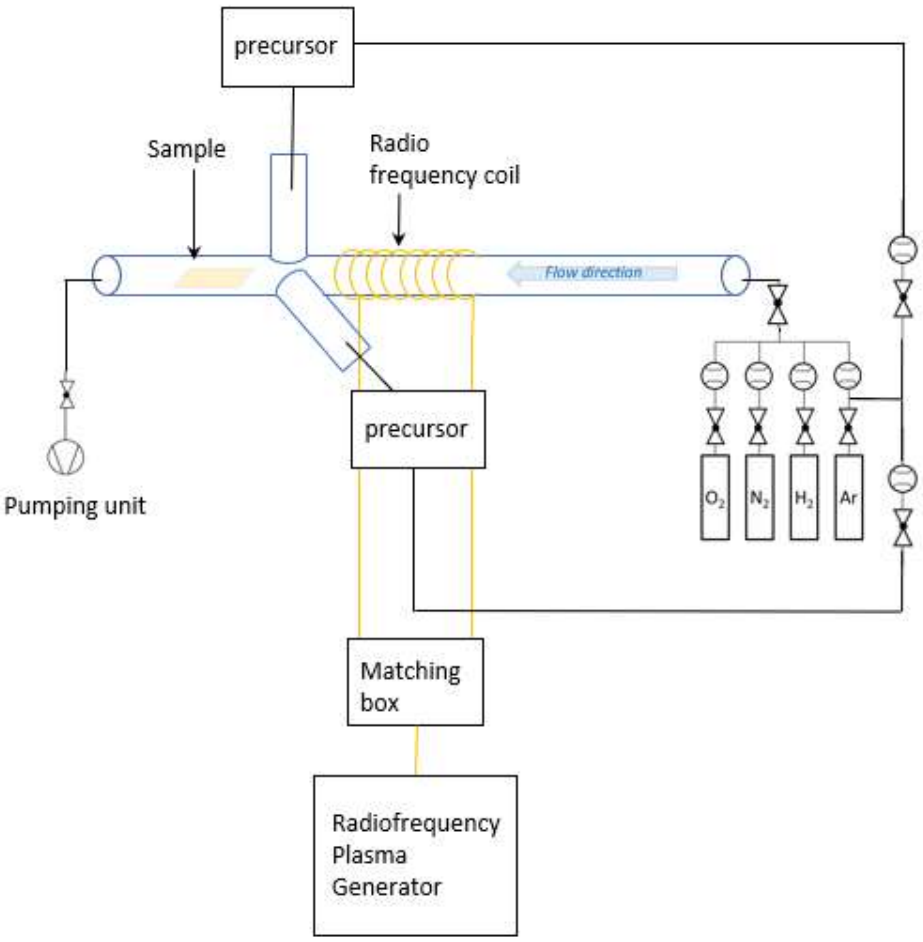

Figure 77. Radiofrequency plasma setup in for the injection of two precursors before the source of plasma i.e. in the afterglow.

Three types of samples were prepared in this study: one with porous substrate with plasma deposited HMDSO only, one with APTES and the final one with both HMDSO and APTES deposited simultaneously. All of the samples were prepared having a sample placed 8 cm from the source of plasma in argon atmosphere with the power of plasma generator at 40 W and the duration of plasma treatment 90 min. The FTIR spectra were recorded for the newly formed layers as shown in figure 78.

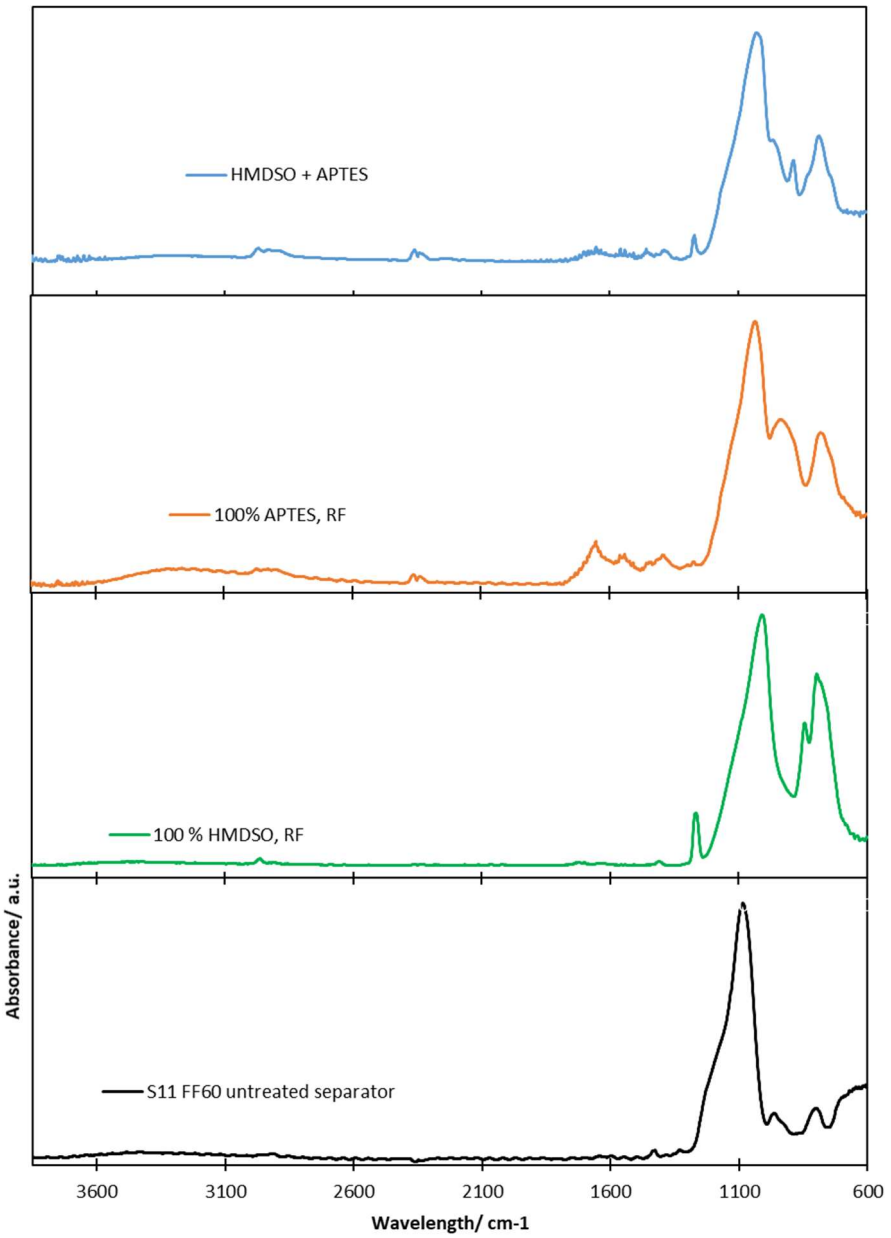

Figure 78. FTIR spectra recorded for untreated PVC-silica separator (black curve), sample treated with HMDSO (green curve), sample treated with APTES (orange curve) and sample with co-deposited HMDSO and APTES (blue curve).

In the spectrum recorded for sample treated with HMDSO and APTES, peak characteristic for sample deposited with HMDSO can be found (1266 cm^{-1}) as well as peaks observed in the spectrum of APTES treated sample (3400–3000 cm^{-1}, 1650 cm^{-1}, 941 cm^{-1}). Thus, it can be concluded that both of the precursors have been successfully deposited. SEM surface image of the sample treated with HMDSO and APTES is presented in figure 79.

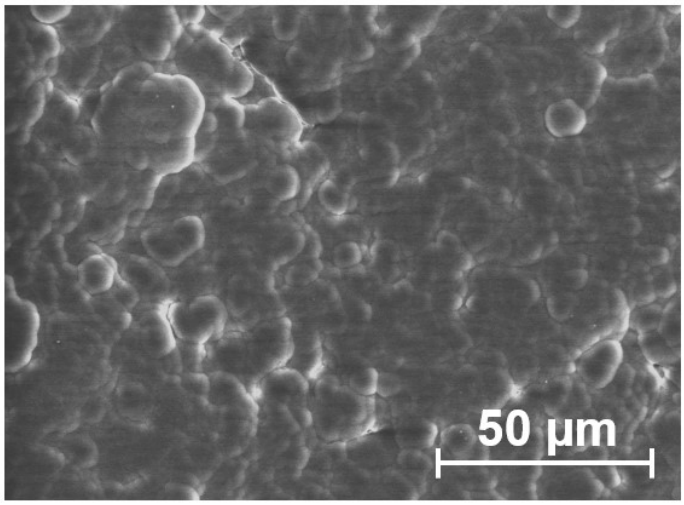

Figure 79. Surface SEM surface image of sample treated with HMDSO and APTES, simultaneously (power – 40 W, time – 90 min, Argon atmosphere).

The obtained sample exhibited slightly improved flexibility in comparison to the one treated using only APTES. However, some cracks were still observed.

A.6. Characterization – resistance and vanadium permeability.

In order to assess the resistance, impedance electrochemical spectroscopy was used. The samples of size 1.44 cm^2 were sandwiched in an electrochemical cell filled up with 1 M HCl electrolyte. The permeability to vanadium ions (VO^{2+}) was tested for samples of size 0.785 cm^2, sandwiched in a permeability cell with one compartment filled up with 150 mL of 1.5 M $MgSO_4$ in 3 M H_2SO_4 and the other with 150 mL of 1.5 M $VOSO_4$ in 3 M H_2SO_4. The results of resistance and permeability are presented in table 12.

Table 12. Resistance and permeability to vanadium species of the plasma deposited samples compared to the untreated substrate and commercial membrane FAP 450.

Sample	TOP LAYER	Resistance [Ω.]	Permeability to VO^{2+} [$cm.min^{-1}$]
1 M HCl	-	0.21	
Porous substrate	-	0.771	$3.12 \cdot 10^{-4}$
FAP 450	-	0.601	$9.86 \cdot 10^{-6}$
APTES_90	APTES	0.87	$5.31 \cdot 10^{-5}$
HA_90	HMDSO + APTES	1.58	$5.80 \cdot 10^{-5}$
DiamSil	DiAmSil	1.273	$9.86 \cdot 10^{-5}$
TriAmSi	TriAmSil	0.87	$2.15 \cdot 10^{-4}$

Table 12 shows that membranes treated with only APTES exhibited the lowest permeability and resistance among other plasma treated membranes. However, still the rate of vanadium crossover is significantly lower in comparison to the commercial membrane Fumasep® FAP 450. Similar permeability results were observed for the sample with co-deposited two precursors. However, the resistance of the sample, 1.58 Ω is too high for a practical application in RFB.

Both samples DiAmSil and TriAmsil exhibited too high vanadium permeability most likely due to the inhomogeneous and uncomplete plasma deposition of the new layer.

A.7. Conclusions.

Samples of PVC-silica substrate with plasma deposited new layers were successfully obtained using radiofrequency plasma generator. Among tested precursors APTES allowed a homogeneous deposition however, the obtained sample was too brittle and samples with dimensions larger than 3 cm by 3 cm were not obtained. Co-deposition of APTES and HMDSO improved the flexibility of the

prepared sample but also led to significant increase of resistivity. Future study should focus on the improvement of flexibility of the samples prepared using APTES precursor.

Bibliography

1. Zhang, H.; Lu, W.; Li, X. Progress and Perspectives of Flow Battery Technologies. *Electrochem. Energy Rev.* **2019**, *2*, 492–506, doi:10.1007/s41918-019-00047-1.

2. Leung, P.; Li, X.; Ponce De León, C.; Berlouis, L.; Low, C.T.J.; Walsh, F.C. Progress in redox flow batteries, remaining challenges and their applications in energy storage. *RSC Adv.* **2012**, *2*, 10125–10156, doi:10.1039/c2ra21342g.

3. Lin, G.; Chong, P.Y.; Yarlagadda, V.; Nguyen, T.V.; Wycisk, R.J.; Pintauro, P.N.; Bates, M.; Mukerjee, S.; Tucker, M.C.; Weber, A.Z. Advanced Hydrogen-Bromine Flow Batteries with Improved Efficiency, Durability and Cost. *J. Electrochem. Soc.* **2016**, *163*, A5049–A5056, doi:10.1149/2.0071601jes.

4. Minke, C.; Turek, T. Materials, system designs and modelling approaches in techno-economic assessment of all-vanadium redox flow batteries – A review. *J. Power Sources* **2018**, *376*, 66–81, doi:10.1016/j.jpowsour.2017.11.058.

5. Arenas, L.F.; Walsh, F.C.; de León, C.P. 3D-Printing of Redox Flow Batteries for Energy Storage: A Rapid Prototype Laboratory Cell. *ECS J. Solid State Sci. Technol.* **2015**, *4*, P3080–P3085, doi:10.1149/2.0141504jss.

6. Bartolozzi, M. Development of redox flow batteries. A historical bibliography. *J. Power Sources* **1989**, *27*, 219–234, doi:10.1016/0378-7753(89)80037-0.

7. Winsberg, J.; Hagemann, T.; Janoschka, T.; Hager, M.D.; Schubert, U.S. Redox-Flow Batteries: From Metals to Organic Redox-Active Materials. *Angew. Chemie - Int. Ed.* **2017**, *56*, 686–711, doi:10.1002/anie.201604925.

8. Weber, A.Z.; Mench, M.M.; Meyers, J.P.; Ross, P.N.; Gostick, J.T.; Liu, Q. Redox flow batteries: A review. *J. Appl. Electrochem.* **2011**, *41*, 1137–1164, doi:10.1007/s10800-011-0348-2.

9. Sum, E.; Rychcik, M.; Skyllas-kazacos, M. Investigation of the V(V)/V(IV) system for use in the positive half-cell of a redox battery. *J. Power Sources* **1985**, *16*, 85–95, doi:10.1016/0378-7753(85)80082-3.

10. Kim, S.; Yan, J.; Schwenzer, B.; Zhang, J.; Li, L.; Liu, J.; Yang, Z.; Hickner, M.A. Cycling performance and efficiency of sulfonated poly(sulfone) membranes in vanadium redox flow batteries. *Electrochem. commun.* **2010**, *12*, 1650–1653, doi:10.1016/j.elecom.2010.09.018.

11. Ye, J.; Yuan, D.; Ding, M.; Long, Y.; Long, T.; Sun, L.; Jia, C. A cost-effective nafion/lignin composite membrane with low vanadium ion permeation for high performance vanadium redox flow battery. *J. Power Sources* **2021**, *482*, 229023, doi:10.1016/j.jpowsour.2020.229023.

12. Minke, C.; Turek, T. Economics of vanadium redox flow battery membranes. *J. Power Sources* **2015**, *286*, 247–257, doi:10.1016/j.jpowsour.2015.03.144.

13. Hanley, E.S.; Amarandei, G.; Glowacki, B.A. Potential of Redox Flow Batteries and Hydrogen as Integrated Storage for Decentralized Energy Systems. **2016**, doi:10.1021/acs.energyfuels.5b02805.

14. Leung, P.; Shah, A.A.; Sanz, L.; Flox, C.; Morante, J.R.; Xu, Q.; Mohamed, M.R.; Ponce de León, C.; Walsh, F.C. Recent developments in organic redox flow batteries: A critical review. *J. Power Sources* **2017**, *360*, 243–283,

doi:10.1016/j.jpowsour.2017.05.057.

15. Choi, C.; Kim, S.; Kim, R.; Choi, Y.; Kim, S.; Jung, H. young; Yang, J.H.; Kim, H.T. A review of vanadium electrolytes for vanadium redox flow batteries. *Renew. Sustain. Energy Rev.* **2017**, *69*, 263–274, doi:10.1016/j.rser.2016.11.188.

16. Vijayakumar, M.; Luo, Q.; Lloyd, R.; Nie, Z.; Wei, X.; Li, B.; Sprenkle, V.; Londono, J.D.; Unlu, M.; Wang, W. Tuning the Perfluorosulfonic Acid Membrane Morphology for Vanadium Redox-Flow Batteries. *ACS Appl. Mater. Interfaces* **2016**, *8*, 34327–34334, doi:10.1021/acsami.6b10744.

17. Modestino, M.A.; Kusoglu, A.; Hexemer, A.; Weber, A.Z.; Segalman, R.A. Controlling nafion structure and properties via wetting interactions. *Macromolecules* **2012**, *45*, 4681–4688, doi:10.1021/ma300212f.

18. Qiu, J.; Li, M.; Ni, J.; Zhai, M.; Peng, J.; Xu, L.; Zhou, H.; Li, J.; Wei, G. Preparation of ETFE-based anion exchange membrane to reduce permeability of vanadium ions in vanadium redox battery. *J. Memb. Sci.* **2007**, *297*, 174–180, doi:10.1016/j.memsci.2007.03.042.

19. Wang, G.; Zhang, M.; He, Z.; Zhang, J.; Chen, J.; Wang, R.; Teng, A.; Dai, Y. Novel amphoteric ion exchange membranes by blending sulfonated poly(ether ether ketone) with ammonium polyphosphate for vanadium redox flow battery applications. *J. Appl. Polym. Sci.* **2021**, *138*, 1–14, doi:10.1002/app.50592.

20. Gubler, L. Membranes and separators for redox flow batteries. *Curr. Opin. Electrochem.* **2019**, *18*, 31–36, doi:10.1016/j.coelec.2019.08.007.

21. Vafiadis, H.; Skyllas-Kazacos, M. Evaluation of membranes for the novel vanadium bromine redox flow cell. *J. Memb. Sci.* **2006**, *279*, 394–402, doi:10.1016/j.memsci.2005.12.028.

22. Zhao, Y.; Yuan, Z.; Lu, W.; Li, X.; Zhang, H. The porous membrane with tunable performance for vanadium flow battery: The effect of charge. *J. Power Sources* **2017**, *342*, 327–334, doi:10.1016/j.jpowsour.2016.12.058.

23. Geise, G.M.; Cassady, H.J.; Paul, D.R.; Logan, B.E.; Hickner, M.A. Specific ion effects on membrane potential and the permselectivity of ion exchange membranes. *Phys. Chem. Chem. Phys.* **2014**, *16*, 21673–21681, doi:10.1039/c4cp03076a.

24. Sharma, P.P.; Tinh, V.D.C.; Kim, D. Enhanced ion cluster size of sulfonated poly (arylene ether sulfone) for proton exchange membrane fuel cell application. *Polymers (Basel).* **2021**, *13*, doi:10.3390/polym13071111.

25. Sukkar, T.; Skyllas-Kazacos, M. Modification of membranes using polyelectrolytes to improve water transfer properties in the vanadium redox battery. *J. Memb. Sci.* **2003**, *222*, 249–264, doi:10.1016/S0376-7388(03)00316-8.

26. Luo, T.; Abdu, S.; Wessling, M. Selectivity of ion exchange membranes: A review. *J. Memb. Sci.* **2018**, *555*, 429–454, doi:10.1016/j.memsci.2018.03.051.

27. Shi, Y.; Eze, C.; Xiong, B.; He, W.; Zhang, H.; Lim, T.M.; Ukil, A.; Zhao, J. Recent development of membrane for vanadium redox flow battery applications: A review. *Appl. Energy* **2019**, *238*, 202–224, doi:10.1016/j.apenergy.2018.12.087.

28. Savari, S.; Sachdeva, S.; Kumar, A. Electrolysis of sodium chloride using composite poly(styrene-co-divinylbenzene) cation exchange membranes. *J. Memb.*

Sci. **2008**, *310*, 246–261, doi:10.1016/j.memsci.2007.10.049.

29. Shin, S.H.; Yun, S.H.; Moon, S.H. A review of current developments in non-aqueous redox flow batteries: Characterization of their membranes for design perspective. *RSC Adv.* **2013**, *3*, 9095–9116, doi:10.1039/c3ra00115f.

30. Maurya, S.; Shin, S.H.; Sung, K.W.; Moon, S.H.; Hwang, C.W.; Park, H.M.; Oh, C.M.; Hwang, T.S.; Shim, J.; Jin, C.S. Anion exchange membrane prepared from simultaneous polymerization and quaternization of 4-vinyl pyridine for non-aqueous vanadium redox flow battery applications. *J. Power Sources* **2014**, *468*, 325–334, doi:10.1016/j.memsci.2014.05.050.

31. Hwang, C.W.; Park, H.M.; Oh, C.M.; Hwang, T.S.; Shim, J.; Jin, C.S. Synthesis and characterization of vinylimidazole-co-trifluoroethylmethacrylate-co-divinylbenzene anion-exchange membrane for all-vanadium redox flow battery. *J. Memb. Sci.* **2014**, *468*, 98–106, doi:10.1016/j.memsci.2014.05.050.

32. Jeevanantham, S.; Hosimin, S.; Vengatesan, S.; Sozhan, G. Quaternized poly(styrene-co-vinylbenzyl chloride) anion exchange membranes: Role of different ammonium cations on structural, morphological, thermal and physio-chemical properties. *New J. Chem.* **2018**, *42*, 380–387, doi:10.1039/c7nj02574b.

33. McRae, W. A., Alexander, S. S. Sulfonating reagent and method of making and using the same in the preparation of cation exchange membranes. U. S. Patent. 2,962,454 A, 29 November **1956**

34. Herman, H.; Slade, R.C.T.; Varcoe, J.R. The radiation-grafting of vinylbenzyl chloride onto poly(hexafluoropropylene-co-tetrafluoroethylene) films with subsequent conversion to alkaline anion-exchange membranes: Optimisation of the experimental conditions and characterisation. *J. Memb. Sci.* **2003**, *218*, 147–163, doi:10.1016/S0376-7388(03)00167-4.

35. Quellmalz, D.; Zschocke, P. Novel ion exchange membranes based on an aromatic polyethersulfone*. *J. Memb. Sci.* **1985**, *22*, 325–332.

36. Gindt, B.P.; Tang, Z.; Watkins, D.L.; Abebe, D.G.; Seo, S.; Tuli, S.; Ghassemi, H.; Zawodzinski, T.A.; Fujiwara, T. Effects of sulfonated side chains used in polysulfone based PEMs for VRFB separator. *J. Memb. Sci.* **2017**, *532*, 58–67, doi:10.1016/j.memsci.2017.03.013.

37. Liao, J.; Zhu, J.; Yang, S.; Pan, N.; Yu, X.; Wang, C.; Li, J.; Shen, J. Long-side-chain type imidazolium-functionalized fluoro-methyl poly(arylene ether ketone) anion exchange membranes with superior electrodialysis performance. *J. Memb. Sci.* **2019**, *574*, 181–195, doi:10.1016/j.memsci.2018.12.066.

38. Komkova, E.N.; Stamatialis, D.F.; Strathmann, H.; Wessling, M. Anion-exchange membranes containing diamines: Preparation and stability in alkaline solution. *J. Memb. Sci.* **2004**, *244*, 25–34, doi:10.1016/j.memsci.2004.06.026.

39. Zhang, S.S. A review on the separators of liquid electrolyte Li-ion batteries. *J. Power Sources* **2007**, *164*, 351–364, doi:10.1016/j.jpowsour.2006.10.065.

40. Bungay, J. K., Bungay, P. M., Lonsdale, H. K., Pinho, M. D. N. Synthetic Membranes:: Science, Engineering and Applications*, Springer,* **2011**, 1 - 37, ISBN 9789400947122

41. Sata, T. Ion Exchange Membranes Preparation, Characterization, Modification and Application, *Royal Society of Chemistry*, **2004**, 35–88, ISBN 9781847551177

42. Peron, J.; Mani, A.; Zhao, X.; Edwards, D.; Adachi, M.; Soboleva, T.; Shi, Z.; Xie, Z.; Navessin, T.; Holdcroft, S. Properties of Nafion ® NR-211 membranes for PEMFCs. **2010**, *356*, 44–51, doi:10.1016/j.memsci.2010.03.025.

43. Siemann, U. Solvent cast technology - A versatile tool for thin film production. *Prog. Colloid Polym. Sci.* **2005**, *130*, 1–14, doi:10.1007/b107336.

44. Xing, D.; Zhang, S.; Yin, C.; Zhang, B.; Jian, X. Effect of amination agent on the properties of quaternized poly (phthalazinone ether sulfone) anion exchange membrane for vanadium redox flow battery application. *J. Memb. Sci.* **2010**, *354*, 68–73, doi:10.1016/j.memsci.2010.02.064.

45. Fang, J.; Shen, P.K. Quaternized poly(phthalazinon ether sulfone ketone) membrane for anion exchange membrane fuel cells. *J. Memb. Sci.* 2006, *285*, 317–322.

46. Yee, R.S.L.; Zhang, K.; Ladewig, B.P. The effects of sulfonated poly(ether ether ketone) ion exchange preparation conditions on membrane properties. *Membranes (Basel).* **2013**, *3*, 182–195, doi:10.3390/membranes3030182.

47. Zhao, S.; Zhang, L.; Wang, Y. Enhanced performance of a Na fi on membrane through ionomer self-organization in the casting solution. *J. Power Sources* **2013**, *233*, 309–312, doi:10.1016/j.jpowsour.2013.01.052.

48. Guan, R.; Dai, H.; Li, C.; Liu, J.; Xu, J. Effect of casting solvent on the morphology and performance of sulfonated polyethersulfone membranes. *J. Memb. Sci.* **2006**, *277*, 148–156, doi:10.1016/j.memsci.2005.10.025.

49. Assumma, L.; Nguyen, H.; Iojoiu, C.; Lyonnard, S. Effects of Block Length and Membrane Processing Conditions on the Morphology and Properties of Per fl uorosulfonated Poly (arylene ether sulfone) Multiblock Copolymer Membranes for PEMFC. ACS Appl. Mater. Interfaces. 2015, 7 (25), 13808-13820, doi:10.1021/acsami.5b01835.

50. Lee, M.; Keun, J.; Lee, H.; Lane, O.; Moore, R.B.; Mcgrath, J.E.; Baird, D.G. Effects of block length and solution-casting conditions on the final morphology and properties of disulfonated poly (arylene ether sulfone) multiblock copolymer films for proton exchange membranes. *Polymer (Guildf).* **2009**, *50*, 6129–6138, doi:10.1016/j.polymer.2009.10.023.

51. Brack, H.P.; Buhrer, H.G.; Bonorand, L.; Scherer, G.G. Grafting of pre-irradiated poly(ethylene-alt-tetrafluoroethylene) films with styrene: Influence of base polymer film properties and processing parameters. *J. Mater. Chem.* **2000**, *10*, 1795–1803, doi:10.1039/b001851l.

52. Hasegawa, S.; Suzuki, Y.; Maekawa, Y. Preparation of poly(ether ether ketone)-based polymer electrolytes for fuel cell membranes using grafting technique. *Radiat. Phys. Chem.* **2008**, *77*, 617–621, doi:10.1016/j.radphyschem.2007.09.007.

53. Wavhal, D.S.; Fisher, E.R. Hydrophilic modification of polyethersulfone membranes by low temperature plasma-induced graft polymerization. *J. Memb. Sci.* **2002**, *209*, 255–269, doi:10.1016/S0376-7388(02)00352-6.

54. Kwak, N.S.; Koo, J.S.; Hwang, T.S. Synthesis and characterization of EFFE-g-(VBTAC-co-HEMA) anion exchange membranes prepared by a 60Co radiation-induced graft copolymerization for redox-flow battery applications. *Macromol. Res.* **2012**, *20*, 205–211, doi:10.1007/s13233-012-0032-3.

55. Espiritu, R.; Mamlouk, M.; Scott, K. Study on the effect of the degree of grafting on the performance of polyethylene-based anion exchange membrane for fuel cell application. *Int. J. Hydrogen Energy* **2016**, *41*, 1120–1133, doi:10.1016/j.ijhydene.2015.10.108.

56. Ennajdaoui, A.; Roualdes, S.; Brault, P.; Durand, J. Membranes produced by plasma enhanced chemical vapor deposition technique for low temperature fuel cell applications. *J. Power Sources* **2010**, *195*, 232–238, doi:10.1016/j.jpowsour.2009.06.090.

57. Hegemann, D. Plasma Polymer Deposition and Coatings on Polymers. Comprehensive Materials Processing. Cameron, D., Ed.; Elsevier Ltd., 2014; Vol. 4, pp 201–228. ISBN: 9780080965321. doi: 10.1016/B978-0-08-096532-1.00426-X

58. Ogumi, Z.; Uchimoto, Y.; Tsujikawa, M.; Takehara, Z.; Foulkes, F.R. Modification of Ion Exchange Membrane Surface by Plasma Process: I . H+ Ion Perm-Selective Membrane from Nafion for Redox-Flow Battery. J. Electrochem. Soc. 1990, 137, 1430–1435, doi: 10.1149/1.2086686.

59. Zeng, R.; Pang, Z.; Zhu, H. Modification of a Nafion ion exchange membrane by a plasma polymerization process. *J. Electroanal. Chem.* **2000**, *490*, 102–106, doi:10.1016/S0022-0728(00)00241-2.

60. Wang, T.; Moon, S.J.; Hwang, D.S.; Park, H.; Lee, J.; Kim, S.; Lee, Y.M.; Kim, S. Selective ion transport for a vanadium redox flow battery (VRFB) in nano-crack regulated proton exchange membranes. *J. Memb. Sci.* **2019**, *583*, 16–22, doi:10.1016/j.memsci.2019.04.017.

61. Matsuoka, K.; Chiba, S.; Iriyama, Y.; Abe, T.; Matsuoka, M.; Kikuchi, K.; Ogumi, Z. Preparation of anion-exchange membrane by plasma polymerization and its use in alkaline fuel cells. *Thin Solid Films* **2008**, *516*, 3309–3313, doi:10.1016/j.tsf.2007.09.032.

62. Rana, D.; Matsuura, T. Surface modifications for antifouling membranes. *Chem. Rev.* **2010**, *110*, 2448–2471, doi:10.1021/cr800208y.

63. Olding, T.; Sayer, M.; Barrow, D. Ceramic sol-gel composite coatings for electrical insulation. *Thin Solid Films* **2001**, *398–399*, 581–586, doi:10.1016/S0040-6090(01)01322-0.

64. Troczyński, T., Yang, Q. Process for making chemically bonded sol-gel ceramics. U. S. Patent 6,284,682 B1, 4 September **2001**

65. Nagarale, R.K.; Gohil, G.S.; Shahi, V.K.; Rangarajan, R. Organic-inorganic hybrid membrane: Thermally stable cation-exchange membrane prepared by the sol-gel method. *Macromolecules* **2004**, *37*, 10023–10030, doi:10.1021/ma048404p.

66. Balaji, J.; Sethuraman, M.G.; Roh, S.H.; Jung, H.Y. Recent developments in sol-gel based polymer electrolyte membranes for vanadium redox flow batteries – A review. *Polym. Test.* **2020**, *89*, 106567, doi:10.1016/j.polymertesting.2020.106567.

67. Mauritz, K.A.; Stefanithis, I.D.; Davis, S. V.; Scheetz, R.W.; Pope, R.K.; Wilkes, G.L.; Huang, H. -H Microstructural evolution of a silicon oxide phase in a perfluorosulfonic acid ionomer by an in situ sol–gel reaction. *J. Appl. Polym. Sci.* **1995**, *55*, 181–190, doi:10.1002/app.1995.070550120.

68. Xi, J.; Wu, Z.; Qiu, X.; Chen, L. Nafion/SiO2 hybrid membrane for vanadium redox flow battery. *J. Power Sources* **2007**, *166*, 531–536,

doi:10.1016/j.jpowsour.2007.01.069.

69. Teng, X.; Zhao, Y.; Xi, J.; Wu, Z.; Qiu, X.; Chen, L. Nafion/organic silica modified TiO2 composite membrane for vanadium redox flow battery via in situ sol-gel reactions. *J. Memb. Sci.* **2009**, *341*, 149–154, doi:10.1016/j.memsci.2009.05.051.

70. Leung, P.K.; Xu, Q.; Zhao, T.S.; Zeng, L.; Zhang, C. Preparation of silica nanocomposite anion-exchange membranes with low vanadium-ion crossover for vanadium redox flow batteries. *Electrochim. Acta* **2013**, *105*, 584–592, doi:10.1016/j.electacta.2013.04.155.

71. Ling, L.; Xiao, M.; Han, D.; Ren, S.; Wang, S.; Meng, Y. Porous composite membrane of PVDF/Sulfonic silica with high ion selectivity for vanadium redox flow battery. *J. Memb. Sci.* **2019**, *585*, 230–237, doi:10.1016/j.memsci.2018.11.082.

72. Zhang, X.; Chen, H.; Zhang, H. Layer-by-layer assembly: From conventional to unconventional methods. *Chem. Commun.* **2007**, 1395–1405, doi:10.1039/b615590a.

73. Saqib, J.; Aljundi, I.H. Membrane fouling and modification using surface treatment and layer-by-layer assembly of polyelectrolytes: State-of-the-art review. *J. Water Process Eng.* **2016**, *11*, 68–87, doi:10.1016/j.jwpe.2016.03.009.

74. Decher, G. Fuzzy nanoassemblies: Toward layered polymeric multicomposites. *Science (80-.).* **1997**, *277*, 1232–1237, doi:10.1126/science.277.5330.1232.

75. Shiratori, S.S.; Rubner, M.F. pH-dependent thickness behavior of sequentially adsorbed layers of weak polyelectrolytes. *Macromolecules* **2000**, *33*, 4213–4219, doi:10.1021/ma991645q.

76. Hyeon, D.H.; Chun, J.H.; Lee, C.H.; Jung, H.C.; Kim, S.H. Composite membranes based on sulfonated poly(ether ether ketone) and SiO2 for a vanadium redox flow battery. *Korean J. Chem. Eng.* **2015**, *32*, 1554–1563, doi:10.1007/s11814-014-0358-y.

77. Teng, X.; Yu, C.; Wu, X.; Dong, Y.; Gao, P.; Hu, H.; Zhu, Y.; Dai, J. PTFE/SPEEK/PDDA/PSS composite membrane for vanadium redox flow battery application. *J. Mater. Sci.* **2018**, *53*, 5204–5215, doi:10.1007/s10853-017-1903-y.

78. Wu, X.; Hu, J.; Liu, J.; Zhou, Q.; Zhou, W.; Li, H. Ion exchange membranes for vanadium redox flow batteries. *Pure Appl. Chem.* **2014**, *86*, 633–649, doi:10.1515/pac-2014-0101.

79. Skyllas-Kazacos, M.; Kasherman, D.; Hong, D.R.; Kazacos, M. Characteristics and performance of 1 kW UNSW vanadium redox battery. *J. Power Sources* **1991**, *35*, 399–404, doi:10.1016/0378-7753(91)80058-6.

80. Ye, R.; Henkensmeier, D.; Yoon, S.J.; Huang, Z.; Kim, D.K.; Chang, Z.; Kim, S.; Chen, R. Redox Flow Batteries for Energy Storage: A Technology Review. *J. Electrochem. Energy Convers. Storage* **2018**, *15*, doi:10.1115/1.4037248.

81. Li, X.; Zhang, H.; Mai, Z.; Zhang, H.; Vankelecom, I. Ion exchange membranes for vanadium redox flow battery (VRB) applications. *Energy Environ. Sci.* **2011**, *4*, 1147–1160, doi:10.1039/c0ee00770f.

82. Chen, D.; Hickner, M.A.; Agar, E.; Kumbur, E.C. Selective anion exchange membranes for high coulombic efficiency vanadium redox flow batteries. *Electrochem. commun.* **2013**, *26*, 37–40, doi:10.1016/j.elecom.2012.10.007.

83. Luo, X.; Lu, Z.; Xi, J.; Wu, Z.; Zhu, W.; Chen, L.; Qiu, X. Influences of permeation of vanadium ions through PVDF-g-PSSA membranes on performances of vanadium redox flow batteries. *J. Phys. Chem. B* **2005**, *109*, 20310–20314, doi:10.1021/jp054092w.

84. Rajput, A.; Khan, H.; Raj, S.K.; Kothandaraman, R.; Kulshrestha, V. Styrene- co -DVB grafted PVDF proton exchange membranes for vanadium redox flow battery applications . *Mater. Adv.* **2020**, *1*, 1930–1938, doi:10.1039/d0ma00496k.

85. Schwenzer, B.; Zhang, J.; Kim, S.; Li, L.; Liu, J.; Yang, Z. Membrane development for vanadium redox flow batteries. *ChemSusChem* **2011**, *4*, 1388–1406, doi:10.1002/cssc.201100068.

86. Chen, D.; Hickner, M.A.; Agar, E.; Kumbur, E.C. Optimizing membrane thickness for vanadium redox flow batteries. *J. Memb. Sci.* **2013**, *437*, 108–113, doi:10.1016/j.memsci.2013.02.007.

87. Chen, D.; Wang, S.; Xiao, M.; Meng, Y. Synthesis and characterization of novel sulfonated poly(arylene thioether) ionomers for vanadium redox flow battery applications. *Energy Environ. Sci.* **2010**, *3*, 622–628, doi:10.1039/b917117g.

88. Abdul Aziz, M.; Oh, K.; Shanmugam, S. A sulfonated poly(arylene ether ketone)/polyoxometalate-graphene oxide composite: A highly ion selective membrane for all vanadium redox flow batteries. *Chem. Commun.* **2017**, *53*, 917–920, doi:10.1039/c6cc08855d.

89. Chen, D.; Wang, S.; Xiao, M.; Meng, Y. Synthesis and properties of novel sulfonated poly(arylene ether sulfone) ionomers for vanadium redox flow battery. *Energy Convers. Manag.* **2010**, *51*, 2816–2824, doi:10.1016/j.enconman.2010.06.019.

90. Li, J.; Liu, S.; He, Z.; Zhou, Z. A novel branched side-chain-type sulfonated polyimide membrane with flexible sulfoalkyl pendants and trifluoromethyl groups for vanadium redox flow batteries. *J. Power Sources* **2017**, *347*, 114–126, doi:10.1016/j.jpowsour.2017.02.055.

91. Wang, N.; Peng, S.; Li, Y.; Wang, H.; Liu, S.; Liu, Y. Sulfonated poly(phthalazinone ether sulfone) membrane as a separator of vanadium redox flow battery. *J. Solid State Electrochem.* **2012**, *16*, 2169–2177, doi:10.1007/s10008-012-1641-7.

92. Winardi, S.; Raghu, S.C.; Oo, M.O.; Yan, Q.; Wai, N.; Lim, T.M.; Skyllas-Kazacos, M. Sulfonated poly (ether ether ketone)-based proton exchange membranes for vanadium redox battery applications. *J. Memb. Sci.* **2014**, *450*, 313–322, doi:10.1016/j.memsci.2013.09.024.

93. Wang, F.; Sylvia, J.M.; Jacob, M.M.; Peramunage, D. Amphiphilic block copolymer membrane for vanadium redox flow battery. *J. Power Sources* **2013**, *242*, 575–580, doi:10.1016/j.jpowsour.2013.05.102.

94. Varcoe, J.R.; Atanassov, P.; Dekel, D.R.; Herring, A.M.; Hickner, M.A.; Kohl, P.A.; Kucernak, A.R.; Mustain, W.E.; Nijmeijer, K.; Scott, K.; et al. Anion-exchange membranes in electrochemical energy systems. *Energy Environ. Sci.* **2014**, *7*, 3135–3191, doi:10.1039/c4ee01303d.

95. Zeng, L.; Zhao, T.S.; Wei, L.; Jiang, H.R.; Wu, M.C. Anion exchange membranes for aqueous acid-based redox flow batteries: Current status and challenges. *Appl.*

Energy **2019**, *233–234*, 622–643, doi:10.1016/j.apenergy.2018.10.063.

96. Merle, G.; Wessling, M.; Nijmeijer, K. Anion exchange membranes for alkaline fuel cells: A review. *J. Memb. Sci.* **2011**, *377*, 1–35, doi:10.1016/j.memsci.2011.04.043.

97. Ding, L.; Wang, Y.; Wang, L.; Zhao, Z.; He, M.; Song, Y. A simple and effective method of enhancing the proton conductivity of polybenzimidazole proton exchange membranes through protonated polymer during solvation. *J. Power Sources* **2020**, *455*, 227965, doi:10.1016/j.jpowsour.2020.227965.

98. Assink, R.A. Fouling mechanism of separator membranes for the iron/chromium redox battery. *J. Memb. Sci.* **1984**, *17*, 205–217, doi:10.1016/S0376-7388(00)82295-4.

99. Mohammadi, T.; Skyllas Kazacos, M. Modification of anion-exchange membranes for vanadium redox flow battery applications. *J. Power Sources* **1996**, *63*, 179–186, doi:10.1016/S0378-7753(96)02463-9.

100. Skyllas-Kazacos, M.; Chakrabarti, M.H.; Hajimolana, S.A.; Mjalli, F.S.; Saleem, M. Progress in Flow Battery Research and Development. *J. Electrochem. Soc.* **2011**, *158*, R55, doi:10.1149/1.3599565.

101. Song, H.B.; Kim, D.H.; Kang, M.S. Thin reinforced poly(2,6-dimethyl-1,4-phenylene oxide)-based anion-exchange membranes with high mechanical and chemical stabilities. *Chem. Lett.* **2019**, *48*, 1500–1503, doi:10.1246/cl.190671.

102. Maurya, S.; Shin, S.H.; Kim, Y.; Moon, S.H. A review on recent developments of anion exchange membranes for fuel cells and redox flow batteries. *RSC Adv.* **2015**, *5*, 37206–37230, doi:10.1039/c5ra04741b.

103. Jung, M.S.J.; Parrondo, J.; Arges, C.G.; Ramani, V. Polysulfone-based anion exchange membranes demonstrate excellent chemical stability and performance for the all-vanadium redox flow battery. *J. Mater. Chem. A* **2013**, *1*, 10458–10464, doi:10.1039/c3ta11459g.

104. Jheng, L. cheng; Hsu, S.L. chung; Lin, B. yun; Hsu, Y. lun Quaternized polybenzimidazoles with imidazolium cation moieties for anion exchange membrane fuel cells. *J. Memb. Sci.* **2014**, *460*, 160–170, doi:10.1016/j.memsci.2014.02.043.

105. Ji, Y.; Tay, Z.Y.; Li, S.F.Y. Highly selective sulfonated poly(ether ether ketone)/titanium oxide composite membranes for vanadium redox flow batteries. *J. Memb. Sci.* **2017**, *539*, 197–205, doi:10.1016/j.memsci.2017.06.015.

106. Maurya, S.; Shin, S.H.; Sung, K.W.; Moon, S.H. Anion exchange membrane prepared from simultaneous polymerization and quaternization of 4-vinyl pyridine for non-aqueous vanadium redox flow battery applications. *J. Power Sources* **2014**, *255*, 325–334, doi:10.1016/j.jpowsour.2014.01.047.

107. Park, S.G.; Kwak, N.S.; Hwang, C.W.; Park, H.M.; Hwang, T.S. Synthesis and characteristics of aminated vinylbenzyl chloride-co-styrene-co-hydroxyethyl acrylate anion-exchange membrane for redox flow battery applications. *J. Memb. Sci.* **2012**, *423–424*, 429–437, doi:10.1016/j.memsci.2012.08.040.

108. Kim, D.S.; Fujimoto, C.H.; Hibbs, M.R.; Labouriau, A.; Choe, Y.K.; Kim, Y.S. Resonance stabilized perfluorinated ionomers for alkaline membrane fuel cells. *Macromolecules* **2013**, *46*, 7826–7833, doi:10.1021/ma401568f.

109. Lin, X.; Wu, L.; Liu, Y.; Ong, A.L.; Poynton, S.D.; Varcoe, J.R.; Xu, T. Alkali resistant and conductive guanidinium-based anion-exchange membranes for alkaline polymer electrolyte fuel cells. *J. Power Sources* **2012**, *217*, 373–380, doi:10.1016/j.jpowsour.2012.05.062.

110. Becerra-Arciniegas, R.A.; Narducci, R.; Ercolani, G.; Antonaroli, S.; Sgreccia, E.; Pasquini, L.; Knauth, P.; Di Vona, M.L. Alkaline stability of model anion exchange membranes based on poly(phenylene oxide) (PPO) with grafted quaternary ammonium groups: Influence of the functionalization route. *Polymer (Guildf).* **2019**, *185*, 121931, doi:10.1016/j.polymer.2019.121931.

111. Xu, T.; Liu, Z.; Yang, W. Fundamental studies of a new series of anion exchange membranes: Membrane prepared from poly(2,6-dimethyl-1,4-phenylene oxide) (PPO) and triethylamine. *J. Memb. Sci.* **2005**, *249*, 183–191, doi:10.1016/j.memsci.2004.10.010.

112. Willdorf-Cohen, S.; Mondal, A.N.; Dekel, D.R.; Diesendruck, C.E. Chemical stability of poly(phenylene oxide)-based ionomers in an anion exchange-membrane fuel cell environment. *J. Mater. Chem. A* **2018**, *6*, 22234–22239, doi:10.1039/C8TA05785K.

113. Lim, H.; Lee, B.; Yun, D.; Al Munsur, A.Z.; Chae, J.E.; Lee, S.Y.; Kim, H.J.; Nam, S.Y.; Park, C.H.; Kim, T.H. Poly(2,6-dimethyl-1,4-phenylene oxide)s with Various Head Groups: Effect of Head Groups on the Properties of Anion Exchange Membranes. *ACS Appl. Mater. Interfaces* **2018**, *10*, 41279–41292, doi:10.1021/acsami.8b13016.

114. Mai, Z.; Zhang, H.; Zhang, H.; Xu, W.; Wei, W.; Na, H.; Li, X. Anion-conductive membranes with ultralow vanadium permeability and excellent performance in vanadium flow batteries. *ChemSusChem* **2013**, *6*, 328–335, doi:10.1002/cssc.201200561.

115. Cha, M.S.; Jeong, H.Y.; Shin, H.Y.; Hong, S.H.; Kim, T.H.; Oh, S.G.; Lee, J.Y.; Hong, Y.T. Crosslinked anion exchange membranes with primary diamine-based crosslinkers for vanadium redox flow battery application. *J. Power Sources* **2017**, *363*, 78–86, doi:10.1016/j.jpowsour.2017.07.068.

116. Hou, J.; Liu, Y.; Ge, Q.; Yang, Z.; Wu, L.; Xu, T. Recyclable cross-linked anion exchange membrane for alkaline fuel cell application. *J. Power Sources* **2018**, *375*, 404–411, doi:10.1016/j.jpowsour.2017.06.073.

117. Shin, D.W.; Guiver, M.D.; Lee, Y.M. Hydrocarbon-Based Polymer Electrolyte Membranes: Importance of Morphology on Ion Transport and Membrane Stability. *Chem. Rev.* **2017**, *117*, 4759–4805, doi:10.1021/acs.chemrev.6b00586.

118. Seo, D.W.; Lim, Y.D.; Lee, S.H.; Hossain, M.A.; Islam, M.M.; Lee, H.C.; Jang, H.H.; Kim, W.G. Preparation and characterization of block copolymers containing multi-sulfonated unit for proton exchange membrane fuel cell. *Electrochim. Acta* **2012**, *86*, 352–359, doi:10.1016/j.electacta.2012.03.125.

119. Dong, X.; Xue, B.; Qian, H.; Zheng, J.; Li, S.; Zhang, S. Novel quaternary ammonium microblock poly (p-phenylene-co-aryl ether ketone)s as anion exchange membranes for alkaline fuel cells. *J. Power Sources* **2017**, *342*, 605–615, doi:10.1016/j.jpowsour.2016.12.114.

120. Zhao, Z.; Wang, J.; Li, S.; Zhang, S. Synthesis of multi-block poly(arylene ether sulfone) copolymer membrane with pendant quaternary ammonium groups for

alkaline fuel cell. *J. Power Sources* **2011**, *196*, 4445–4450, doi:10.1016/j.jpowsour.2011.01.081.

121. Li, X.; Yu, Y.; Liu, Q.; Meng, Y. Synthesis and properties of anion conductive multiblock copolymers containing tetraphenyl methane moieties for fuel cell application. *J. Memb. Sci.* **2013**, *436*, 202–212, doi:10.1016/j.memsci.2013.02.041.

122. Tanaka, M.; Fukasawa, K.; Nishino, E.; Yamaguchi, S.; Yamada, K.; Tanaka, H.; Bae, B.; Miyatake, K.; Watanabe, M. Anion conductive block poly(arylene ether)s: Synthesis, properties, and application in alkaline fuel cells. *J. Am. Chem. Soc.* **2011**, *133*, 10646–10654, doi:10.1021/ja204166e.

123. Cha, M.S.; Lee, J.Y.; Kim, T.H.; Jeong, H.Y.; Shin, H.Y.; Oh, S.G.; Hong, Y.T. Preparation and characterization of crosslinked anion exchange membrane (AEM) materials with poly(phenylene ether)-based short hydrophilic block for use in electrochemical applications. *J. Memb. Sci.* **2017**, *530*, 73–83, doi:10.1016/j.memsci.2017.02.015.

124. Si, J.; Lv, Y.; Lu, S.; Xiang, Y. Microscopic phase-segregated quaternary ammonia polysulfone membrane for vanadium redox flow batteries. *J. Power Sources* **2019**, *428*, 88–92, doi:10.1016/j.jpowsour.2019.04.100.

125. Hwang, G.J.; Kim, S.W.; In, D.M.; Lee, D.Y.; Ryu, C.H. Application of the commercial ion exchange membranes in the all-vanadium redox flow battery. *J. Ind. Eng. Chem.* **2018**, *60*, 360–365, doi:10.1016/j.jiec.2017.11.023.

126. Mohammadi, T.; Chieng, S.C.; Kazacos, M.S. Water transport study across commercial ion exchange membranes in the vanadium redox flow battery. *J. Memb. Sci.* **1997**, *133*, 151–159, doi:10.1016/S0376-7388(97)00092-6.

127. Lee, M.S.; Kang, H.G.; Jeon, J.D.; Choi, Y.W.; Yoon, Y.G. A novel amphoteric ion-exchange membrane prepared by the pore-filling technique for vanadium redox flow batteries. *RSC Adv.* **2016**, *6*, 63023–63029, doi:10.1039/c6ra07790k.

128. Kerres, J.; Ullrich, A.; Häring, T.; Baldauf, M.; Gebhardt, U.; Preidel, W. Preparation, characterization and fuel cell application of new acid-base blend membranes. *J. New Mater. Electrochem. Syst.* **2000**, *3*, 229–239.

129. Liu, S.; Wang, L.; Ding, Y.; Liu, B.; Han, X.; Song, Y. Novel sulfonated poly (ether ether keton)/polyetherimide acid-base blend membranes for vanadium redox flow battery applications. *Electrochim. Acta* **2014**, *130*, 90–96, doi:10.1016/j.electacta.2014.02.144.

130. Yan, X.; Zhang, C.; Dong, Z.; Jiang, B.; Dai, Y.; Wu, X.; He, G. Amphiprotic Side-Chain Functionalization Constructing Highly Proton/Vanadium-Selective Transport Channels for High-Performance Membranes in Vanadium Redox Flow Batteries. *ACS Appl. Mater. Interfaces* **2018**, *10*, 32247–32255, doi:10.1021/acsami.8b11993.

131. Qiu, J.; Zhai, M.; Chen, J.; Wang, Y.; Peng, J.; Xu, L.; Li, J.; Wei, G. Performance of vanadium redox flow battery with a novel amphoteric ion exchange membrane synthesized by two-step grafting method. *J. Memb. Sci.* **2009**, *342*, 215–220, doi:10.1016/j.memsci.2009.06.043.

132. Liao, J.; Chu, Y.; Zhang, Q.; Wu, K.; Tang, J.; Lu, M.; Wang, J. Fluoro-methyl sulfonated poly(arylene ether ketone-co-benzimidazole) amphoteric ion-exchange membranes for vanadium redox flow battery. *Electrochim. Acta* **2017**, *258*, 360–

370, doi:10.1016/j.electacta.2017.11.063.

133. Watt-Smith, M.J.; Ridley, P.; Wills, R.G.A.; Shah, A.A.; Walsh, F.C. The importance of key operational variables and electrolyte monitoring to the performance of an all vanadium redox flow battery. *J. Chem. Technol. Biotechnol.* **2013**, *88*, 126–138, doi:10.1002/jctb.3870.

134. Gong, K.; Xu, F.; Grunewald, J.B.; Ma, X.; Zhao, Y.; Gu, S.; Yan, Y. All-Soluble All-Iron Aqueous Redox-Flow Battery. *ACS Energy Lett.* **2016**, *1*, 89–93, doi:10.1021/acsenergylett.6b00049.

135. Sanz, L.; Lloyd, D.; Magdalena, E.; Palma, J.; Kontturi, K. Description and performance of a novel aqueous all-copper redox flow battery. *J. Power Sources* **2014**, *268*, 121–128, doi:10.1016/j.jpowsour.2014.06.008.

136. Koros, W.J.; Ma, Y.H.; Shimidzu, T. Terminology for membranes and membrane processes (IUPAC Recommendations 1996). *Pure Appl. Chem.* **1996**, *68*, 1479–1489, doi:10.1351/pac199668071479.

137. Nagarjuna, G.; Hui, J.; Cheng, K.J.; Lichtenstein, T.; Shen, M.; Moore, J.S.; Rodríguez-López, J. Impact of redox-active polymer molecular weight on the electrochemical properties and transport across porous separators in nonaqueous solvents. *J. Am. Chem. Soc.* **2014**, *136*, 16309–16316, doi:10.1021/ja508482e.

138. Janoschka, T.; Martin, N.; Martin, U.; Friebe, C.; Morgenstern, S.; Hiller, H.; Hager, M.D.; Schubert, U.S. An aqueous, polymer-based redox-flow battery using non-corrosive, safe, and low-cost materials. *Nature* **2015**, *527*, 78–81, doi:10.1038/nature15746.

139. Zhang, H.; Zhang, H.; Li, X.; Mai, Z.; Zhang, J. Nanofiltration (NF) membranes: The next generation separators for all vanadium redox flow batteries (VRBs)? *Energy Environ. Sci.* **2011**, *4*, 1676–1679, doi:10.1039/c1ee01117k.

140. Zhang, H.; Zhang, H.; Li, X.; Mai, Z.; Wei, W. Silica modified nanofiltration membranes with improved selectivity for redox flow battery application. *Energy Environ. Sci.* **2012**, *5*, 6299–6303, doi:10.1039/c1ee02571f.

141. Wei, X.; Nie, Z.; Luo, Q.; Li, B.; Sprenkle, V.; Wang, W. Polyvinyl Chloride/Silica Nanoporous Composite Separator for All-Vanadium Redox Flow Battery Applications. *J. Electrochem. Soc.* **2013**, *160*, A1215–A1218, doi:10.1149/2.087308jes.

142. Mohammadi, T.; Skyllas-Kazacos, M. Characterisation of novel composite membrane for redox flow battery applications. *J. Memb. Sci.* **1995**, *98*, 77–87, doi:10.1016/0376-7388(94)00178-2.

143. Kang, M.-S. Development of Pore-filled Ion-exchange Membranes for Efficient All Vanadium Redox Flow Batteries. *J. Korean Electrochem. Soc.* **2013**, *16*, 204–210, doi:10.5229/jkes.2013.16.4.204.

144. Yamaguchi, T.; Miyata, F.; Nakao, S.I. Pore-filling type polymer electrolyte membranes for a direct methanol fuel cell. *J. Memb. Sci.* **2003**, *214*, 283–292, doi:10.1016/S0376-7388(02)00579-3.

145. Jung, H.; Fujii, K.; Tamaki, T.; Ohashi, H.; Ito, T.; Yamaguchi, T. Low fuel crossover anion exchange pore-filling membrane for solid-state alkaline fuel cells. *J. Memb. Sci.* **2011**, *373*, 107–111, doi:10.1016/j.memsci.2011.02.044.

146. Agarwal, C.; Cattrall, R.W.; Kolev, S.D. Donnan dialysis based separation of gold(III) from electronic waste solutions using an anion exchange pore-filled membrane. *J. Memb. Sci.* **2016**, *514*, 210–216, doi:10.1016/j.memsci.2016.04.033.

147. Ahn, Y.; Kim, D. Ultra-low vanadium ion permeable electrolyte membrane for vanadium redox flow battery by pore filling of PTFE substrate. *Energy Storage Mater.* **2020**, *31*, 105–114, doi:10.1016/j.ensm.2020.06.035.

148. Li, Z.; Zhang, B.; Qu, L.; Ren, J.; Li, Y. A novel atmospheric dielectric barrier discharge (DBD) plasma graft-filling technique to fabricate the composite membranes for pervaporation of aromatic/aliphatic hydrocarbons. *J. Memb. Sci.* **2011**, *371*, 163–170, doi:10.1016/j.memsci.2011.01.035.

149. Wang, M.; An, Q.F.; Wu, L.G.; Mo, J.X.; Gao, C.J. Preparation of pH-responsive phenolphthalein poly(ether sulfone) membrane by redox-graft pore-filling polymerization technique. *J. Memb. Sci.* **2007**, *287*, 257–263, doi:10.1016/j.memsci.2006.10.049.

150. Kuzume, A.; Miki, Y.; Ito, M. Characterisation of PAMPS-PSS pore-filling membrane for direct methanol fuel cell. *J. Memb. Sci.* **2013**, *446*, 92–98, doi:10.1016/j.memsci.2013.06.032.

151. Wang, N.; Wang, L.; Zhang, R.; Li, J.; Zhao, C.; Wu, T.; Ji, S. Highly stable "pore-filling" tubular composite membrane by self-crosslinkable hyperbranched polymers for toluene/n-heptane separation. *J. Memb. Sci.* **2015**, *474*, 263–272, doi:10.1016/j.memsci.2014.09.041.

152. Kim, D.H.; Park, J.H.; Seo, S.J.; Park, J.S.; Jung, S.; Kang, Y.S.; Choi, J.H.; Kang, M.S. Development of thin anion-exchange pore-filled membranes for high diffusion dialysis performance. *J. Memb. Sci.* **2013**, *447*, 80–86, doi:10.1016/j.memsci.2013.07.017.

153. Oshiba, Y.; Tomatsu, J.; Yamaguchi, T. Thin pore-filling membrane with highly packed-acid structure for high temperature and low humidity operating polymer electrolyte fuel cells. *J. Power Sources* **2018**, *394*, 67–73, doi:10.1016/j.jpowsour.2018.05.013.

154. Miyake, S., Tokuda, N. Battery diaphragm. U. S. Patent 6,461,772 B1, 8 October **2002**

155. Maurya, S.; Shin, S.H.; Kim, M.K.; Yun, S.H.; Moon, S.H. Stability of composite anion exchange membranes with various functional groups and their performance for energy conversion. *J. Memb. Sci.* **2013**, *443*, 28–35, doi:10.1016/j.memsci.2013.04.035.

156. Kim, D.H.; Kang, M.S. Pore-filled anion-exchange membranes with double cross-linking structure for fuel cells and redox flow batteries. *Energies* **2020**, *13*, doi:10.3390/en13184761.

157. Khoiruddin; Ariono, D.; Subagjo; Wenten, I.G. Surface modification of ion-exchange membranes: Methods, characteristics, and performance. *J. Appl. Polym. Sci.* **2017**, *134*, 1–13, doi:10.1002/app.45540.

158. Luo, Q.; Zhang, H.; Chen, J.; Qian, P.; Zhai, Y. Modification of Nafion membrane using interfacial polymerization for vanadium redox flow battery applications. *J. Memb. Sci.* **2008**, *311*, 98–103, doi:10.1016/j.memsci.2007.11.055.

159. Jia, C.; Liu, J.; Yan, C. A significantly improved membrane for vanadium redox

flow battery. *J. Power Sources* **2010**, *195*, 4380–4383, doi:10.1016/j.jpowsour.2010.02.008.

160. Lee, W.; Jung, M.; Serhiichuk, D.; Noh, C.; Gupta, G.; Harms, C.; Kwon, Y.; Henkensmeier, D. Layered composite membranes based on porous PVDF coated with a thin, dense PBI layer for vanadium redox flow batteries. *J. Memb. Sci.* **2019**, *591*, 117333, doi:10.1016/j.memsci.2019.117333.

161. Zhou, X.L.; Zhao, T.S.; An, L.; Wei, L.; Zhang, C. The use of polybenzimidazole membranes in vanadium redox flow batteries leading to increased coulombic efficiency and cycling performance. *Electrochim. Acta* **2015**, *153*, 492–498, doi:10.1016/j.electacta.2014.11.185.

162. Jang, J.K.; Kim, T.H.; Yoon, S.J.; Lee, J.Y.; Lee, J.C.; Hong, Y.T. Highly proton conductive, dense polybenzimidazole membranes with low permeability to vanadium and enhanced H2SO4 absorption capability for use in vanadium redox flow batteries. *J. Mater. Chem. A* **2016**, *4*, 14342–14355, doi:10.1039/c6ta05080h.

163. Peng, S.; Yan, X.; Wu, X.; Zhang, D.; Luo, Y.; Su, L.; He, G. Thin skinned asymmetric polybenzimidazole membranes with readily tunable morphologies for high-performance vanadium flow batteries. *RSC Adv.* **2017**, *7*, 1852–1862, doi:10.1039/c6ra24801b.

164. Wang, N.; Peng, S.; Wang, H.; Li, Y.; Liu, S.; Liu, Y. SPPEK/WO 3 hybrid membrane fabricated via hydrothermal method for vanadium redox flow battery. *Electrochem. commun.* **2012**, *17*, 30–33, doi:10.1016/j.elecom.2012.01.012.

165. Yang, C.C.; Chiu, S.S.; Kuo, S.C.; Liou, T.H. Fabrication of anion-exchange composite membranes for alkaline direct methanol fuel cells. *J. Power Sources* **2012**, *199*, 37–45, doi:10.1016/j.jpowsour.2011.10.020.

166. Vinodh, R.; Sangeetha, D. Comparative study of composite membranes from nano-metal-oxide-incorporated polymer electrolytes for direct methanol alkaline membrane fuel cells. *J. Appl. Polym. Sci.* **2013**, *128*, 1930–1938, doi:10.1002/app.38266.

167. Dai, W.; Shen, Y.; Li, Z.; Yu, L.; Xi, J.; Qiu, X. SPEEK/Graphene oxide nanocomposite membranes with superior cyclability for highly efficient vanadium redox flow battery. *J. Mater. Chem. A* **2014**, *2*, 12423–12432, doi:10.1039/c4ta02124j.

168. Wu, C.; Bai, H.; Lv, Y.; Lv, Z.; Xiang, Y.; Lu, S. Enhanced membrane ion selectivity by incorporating graphene oxide nanosheet for vanadium redox flow battery application. *Electrochim. Acta* **2017**, *248*, 454–461, doi:10.1016/j.electacta.2017.07.122.

169. Wu, C.; Lu, S.; Wang, H.; Xu, X.; Peng, S.; Tan, Q.; Xiang, Y. A novel polysulfone-polyvinylpyrrolidone membrane with superior proton-to-vanadium ion selectivity for vanadium redox flow batteries. *J. Mater. Chem. A* **2015**, *4*, 1174–1179, doi:10.1039/c5ta08593d.

170. Shukla, G.; Shahi, V.K. Amine functionalized graphene oxide containing C16 chain grafted with poly(ether sulfone) by DABCO coupling: Anion exchange membrane for vanadium redox flow battery. *J. Memb. Sci.* **2019**, *575*, 109–117.

171. Tsehaye, M.T.; Yang, X.; Janoschka, T.; Hager, M.D.; Schubert, U.S.; Alloin, F.; Iojoiu, C. Study of Anion Exchange Membrane Properties Incorporating N -

Spirocyclic Quaternary Ammonium Cations and Aqueous Organic Redox Flow Battery Performance. *Membranes (Basel).* **2021**, *11 (5)*, 367, doi:10.3390/membranes11050367

172. Zhang, S.; Zhang, B.; Zhao, G.; Jian, X. Anion exchange membranes from brominated poly(aryl ether ketone) containing 3,5-dimethyl phthalazinone moieties for vanadium redox flow batteries. *J. Mater. Chem. A* **2014**, *2*, 3083–3091, doi:10.1039/c3ta14503d.

173. Chen, D.; Kim, S.; Li, L.; Yang, G.; Hickner, M.A. Stable fluorinated sulfonated poly(arylene ether) membranes for vanadium redox flow batteries. *RSC Adv.* **2012**, *2*, 8087–8094, doi:10.1039/c2ra20834b.

174. Dai, Q.; Liu, Z.; Huang, L.; Wang, C.; Zhao, Y.; Fu, Q.; Zheng, A.; Zhang, H.; Li, X. Thin-film composite membrane breaking the trade-off between conductivity and selectivity for a flow battery. *Nat. Commun.* **2020**, *11*, 1–9, doi:10.1038/s41467-019-13704-2.

175. Yoo, S.H.; Kim, J.H.; Jho, J.Y.; Won, J.; Kang, Y.S. Influence of the addition of PVP on the morphology of asymmetric polyimide phase inversion membranes: Effect of PVP molecular weight. *J. Memb. Sci.* **2004**, *236*, 203–207, doi:10.1016/j.memsci.2004.02.017.

176. Han, M.J.; Nam, S.T. Thermodynamic and rheological variation in polysulfone solution by PVP and its effect in the preparation of phase inversion membrane. *J. Memb. Sci.* **2002**, *202*, 55–61, doi:10.1016/S0376-7388(01)00718-9.

177. Li, A.; Wang, G.; Wei, X.; Li, F.; Zhang, M.; Zhang, J.; Chen, J.; Wang, R. Highly selective sulfonated poly(ether ether ketone)/polyvinylpyrrolidone hybrid membranes for vanadium redox flow batteries. *J. Mater. Sci.* **2020**, *55*, 16822–16835, doi:10.1007/s10853-020-05228-8.

178. Zeng, L.; Zhao, T.S.; Wei, L.; Zeng, Y.K.; Zhang, Z.H. Polyvinylpyrrolidone-based semi-interpenetrating polymer networks as highly selective and chemically stable membranes for all vanadium redox flow batteries. *J. Power Sources* **2016**, *327*, 374–383, doi:10.1016/j.jpowsour.2016.07.081.

179. Wang, Z.X.; Yang, B. Chemical transformations of quaternary ammonium salts: Via C-N bond cleavage. *Org. Biomol. Chem.* **2020**, *18*, 1057–1072, doi:10.1039/c9ob02667c.

180. Dang, H.S.; Weiber, E.A.; Jannasch, P. Poly(phenylene oxide) functionalized with quaternary ammonium groups via flexible alkyl spacers for high-performance anion exchange membranes. *J. Mater. Chem. A* **2015**, *3*, 5280–5284, doi:10.1039/c5ta00350d.

181. Yang, J.; Jiang, H.; Gao, L.; Wang, J.; Ye, N.; Xu, Y.; He, R. Formation and investigation of dual cross-linked high temperature proton exchange membranes based on vinylimidazolium-functionalized poly(2,6-dimethyl-1,4-phenylene oxide) and polystyrene. *Polym. Chem.* **2018**, *9*, 5462–5469, doi:10.1039/c8py01148f.

182. Zhang, N.; Huo, J.; Yang, B.; Ruan, X.; Zhang, X.; Bao, J.; Qi, W.; He, G. Understanding of imidazolium group hydration and polymer structure for hydroxide anion conduction in hydrated imidazolium-g-PPO membrane by molecular dynamics simulations. *Chem. Eng. Sci.* **2018**, *192*, 1167–1176, doi:10.1016/j.ces.2018.08.051.

183. Gao, L.; He, G.; Pan, Y.; Zhao, B.; Xu, X.; Liu, Y.; Deng, R.; Yan, X. Poly(2,6-dimethyl-1,4-phenylene oxide) containing imidazolium-terminated long side chains as hydroxide exchange membranes with improved conductivity. *J. Memb. Sci.* **2016**, *518*, 159–167, doi:10.1016/j.memsci.2016.07.012.

184. Tan, Q.; Lu, S.; Si, J.; Wang, H.; Wu, C.; Li, X.; Xiang, Y. A Bunch-Like Tertiary Amine Grafted Polysulfone Membrane for VRFBs with Simultaneously High Proton Conductivity and Low Vanadium Ion Permeability. *Macromol. Rapid Commun.* **2017**, *38*, 1–8, doi:10.1002/marc.201600710.

185. Cho, H.; Krieg, H.M.; Kerres, J.A. Performances of anion-exchange blend membranes on vanadium redox flow batteries. *Membranes (Basel).* **2019**, *9*, doi:10.3390/membranes9020031.

186. Haisch, T.; Ji, H.; Weidlich, C. Monitoring the state of charge of all-vanadium redox flow batteries to identify crossover of electrolyte. *Electrochim. Acta* **2020**, *336*, doi:10.1016/j.electacta.2019.135573.

187. Düerkop, D.; Widdecke, H.; Schilde, C.; Kunz, U.; Schmiemann, A. Polymer Membranes for All-Vanadium Redox Flow Batteries: A Review. *Membranes (Basel).* **2021**, *11*, 214, doi:10.3390/membranes11030214.

188. Poli, N.; Schäffer, M.; Trovò, A.; Noack, J.; Guarnieri, M.; Fischer, P. Novel electrolyte rebalancing method for vanadium redox flow batteries. *Chem. Eng. J.* **2021**, *405*, 126583, doi:10.1016/j.cej.2020.126583.

189. Haladjova, E.; Mountrichas, G.; Pispas, S.; Rangelov, S. Poly(vinyl benzyl trimethylammonium chloride) Homo and Block Copolymers Complexation with DNA. *J. Phys. Chem. B* **2016**, *120*, 2586–2595, doi:10.1021/acs.jpcb.5b12477.

190. Matsumoto, H.; Sakaebe, H.; Tatsumi, K. Preparation of room temperature ionic liquids based on aliphatic onium cations and asymmetric amide anions and their electrochemical properties as a lithium battery electrolyte. *J. Power Sources* **2005**, *146*, 45–50, doi:10.1016/j.jpowsour.2005.03.103.

191. Rogińska, J., Belmonte, T., Etienne, M. Plasma treatment of porous membranes for selectivity improvement, Internal report, **2017**